Laser-based Gain Monitoring System for HERMES Experiment

Master Thesis

Hidekazu Tanaka

Department of Physics
Tokyo Institute of Technology

October 7, 2002

Abstract

The HERMES experiment is an experiment at DESY-HERA, designed to study the spin structure of the nucleon by deep inelastic scattering (DIS) of polarized positrons (electrons) at 27.6 GeV (27.5 GeV) off polarized internal gas targets (H, ^{3}He, D). Measurements with heavier targets are also carried out for nuclear physics.

To investigate the nucleon spin structure the inclusive and semi-inclusive measurement of spin asymmetries have been carried out. HERMES has a highly efficient particle identification (PID) system. The HERMES PID method uses several PID detectors such as calorimeter, preshower counter, Transition Radiation Detector (TRD) and Ring Imaging Cherenkov counter (RICH). The calorimeter and preshower counter play important roles in the PID process. With those detector combination, hadron-electron separation reaches 97 %.

More than 900 Photo-Multiplyer Tubes (PMT) are used for the PID detectors and other important detectors. Their gain stabilities are checked continuously with the Gain Monitoring System (GMS). The GMS sends light pulses of different intensities to the particle detectors as well as to an array of reference detectors via an optical fiber network. The different intensities of the light pulses are obtained by rotating a wheel with several attenuation plates in front of the Nitrogen Laser light source. The responses of the detectors to those pulses are measured in the same way as pulses from real deep inelastic scattering events. The GMS is however designed not to interfere with the measurement of the real deep inelastic scattering events. The responses of the particle detectors are compared with the reference photo-diode and the relative gain is calculated.

This work describes the GMS and how to analyze the relative gains. The performance of the reference detectors is discussed in connection with the Laser monitoring system which was built newly in this work. The detector gain is evaluated using the relative gain, and is discussed in the context of detector stability for long term measurements.

Contents

Chapter 1

Introduction

The main subject of the HERMES research program is the polarized structure functions of the nucleon and the decomposition of the contributions to the nucleon spin from the different quark flavors. The HERMES experiment is located in the HERA East Hall of DESY. HERMES uses a polarized positron beam of 27.6 GeV and gaseous fixed internal target. HERMES does not use the HERA proton beam.

Beside HERMES three experiments are running at HERA. The HERA positron-proton collider ring at DESY, Hamburg, provides two interaction areas where the positron and proton beams are brought to collision. The two experiments H1 and ZEUS, are running in the collider mode. HERA-B was set up in HERA West Hall and uses the HERA proton beam and a fixed target to study the CP violation in the B meson system.

One of the main tasks of the HERMES Experiment is the determination of the quark spin distributions with semi-inclusive measurements in deep inelastic scattering (DIS). Semi-inclusive measurement means a detection of hadrons in coincidence with the scattered positron. Semi-inclusive measurements allow us to study the spin contributions of each quark in the nucleon by tagging the struck quark with help of the identification of the leading hadron in the final state. For the particle identification (PID), HERMES uses several types of PID methods, and those PID methods are combined for the final identification of the particle. To use the DIS process as a way to access the quark spin, it is most important to separate the scattered positron (electron) from produced hadrons. The calorimeter and preshower counter are used for the positron-hadron separation. This PID method is called "PID2". Combining PID2 with the signal from the Transition Radiation Detector (TRD), the positron-hadron separation probability reaches more than 97% [2].

The PID at HERMES is not only for the positron-hadron separation, but also pion, kaon proton are identified in semi-inclusive measurement with Ring Imaging Cherenkov counter (RICH). To access the nucleon spin contribution from sea-quark, the spin asymmetries in the productions of those hadrons are extracted[3]. Especially, the negative kaon consists of only sea-quarks ($\bar{u}s$). So, the spin asymmetry in kaon production is one of the most interesting subjects.

Stability of the PID detectors, calorimeter and preshower counter etc, are monitored by the Gain Monitoring System (GMS). The GMS monitors not only the PID detectors but also the luminosity monitor, the H0 hodoscope, and the longitudinal polarimeter (LPol). The main aim is to measure the gain of photo-multiplier tube (PMT) of those detectors. The GMS is operating since the start-up of the HERMES experiment in 1995. Various improvements were made recently as described in this thesis.

The GMS operation includes the light transmission to the detector, the production of electrical signals by photo-sensitive detectors, signal processing (amplification, shaping), and digitization. The GMS injects the Laser light to the PMTs, and at the same time, to an array of reference detectors via the optical fiber network. The light can be attenuated by means of filters mounted on a rotating wheel. The generation of a GMS event begins when one of the filters is in front of the light source with a rate of a few Hz. When the filter is in position the light source, a nitrogen/dye laser, is triggered to generate an intense pulse of light. The data which are tagged with the current filter number are included in the event data stream in a special GMS event. Comparing the initial response of a detector to the response later in the experiment the stability of the detector response is monitored.

In this thesis, following topics are covered.
The second chapter describes physics of the DIS process. The semi-inclusive measurement which is used to access the quark spin at the HERMES experiment is explained. The detector components of the HERMES experiment are described in the third chapter. Then in the fourth chapter, GMS hardware components and their specification are discussed. The principle and the result of gain monitoring are described in the last chapter.

Chapter 2

Deep Inelastic Scattering(DIS)

Deep inelastic scattering (DIS) has played an essential role in the study of quarks and gluons. The lepton-hadron scattering with high momentum transfer produces one or more hadrons. Hence, it is described as:

$$e + N \rightarrow e' + h + X$$

where e is the initial lepton, N is the target nucleon and e' is the scattered lepton, h is one or more hadrons inside the detector acceptance, X stands for other undetected hadrons.

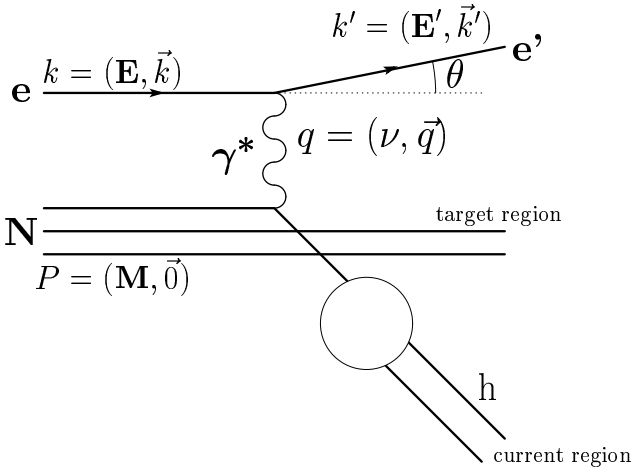

Figure 2.1: Diagram of a deep inelastic scattering.

Figure 2.1 shows a schematic diagram of deep inelastic scattering. The initial lepton has four-momentum k and the final lepton has k'. Assuming one

photon exchange with the nucleon as a target, the differential cross section for the final lepton detected in the solid angle $d\Omega$ and in the final energy range $(E, E' + dE')$ is written as

$$\frac{d^2\sigma}{d\Omega dE'} = \frac{\alpha 2}{2Mq^4}\frac{E'}{E}L_{\mu\nu}W^{\mu\nu} \tag{2.1}$$

where $q = k - k'$ and α is the fine structure constant. The other kinematic variables are summarized below:

$$\begin{array}{ll}
Q^2 = -\boldsymbol{q}^2 = -(\boldsymbol{k} - \boldsymbol{k}')^2 \simeq 4EE'\sin^2\frac{\theta}{2} & \\
\nu = \frac{\vec{P}\cdot\vec{q}}{M} = E - E' & \text{energy transfer} \\
x = -\frac{\vec{q}^2}{2\vec{P}\cdot\vec{q}} = \frac{Q^2}{2M\nu} & \text{momentum fraction} \\
 & \text{carried by quark} \\
y = \frac{\vec{P}\cdot\vec{q}}{\vec{P}\cdot\vec{k}} = \frac{\nu}{E} & \text{energy fraction} \\
W^2 = (\vec{P} + \vec{q})^2 = M^2 + 2M\nu - Q^2 & \text{invariant mass of the} \\
 & \text{final state hadrons}
\end{array} \tag{2.2}$$

2.1 The Unpolarized Cross Section

The inclusive DIS cross-section can be expressed in terms of the lepton and hadron tensors, $L^{\mu\nu}$ and $W_{\mu\nu}$:

$$\frac{d^2\sigma}{d\Omega dE'} = \frac{\alpha^2}{Q^4}\frac{E'}{E}L^{\mu\nu}W_{\mu\nu}, \tag{2.3}$$

where $\alpha = \frac{1}{137.04}$ is the fine structure constant. The lepton tensor is calculated from the spinors according to the Feynman rules:

$$L^{\mu\nu} = \sum_{s_l'}(\bar{u}(k', s_l')\gamma^\mu u(k, s_l)) \cdot (\bar{u}(k, s_l)\gamma^\nu u(k', s_l'))\,. \tag{2.4}$$

When the beam and target are unpolarized, the initial spins s_l are averaged and the leptonic tensor becomes:

$$L^{\mu\nu} = 2\left[k^{\mu'}k^\nu + k^\mu k^{\nu'} + (m_e^2 - k\cdot k')g^{\mu\nu}\right], \tag{2.5}$$

where m_e is the electron mass and can be neglected. $g^{\mu\nu}$ is the metric tensor. The hadronic tensor reflects the structure of the nucleon and can be reduced to two real functions, W_1 and W_2:

$$W_{\mu\nu} = W_1(Q^2, \nu)(-g_{\mu\nu} + \frac{q_\mu q_\nu}{q^2}) + \frac{W_2(Q_2, \nu)}{M^2}(p_\mu - \frac{p\cdot q}{q^2}q_\mu)(p_\nu - \frac{p\cdot q}{q^2}q_\nu) \tag{2.6}$$

If we introduce dimensionless structure functions:

$$F_1(x, Q^2) = MW_1(Q^2, \nu), \tag{2.7}$$

$$F_2(x, Q^2) = \nu W_2(Q^2, \nu), \tag{2.8}$$

the unpolarized cross-section becomes:

$$\frac{d^2\sigma}{d\Omega dE'} = \frac{4\pi\alpha^2}{Q^4} \cdot \left\{ y^2 F_1(x, Q^2) + \left(1 - y - \frac{Mxy}{2E}\right) \frac{F_2(x, Q^2)}{x} \right\}. \tag{2.9}$$

The measurement of the structure functions of proton reveals that they depend only very weakly on Q^2, which is called Bjorken scaling. This indicates that the proton consists of point like sub-particles called partons. Furthermore, the Callen-Gross relation

$$F_2(x) = 2xF_1(x) \tag{2.10}$$

is measured to be valid to high degree. This relation is a direct consequence of the spin-$\frac{1}{2}$ property of the quarks inside the proton because the relation is only true for the scattering of point-like spin-$\frac{1}{2}$ particles by exchange of a vector boson.

The unpolarized cross-section can alternatively be described in terms of absorption cross-section for longitudinally σ_L and transversely σ_T polarized photons:

$$\frac{d^2\sigma}{d\Omega dE'} = \Gamma \left(\sigma_T + \epsilon\sigma_L\right), \tag{2.11}$$

Γ denotes the flux of virtual photons.

2.2 The Polarized Cross Section

Consider the deep inelastic scattering of polarized leptons and polarized nucleons. The polarized cross-section contains additional terms to take into account the azimuthal angle ϕ:

$$\frac{d^3\sigma}{d\cos\theta d\phi dE'} = \frac{\alpha^2}{Q^4}\frac{E'}{E} L^{\mu\nu} W_{\mu\nu}. \tag{2.12}$$

The lepton tensor in Eq.2.4 becomes:

$$L^{\mu\nu} = 2\left[k^{\mu'}k^{\nu} + k^{\mu}k^{\nu'} - k \cdot k' g^{\mu\nu} - i\epsilon^{\mu\nu\alpha\beta} q_\alpha s_{l\beta}\right], \tag{2.13}$$

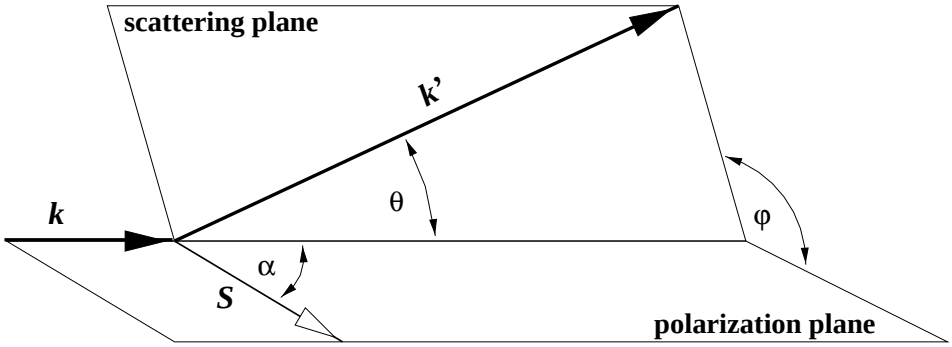

Figure 2.2: Scattering angles in polarized DIS. The four-momentum vectors, k and k' are for the incident and scattered leptons. The angles θ, ϕ and α are defined as the angles between k and k'.

where $s_{l\beta}$ is the spin four-vector of the incoming lepton and $\epsilon^{\mu\nu\alpha\beta}$ is the totally anti-asymmetric Levi-Civita tensor. The general form of the hadronic tensor in the polarized case is

$$\begin{aligned} W_{\mu\nu} &= W_1(Q^2,\nu)(-g_{\mu\nu}+\tfrac{q_\mu q_\nu}{q^2})+\tfrac{W_2(Q^2,\nu)}{M^2}(p_\mu-\tfrac{p\cdot q}{q^2}q_\mu)(p_\nu-\tfrac{p\cdot q}{q^2}q_\nu) \\ &\quad +G_1(Q^2,\nu)Mi\epsilon_{\mu\nu\lambda\sigma}q^\lambda s_h^\sigma+\tfrac{G_2(Q^2,\nu)}{M}i\epsilon_{\mu\nu\lambda\sigma}q^\lambda(p\cdot qs_h^\sigma-s_h\cdot qp^\sigma), \end{aligned} \tag{2.14}$$

where s_h is the axial polarized vector of a spin-$\frac{1}{2}$ target. Because of the symmetries of the leptonic and hadronic tensors, the polarization asymmetry of the cross-section is completely determined by the anti-asymmetric part of $W_{\mu\nu}$.

In analogy to the unpolarized case, two dimensionless spin structure functions are introduced:

$$g_1(x,Q^2)=M^2\nu G_1(Q^2,\nu), \tag{2.15}$$

$$g_s(x,Q^2)=M\nu^2 G_2(Q^2,\nu). \tag{2.16}$$

With these definitions, the spin-dependent part of the polarized DIS cross-section is given by

$$\begin{aligned} \tfrac{d^3(\sigma(\alpha)-\sigma(\pi+\alpha))}{dxdyd\phi} &= \tfrac{e^4}{4\pi^2Q^2}\Big[\cos\alpha\Big(\Big[1-\tfrac{y}{2}-\tfrac{y^2}{4}\gamma^2\Big]g_1(x,Q^2)-\tfrac{y}{2}\gamma^2 g_2(x,Q^2)\Big) \\ &\quad -\sin\alpha\cos\phi\sqrt{\gamma^2\Big[1-y-\tfrac{y^2}{4}\gamma^2\Big]}\Big(\tfrac{y}{2}g_1(x,Q^2)+g_2(x,Q^2)\Big)\Big], \end{aligned}$$

where γ is defined as $\gamma=\sqrt{Q^2}/\nu$ and α is defined in Figure 2.2.

2.3 Cross Section Asymmetries

The experimentaly measured asymmetries $A_\parallel$ and $A_\perp$ are obtained by reversing the spin of the longitudnally and transversely polarized target:

$$A_\parallel = \frac{\sigma^{\uparrow\downarrow} - \sigma^{\uparrow\uparrow}}{\sigma^{\uparrow\downarrow} + \sigma^{\uparrow\uparrow}}, \tag{2.17}$$

$$A_\perp = \frac{\sigma^{\uparrow\rightarrow} - \sigma^{\uparrow\leftarrow}}{\sigma^{\uparrow\rightarrow} + \sigma^{\uparrow\leftarrow}}. \tag{2.18}$$

These cross-section asymmetries are related to the asymmetries of the virtual photon absorption cross section by

$$A_\parallel = \mathcal{D} \cdot (A_1 + \eta \cdot A_2), \tag{2.19}$$

$$A_\perp = d \cdot (A_2 - \xi \cdot A_1). \tag{2.20}$$

The kinematic factors are defined as follows:

$$\mathcal{D} = \frac{y(2-y)}{y^2 + 2(1 - y(1+R))}, \tag{2.21}$$

$$\eta = \frac{2\gamma(1-y)}{2-y}, \tag{2.22}$$

$$d = \mathcal{D}\sqrt{\frac{2\epsilon}{1+\epsilon}}, \tag{2.23}$$

$$\xi = \eta\frac{1+\epsilon}{2\epsilon}, \tag{2.24}$$

where ϵ is the degree of transverse polarization of the virtual photon and $R(x, Q^2)$ is the ratio of cross-section for longitudinally and transversely polarized photons. $\mathcal{D}$ is the depolarization factor, measuring the depolarization of the photon relative to the polarization of the scattered lepton.

A_1 and A_2 have relations to g_1 and g_2. They are written as:

$$A_1 = \frac{g_1 - \gamma^2 g_2}{F_1}, \tag{2.25}$$

$$A_2 = \frac{\gamma(g_1 + g_2)}{F_1}. \tag{2.26}$$

Eliminating g_2 from Eq.2.25 and Eq.2.26 yields the relation between A_1 and the structure function ratio g_1/F_1:

$$A_1 = (1+\gamma^2)\frac{g_1}{F_1} - \gamma A_2. \tag{2.27}$$

Inverting the Eq.2.20 yields the formula to determine A_1 from the measured raw asymmetry $A_\parallel$:

$$A_1 = \frac{A_\parallel}{\mathcal{D}} - \eta A_2. \tag{2.28}$$

Eliminating A_1 from Eq.2.27 and Eq.2.28 yields the formula to determine g_1/F_1 from the measured raw asymmetry $A_\parallel$:

$$\frac{g_1}{F_1} = \frac{1}{1+\gamma^2}\left[\frac{A_\parallel}{\mathcal{D}} + (\gamma - \eta)A_2\right]. \tag{2.29}$$

Using the relation between F_1 and F_2:

$$\frac{1+R(x,Q^2)}{1+\gamma^2} = \frac{F_2(x,Q^2)}{2xF_1(x,Q^2)}, \tag{2.30}$$

where R is the ratio of longitudinal and transverse photon absorption cross sections: $R = \sigma_L/\sigma_T$ in Eq. 2.29 F_1 can be replaced by F_2 structure function which has already been measured with high accuracy. Finally one obtains the formula to determine the g_1 structure function from the measured asymmetry $A_\parallel$:

$$g_1 = \frac{F_2}{2x(1+R)}\left[\frac{A_\parallel}{\mathcal{D}} + \gamma\frac{y}{2-y}A_2\right]. \tag{2.31}$$

The approximate determination of $A_1(x,Q^2)$ and $g_1(x,Q^2)$ by only measuring $A_\parallel$ is possible by assuming $\gamma A_2 \simeq 0$.

$$A_1 = \frac{A_\parallel}{\mathcal{D}}, \tag{2.32}$$

$$g_1 = \frac{F_2}{2x(1+R)}\frac{A_\parallel}{\mathcal{D}}. \tag{2.33}$$

2.4 Semi-Inclusive Measurement of Deep Inelastic Scattering

In Figure2.1 the scattered lepton e' is measured in coincidence with the hadrons h. The scattered lepton has the information of the kinematics of the struck quark. The produced hadrons have the information of the flavor of the struck quark. This kind of flavor tagging works on the statistical basis and requires knowledge of the hadronization.

The quark parton model will be extended by a fragmentation model which allows to relate the appearance of certain hadrons h in the final state to the parton distribution functions for different flavors by so called "fragmentation functions". Figure 2.1 shows the semi-inclusive measurement of the DIS process. The cross-section of the semi-inclusive measurement with a hadron h in the final state is given by

$$\frac{d^3\sigma_h}{dxdQ^2dz}(x,Q^2,z) = \frac{\sum_q e_q^2(x)D_q^h(z)}{\sum_q e_q^2 q(x)} \cdot \frac{d^2\sigma}{dxdQ^2}(x,Q^2), \tag{2.34}$$

where $D_q^h(z)$ is the fragmentation function defined as the number density to produce a hadron with the energy fraction $z = E_h/\nu$ after a quark of flavor q is struck.

The kinematical variables of semi-inclusive measurements are summarized as:

$$\begin{array}{ll} z = \frac{E_h}{\nu} & \text{Fractional energy of a hadron in lab. frame} \\ \boldsymbol{p}_\parallel = \frac{\boldsymbol{p}_h \boldsymbol{q}}{\sqrt{\boldsymbol{q}^2}} & \text{Parallel momentum of hadron in } \gamma N \text{ frame} \\ \boldsymbol{p}_T = \boldsymbol{p} - \boldsymbol{p}_\parallel & \text{Transverse momentum of hadron in } \gamma N \text{ frame} \\ x_F = \left(\frac{2||\boldsymbol{p}^2||}{\sqrt{W^2}}\right)_{c.m.} & \text{Feynman's scaling variable} \end{array} \tag{2.35}$$

The fragmentation functions don't depend on any kinematical variables which appear in the inclusive measurement (e.g. x and Q^2) to the approximation. This fact leads to the assumption that the two processes are independent of each other and is called factorization. The factorization is a direct consequence of quasi-free partons in the quark parton model. The mean hadron multiplicity n^h per event is calculated as:

$$\frac{d^3n^h}{dxdQ^2dz}(x,Q^2,z) = \frac{\sum_q e_q^2(x)D_q^h(z)}{\sum_q e_q^2 q(x)}. \tag{2.36}$$

The measured semi-inclusive asymmetry of a hadron h is defined as

$$A_\parallel^h = \frac{\sigma_h^{\uparrow\downarrow} - \sigma_h^{\uparrow\uparrow}}{\sigma_h^{\uparrow\downarrow} + \sigma_h^{\uparrow\uparrow}}. \tag{2.37}$$

Furthermore, we define

$$g_1^h(x,z) = \frac{1}{2}\sum_q e_q^2 D_q^h(z)\Delta q, \tag{2.38}$$

and

$$F_2^h(x,z) = 2x\frac{1}{2}\sum_q e_q^2 D_q^h(z)\Delta q. \tag{2.39}$$

We can use the relation Eq.2.29 analogously to derive the relation between the spin asymmetry of the hadron $A_\parallel^h$ and the polarized and unpolarized parton distribution functions using Eq.2.38 and Eq.2.39:

$$\frac{\sum_q e_q^2 D_q^h(z)\Delta q}{\sum_{q'} e_{q'}^2 D_{q'}^h(z)\Delta q'}\left[1 + R(x,Q^2)\right] = \frac{A_\parallel^h}{\mathcal{D}}. \tag{2.40}$$

The measured longitudinal asymmetries corrected with the depolarization factor $\mathcal{D}$ is written as:

$$A^h(x,z) = \frac{A_\parallel^h}{\mathcal{D}}. \tag{2.41}$$

If we have enough information on the asymmetries, it is possible to decompose the polarized parton distribution functions Δq for each flavor. The simple and best solution is to identify the hadrons (e.g. π, K and p) in the final state.

Chapter 3

HERMES Experiment

The HERMES experiment has been designed to study the spin structure of the nucleon. The experiment is studying the nucleon spin structure with "Hadron Elektron Ring Anlage" (HERA) synchrotron accelerator of the "Deutsches Elektronen Synchrotoron" (DESY), and takes data on Deep Inelastic Scattering (DIS) of polarized positrons (electrons) and polarized nucleon gas targets.

It was discovered that quark spin contribution to the nucleon spin is very small by EMC[4][5] of CERN. Semi-inclusive DIS can provide a way to clarify the distribution of each quark spin. Especially, to know spin distribution of the sea-quark, it is important to identify the hadron type of produced hadrons in DIS event. HERMES has highly efficient particle identification (PID) detectors. The PID detectors can separate not only between electron and hadron, but also pion, kaon and proton.

The spectrometer used in HERMES is a forward spectrometer with a large acceptance to detect the scattered lepton and produced hadrons in DIS processes. The overview of the spectrometer can be seen in Figure 3.1.

In the figure a part of detector is cut away the detector to show the beam pipe. The horizontal line positron (electron) beam pipe. In sequence, HERMES spectrometers consists of VC(Vertex Chamber), FC(Front Chamber), Hodoscope (H1, H2, H0), Spectrometer magnet, BC(Back Chamber), RICH, TRD (Transition Radiation Detector), and Calorimeter. The total length is about 10 m.

3.1 The Beam

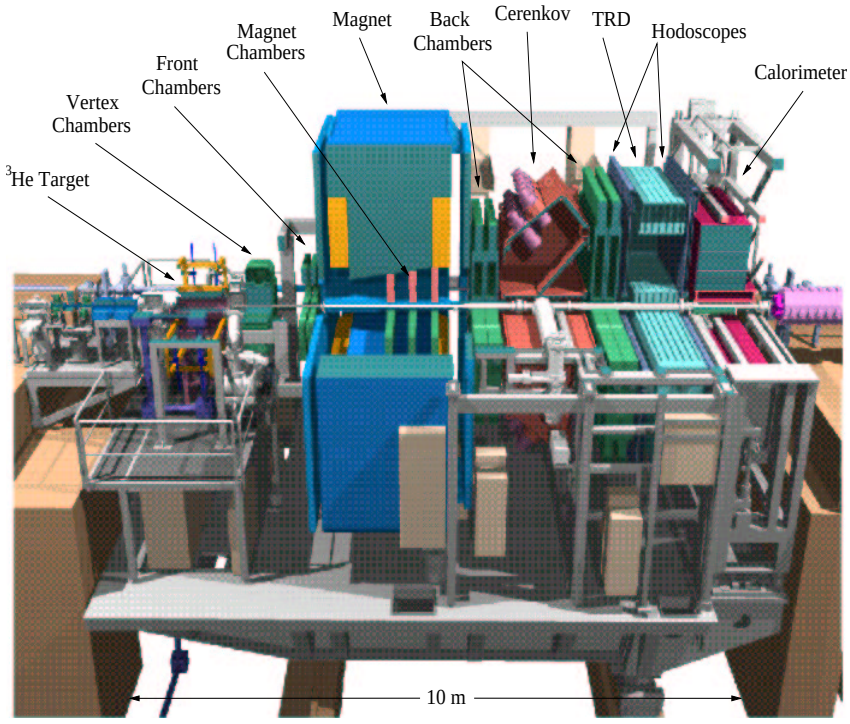

Figure 3.1: A three dimensional CAD diagram of the HERMES Spectrometer.

The HERMES experiment is located in the east straight section of the HERA facility at the DESY laboratory in Hamburg, Germany. HERA consists of two storage rings, with a 27.5 GeV positron (electron) beam and a 820 GeV proton beam.

The experiment uses the 27.5 GeV positron beam with maximum current of 40 mA.

Figure 3.2 shows the HERA lepton (electron or positron) ring. The beam becomes polarized transversely to the beam plane due to the asymmetry in the emission of synchrotron radiation (Sokolov-Ternov mechanism [6]). The beam polarization $P(t)$ is given as function of time t:

$$P(t) = p_{max}(1 - e^{-t/\tau}), \tag{3.1}$$

where τ is the polarization build up time and p_{max} is the equilibrium polarization. At HERA the beam reaches 60% polarization in about 30 minutes after the beam injection.

Because it is necessary to obtain the longitudinal beam polarization at HERMES, two spin rotators are located up and downstream of the HERMES spectrometer. The first rotates the lepton spin to the longitudinal direction the second one rotates back to transverse. The beam polarization is measured by a transverse polarimeter in the West Hall of HERA. The polarization is constant in the whole storage ring. The polarization after passing through the first spin rotator is measured by LPol (Longitudinal Polarimeter). Figure 3.3 shows the actual longitudinal polarization during the experiment.

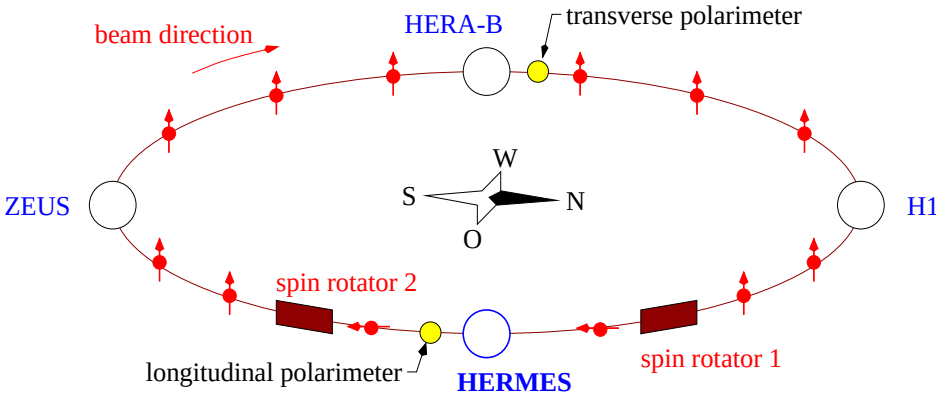

Figure 3.2: The HERA storage ring with HERMES and the other three experiments, ZEUS, H1 and HERA-B. Because the longitudinal beam polarization is needed for HERMES, the two spin rotators are located up and downstream of the HERMES experiment.

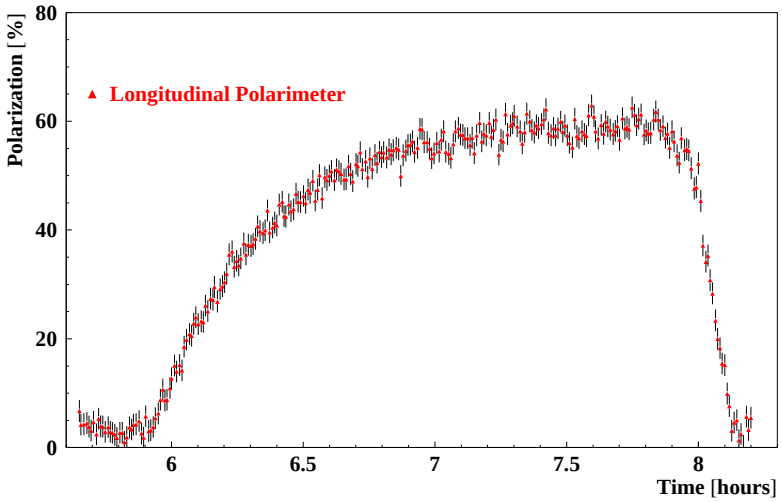

Figure 3.3: The longitudinal polarization of HERA beam. The polarization reaches up to 60 % in about 30 minutes. This polarization is measured by Longitudinal Ploarimeter(See Section 3.4)

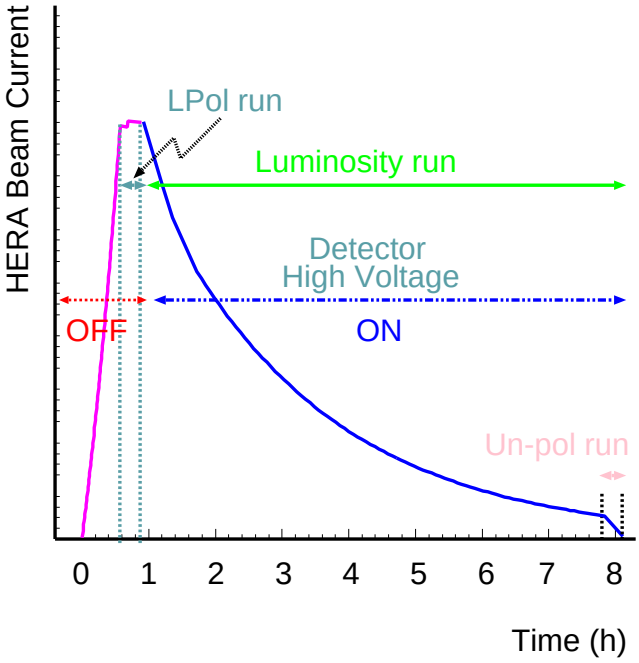

Figure 3.4: Time scale during the experiment from beam injection to beam dump.

The Figure 3.4 shows a time scale of HERA positron beam and HERMES experiment. After the HERA positron beam current reaches the maximum, there is a time zone which is called "LPol run". In this zone, high voltage of all detector (except LPol) is still not turned on, but the DAQ system is running. One luminosity run is for about 8 hours. The "Un-pol run" at the end is the high density run with unpolarized targets.

3.2 The Target

It is technically difficult to polarize the nucleon of a pure solid material to a high degree and use them as a target in a lepton beam. Instead, HERMES uses internal gas targets, together with a storage cell technique to enhance the target density.

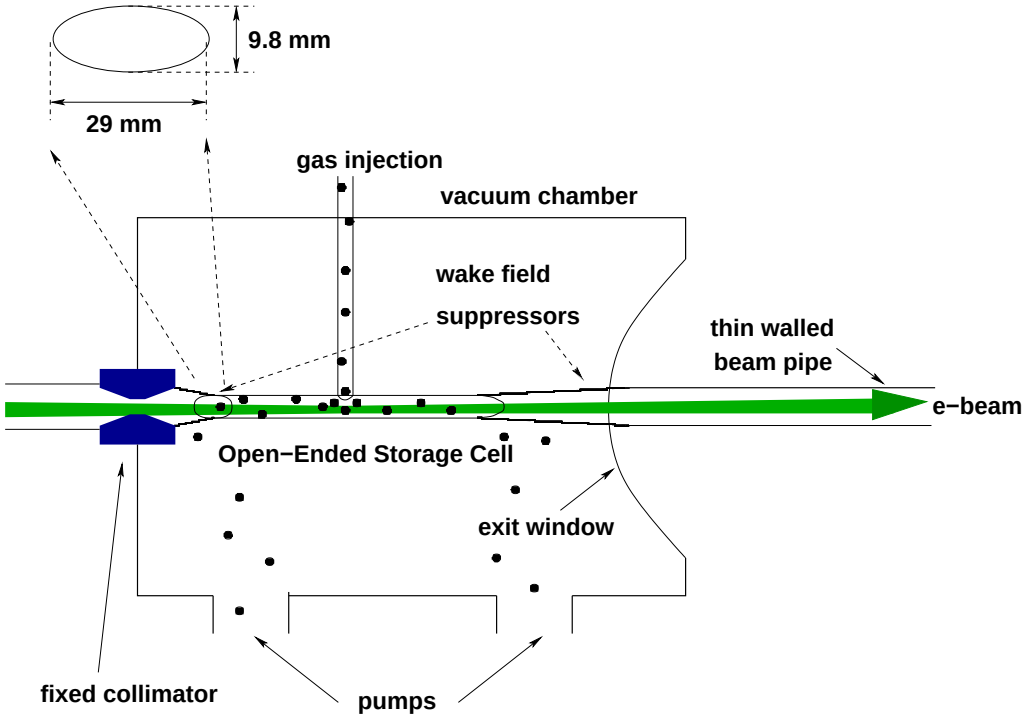

Figure 3.5: Schematic view of the HERMES together with storage cell.

Figure 3.5 shows the schematic view of the target. From one side the gas atoms are injected into a thin-walled, T-shaped tube which is called "storage

cell". The storage cell is made of aluminum with its length of 400 mm and its wall thickness of 0.125 mm. The target atoms remain inside the cell for typically 3 ms and cross the interaction region many times. When the target atoms are in the target cell, the following interactions are needed to be considered ;

- Recombination: the atoms inside the target cell hit the cell walls and form molecules.
- Wall depolarization: the atoms attached to the wall by collision lead to a relaxation of the atom polarization by the interaction with surface magnetic fields.
- Spin exchange collisions: a collision of the atoms may lead to a spin exchange between the hyperfine states of the atoms and cause exchange of electron and proton spin.

Now the target thickness achieved is 7×10^{13} atoms/cm^2, which is more than two order of magnitude higher compared to the target thickness by a free jet target, usually 2×10^{11} atoms/cm^2 [7].

3.3 The Detector Components

HERMES spectrometer has a large acceptance and is a forward angle detector. This spectrometer is shown in Fig.3.6 and Fig.3.1 [1]. With the HERMES detector, scattering angles of particles are accepted between $\pm$ 170 mrad in the horizontal direction and between +/(-)40 mrad and +/(-)140 mrad in the vertical direction[9].

A spectrometer magnet and several detectors for particle tracking allow the determination of particle momenta. The tracking system consists of microstrip gas chambers, drift chambers and three proportional chambers in the magnet.

For semi-inclusive measurements in DIS, HERMES needs a very good particle identification (PID), not only to separate leptons and hadrons, but also to identify the hadrons. To achieve this high quality particle identification, the HERMES spectrometer is equipped with four special PID detectors, an electromagnetic lead-glass calorimeter, a preshower hodoscope, a transition radiation detector (TRD) and Cherenkov Counter. The original threshold Cherenkov has been replaced in 1998 by a Ring Imaging Cherenkov Counter

(RICH) to allow a clean hadron identification over the momentum range of $2 \sim 15$ GeV/c.

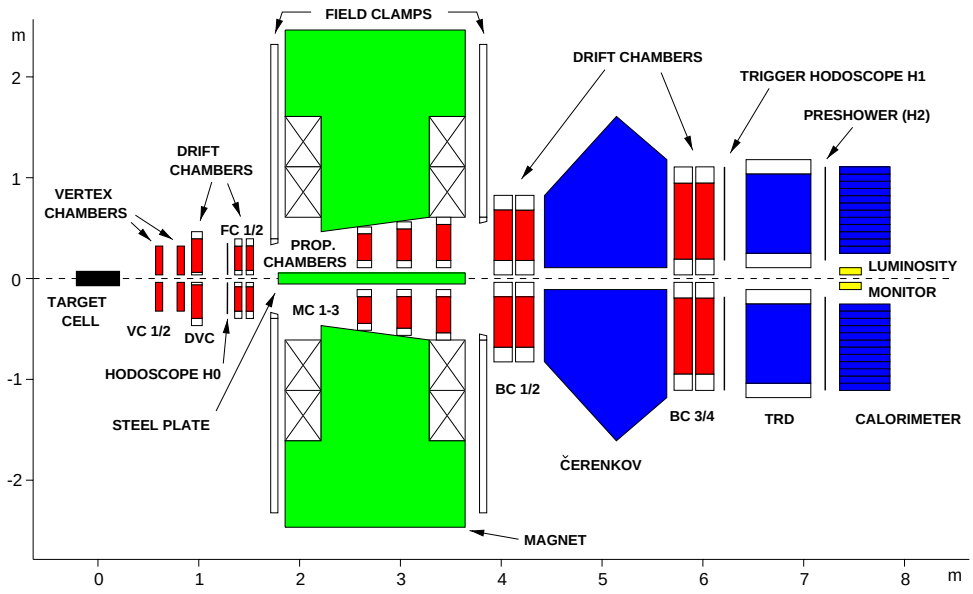

Figure 3.6: The HERMES Spectrometer. Two identical detectors are built above and below the beam line. The Cherenkov Counter was operated as a threshold Cherenkov Counter during 1995 - 1997 data taking. Since 1998, a Ring Imaging Cherenkov Counter is installed to identify produced hadrons.

3.3.1 The Tracking System

Spectrometer Magnet

The HERMES spectrometer has a H-type magnet with a deflecting power of 1.5 Tm and it is usually operated at 1.3 Tm for the momentum measurement. The lepton beam line is protected by a horizontal septum plate with compensator coils which is arranged in the beam plane. The angular acceptance is 40 mrad $< |\theta_y| <$ 140 mrad vertically, and $|\theta_x| <$ 170 mrad

horizontally, where the lower vertical limit is given by the septum plate. The total acceptance of scattering angles is 40 mrad $< |\theta| <$ 220 mrad[9].

Vertex and Front Chambers

In upstream region of the spectrometer magnet, the drift vertex chambers DVC and the drift front chambers FC1/2 are installed to reconstruct the particle vertex and to determine the scattering angle.

The FC's is a pair of drift chambers, each chamber has 6 planes. The size of drift cell is 7 mm (3.5 mm maximum drift length), and the used gas is $Ar/CO_2/CF_4$ ($Ar:CO_2:CF_4$ 90:5:5) like in all other HERMES drift chambers.

The DVC acceptance is vertically $\pm$ 35 mrad $\sim \pm$ 270 mrad and horizontally $\pm$ 200 mrad. The DVC drift cell is smaller than the FC's.

Magnet Chambers

The proportional wire chambers MC1/2/3 are installed in the gap of the spectrometer magnet. They were originally installed to analyze multiple tracks in high multiplicity events.

It has turned out that they are also particularly useful for the analysis of particles with low energy which are deflected by the magnet so that they don't come out of the magnet ; pion from the Λ-decays, for example. Each chamber consists of 3 modules. The distance between anode and cathode planes is 4.00$\pm$0.03 mm. The gas is the same as the drift chambers but the proportions of the mixture is different ($Ar:CO_2:CF_4$ 65:30:5).

Back Chambers

In the region downstream of the spectrometer magnet two sets of the back drift chambers BC1/2 and BC3/4 are mounted. The difference between BC1/2 and BC3/4 is the detector size. The active areas of these modules depend on their z-position and the acceptance of the spectrometer. The BC1/2 active area is horizontally 1880 mm and vertically 520 mm, and the BC3/4's is 2890 mm and 710 mm. Each set of chambers has two modules with 6 planes. The efficiency of the drift chamber depends on the drift distance and the typical efficiency is well above 99%. The details are shown in [10]. These detectors are shown in Fig.3.7.

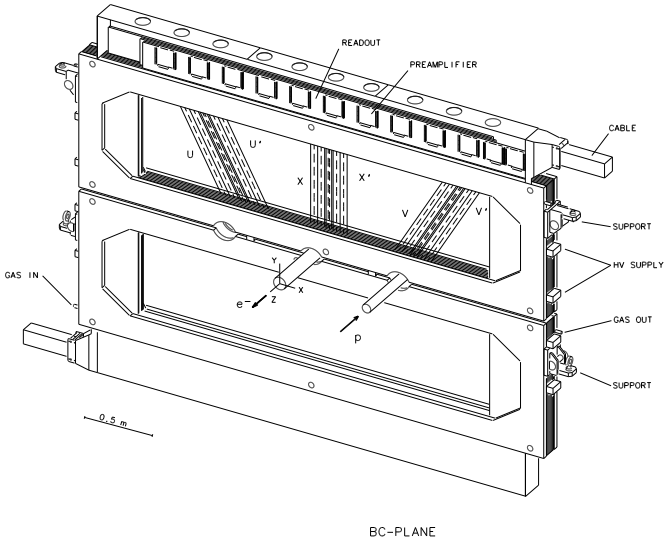

Figure 3.7: Schematic view of the HERMES BC module.

3.3.2 The Particle Identification System

As mentioned before, a clean particle identification is very important at HERMES. The PID is performed in two steps : first a lepton-hadron separation and second the identification of the hadron. Especially the second point is essential for the study of the quark spin distribution. As for the lepton-hadron separation, the hadron rejection factor (HRF) of the system is designed to be 10^4 at least, where HRF is defined as the total number of hadrons divided by the number of hadrons misidentified as leptons.

This value depends on the efficiency for the lepton identification. The contamination of the lepton sample by hadrons is below 1% for the whole kinematic range. This hadron rejection is done by the calorimeter, the preshower hodoscope and the TRD. The second step, the hadron identification is done by the fourth PID detector, the RICH. These four detectors are described in the following.

Calorimeter

The calorimeter (Fig.3.10) provides a first level trigger for scattered positrons (electrons). It consists of two modules which have 420 blocks each above and below the beam line. All 840 blocks are made by identical lead-glass blocks

with size of 9 × 9 × 50 cm (about 18 radiation length), and are arranged in a 42 × 10 array for each module. The lead glass is chosen F101 which has a durability for radiation damage[14]. The blocks are polished, wrapped with 50 μm thick alminized mylar foil and covered with a 125 μm thick tedlar foil to provide light insulation. Each block is coupled to a 7.5 cm Philips XP3461 photo-multiplier with a silicon glue (SILGARD 184) with a refraction index of 1.41. Each block is readout by a photo-multiplier tube (PMT). Both the calorimeter walls can be moved 50 cm vertically from the beam pipe to prevent radiation damage during beam injection or dump.

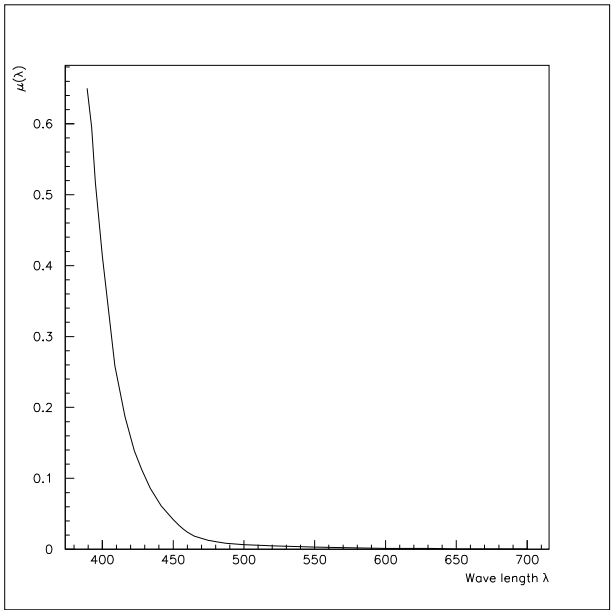

Figure 3.8: Attenuation for F101.

The energy resolution of this detector is parameterized by the following function ;

$$\frac{\sigma_E}{E}[\%] = \frac{5.1 \pm 1.1}{\sqrt{E[GeV]}} + (2.0 \pm 0.5) + \frac{10.0 \pm 2.0}{E(GeV)} \tag{3.2}$$

which is slightly degraded compared to the test beam results ($\sigma_E/E = 1.5 \pm 0.5 + (5.1 \pm 1.1)/\sqrt{E(GeV)}$) [15]. Combined with the preshower counter, the efficiency for the detection of lepton is about 95%. The actual energy resolution of the calorimeter can be seen in Figure 3.11.

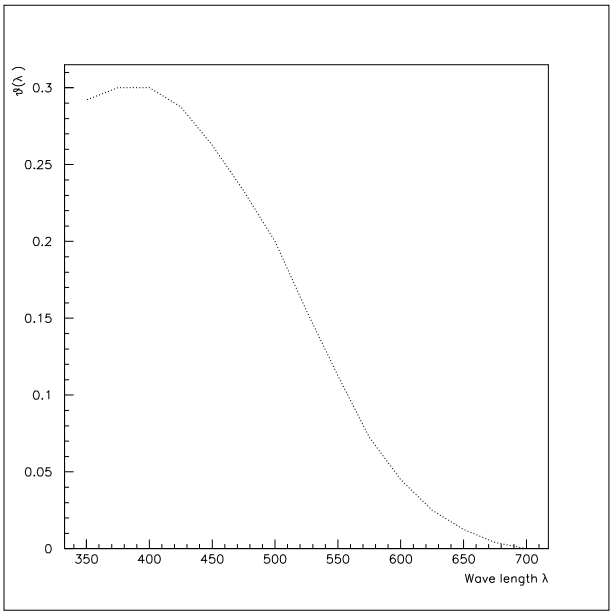

Figure 3.9: Quantum efficiency for Philips PMT.

Calorimeter basically evaluates the energy of the incident particle by the number of Cherenkov photons. Incoming particle produces electrons in the lead glass, then the shower electrons emit Cherenkov photons. The calorimeter PMT reads out the number of the emitted photons. The shower which was produced by incident particle is spread to the neighboring eight blocks. To estimate the incoming particle energy it is summed over all lead glass blocks on which the preshower spreaded. Usually the sum is taken for 9 blocks.

Actually, calorimeter's lead glass block and PMT are tested using 3 GeV beam. In this case, mean value of the PMT ADC value can be seen in Figure 5.16. Thus the relation between PMT read-out ADC value and particle energy is, ADC : Energy = 600 (ADC channels) : 3 (GeV). Therefore the equation to transform ADC channels to energy (E) is ;

$$E = C_0 + x(C_1 + x(C_2 + C_3 x)). \tag{3.3}$$

where $C_0 = 0.19169$, $C_1 = 0.0043086$, $C_2 = -1.02 \cdot 10^{-7}$, $C_3 = 1.02 \cdot 10^{-11}$. The C_1 corresponds to (3 (GeV)/600 (ADC))$^{-1}$. The x is sum of the ADC

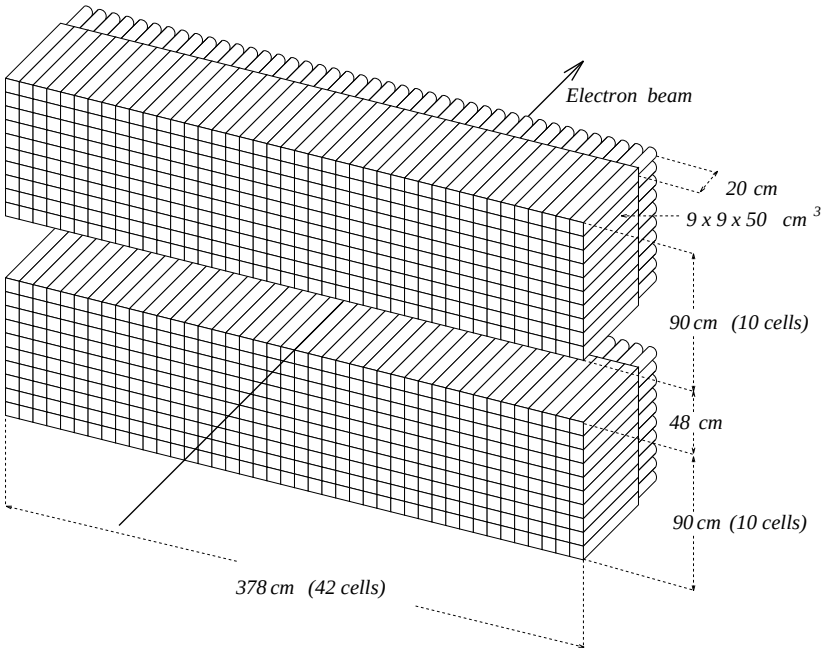

Figure 3.10: Isometric view of the HERMES Calorimeter.

values over the 9 blocks (cells) :

$$x = \sum_{i=1}^{9\text{cells}} (\text{ADC}_i - \text{pedestal}_i). \tag{3.4}$$

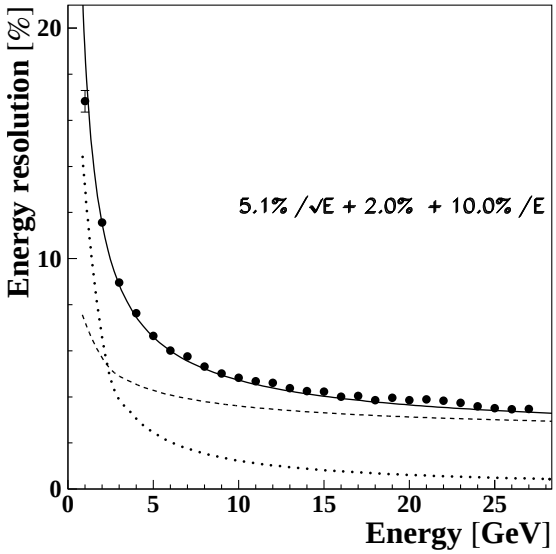

Figure 3.11: Energy resolution of the calorimeter. The circles are real data corrected by Monte Carlo. The solid line is sum of the calibrations from the lead glass (dashed curve) and from the preshower (dotted curve).

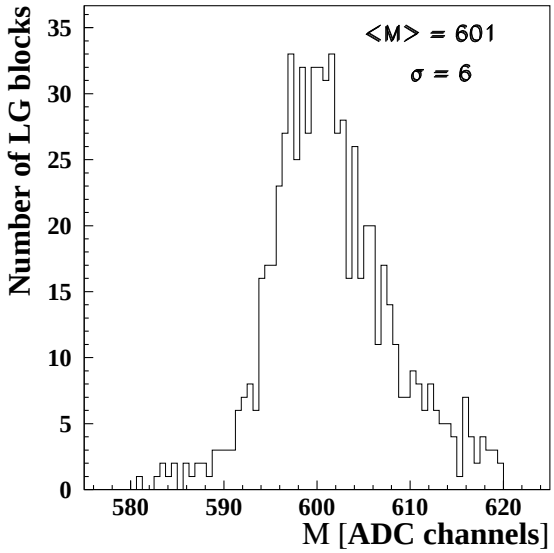

Figure 3.12: Energy and ADC value relation for the calorimeter. Equalization of the 840 lead-glass (LG) blocks in a 3 GeV electron beam. This figure shows the distribution of the value M of the ADC values.

Hodoscopes

There are two hodoscopes H1 and H2, which are plastic scintillators. H2 is behind the 11 mm Pb radiator (two radiation lengths) sandwiched between two 1.3 mm stainless steel sheets and used as a preshower counter in front of the calorimeter.

The first level trigger is obtained by a combination with the calorimeter and H1, where H2 gives a discrimination between leptons and hadrons. Both the hodoscopes consist of 42 vertical scintillator modules each in the upper and lower detector. The size of the modules is $9.3 \times 91 \times 1$ cm^3 and they are read out by PMTs of 5.2 cm diameter.

Transition Radiation Detector

The transition radiation detector (TRD) is used for the discrimination between leptons and hadrons [11]. Only leptons emit transition radiation in the HERMES energy region.

The HERMES TRD is a multiwire proportional chamber constructed by 6 modules above and below the beam. Each module has polyethylene/ polypropylene fibers as radiators and Xe/CH_4 gas (90:10) in the proportional chamber. The fibers used for the radiators are 17-20 μm in diameter and have a material density of 0.059 g/cm^3. The radiators are 6.35 cm thick, and Xe/CH_4 has been chosen because of its efficient X-ray absorption.

The chambers are 2.54 cm thick and the wire diameter was unusually large 75 μm to allow operation at high voltage while limiting the gas gain to about 10^4. The original purpose of the TRD is to obtain the pion rejection factor (PRF) of at least 100 with 90% lepton efficiency at 5 GeV and above, accordingly the energy averaged PRF is about 300 [11] with 90% lepton efficiency. When we analyze the data as the function of momentum, the PRF of 130 is obtained at 5 GeV. The design goal is therefore accomplished.

Ring Imaging Cherenkov Counter

To study the quark spin structure, it is necessary that produced hadrons (pions, kaons, protons) are identified separately. Until 1998, a threshold Cherenkov Counter was used to identify pions which are produced in DIS scattering. This threshold Cherenkov Counter had good performance for pion separation from hadrons. The efficiency of this counter was above 99%. In 1998 a Ring Imaging Cherenkov Counter (RICH) has been installed as a substitute for the threshold Cherenkov Counter. The HERMES RICH is designed to identify pions, kaons and protons in a momentum region of $2 \sim 15$ GeV/c. This RICH has two radiators : aerogel and C_4F_{10} gas. Measuring

two ring images produced by Cherenkov photons on the PMT plane, we can identify and separate each particle. Actual efficiency of the pion identification reaches 98%, kaon identification efficiency reaches 93%[8].

3.4 Beam Polarimeter

There are two beam polarimeters in the HERA ring, a Transverse Polarimeter and a Longitudinal Polarimeter (LPol)[1]. The LPol belongs to HERMES and this polarimeter measures the positron (electron) beam polarization before the second spin rotator. At this point the beam is polarized in the longitudinal direction.

The LPol uses a high-power pulsed Nd:YAG laser with an energy-doubled wavelength of 532 nm. In contrast to the Transverse Polarimeter where the energy of the individual Compton photons is analyzed, the LPol measures the total energy deposited in the detector by $10^3 \sim 10^4$ Compton photons per bunch.

The optical system has been built following the modified optical system of the transverse polarimeter. A laser beam, which is switched between the two helicity states of circular polarization by a Pockels cell, is sent from the HERA East hall by means of a computer controlled mirror system down to the HERA beam pipe. It hits the electron beam about 52 m downstream of the HERMES internal gas target with a crossing angle of 9 mrad. The laser light is guided entirely in a vacuum tube to avoid pointing instabilities from convection due to temperature differences between the tunnel and the laser lab, to insure laser safety by monitoring the pressure in the tube and to keep the surfaces of all optical elements in the transport system clean[12]. The LPol components and its layout can be seen in Figure 3.13.

3.5 Luminosity Monitor

The luminosity monitor is based on the detection of Møller or Bhabha scattering off electrons from the shell of the target atom. Two calorimeter on both sides of the beam pipe measure symmetric scattering with an angular acceptance of 4.5 to 8.2 mrad. The coincidence rates depend on the type of the beam : For a nominal beam current of 56 mA and a nominal H target density of 1×10^{14} atoms/cm^2 in the case of the electron beam (Møller

[1]The location of those are Figure 3.2

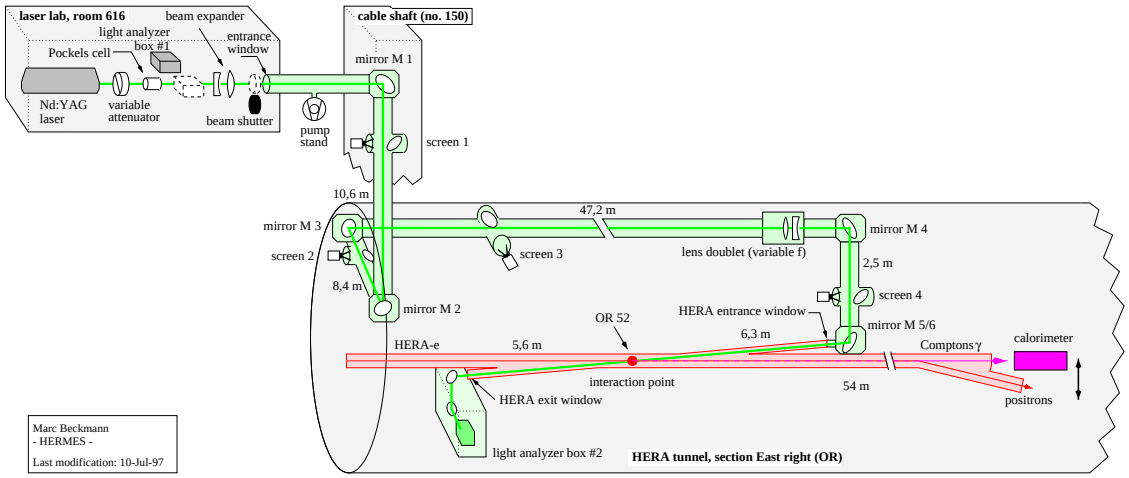

Figure 3.13: Schematic view of positron(electron) beam polarimeter.The most right of the figure is calorimeter.In case of LPol, the calorimeter is used crystal calorimeter.

scattering) the coincidence rate is 116 Hz and in case of the positron beam (Bhabha scattering and pair production) the coincidence rate is 86 Hz. The energy of scattered electrons and positrons are in range of 10 to 20 GeV when they are in the acceptance of the detector. Each calorimeter consists of 12 $NaBi(WO_4)_2$ crystals which have a size of $22 \times 22 \times 200 mm^3$. They are Cherenkov radiators, are insensitive to low energy background and have a good time resolution. To reduce radiation damage, the counter can be horizontally moved away from the positron (electron) beam pipe during injection time of the beam.

The luminosity monitor is also of interest for detecting electron scattering at low angles. The idea behind this is to detect the scattered electron from resonance production processes and from J/ψ decay.

Chapter 4

Gain Monitoring System(GMS)

The Gain Monitoring System (GMS) was installed in the HERMES experiment to monitor various HERMES detectors which have photo-multiplier (PMT). The gain stability of the PMTs of the calorimeter, luminosity monitor, preshower counter (hodoscope 2), longitudinal polarimeter, and hodoscope (H0) are checked continuously with this system.

The GMS provides light pulses of various intensities to the PMTs via optical fibers, as well as to an array of reference detectors of GMS. The fiber wiring (fiber network) can be seen in Figure 4.3.

The responses of the detectors to these pulses are measured in the same way as for signal from the real deep inelastic scattering event during the experiment. Then, the responses of the detectors are evaluated as gain (which is defined in following section) in comparison with the response of the reference detector.

4.1 GMS Hardware Component

The GMS hardware components are as follows ;

1. Light source
2. Light filtering system
3. Light distributing system
4. Reference detector
5. Electronics modules

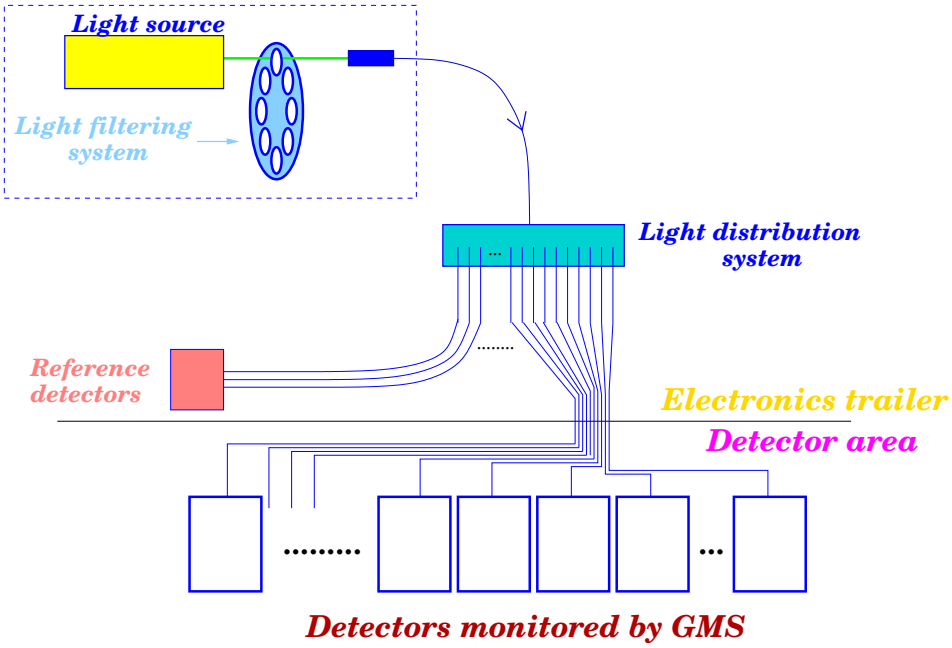

Figure 4.1: Overview of the GMS components.

The overview of the GMS components can be seen in Figure 4.1. The GMS sends the light pulses to the detectors via optical fibers. This process has two steps. The first step is the generation of the light pulse with the light source. The generated light is attenuated with the light filtering system. In the second step, the pulses are split and send to the detectors and the reference detector with light distribution system.

The experimental area of HERMES is divided into the detector area and electronics area (Electronics Trailer = E.T). The detectors are placed at the detector area while many electronic modules are on E.T. The GMS electronics devices, light source, light filtering system and reference detectors are also located on E.T.

Each component will be described in detail in the following sections.

4.1.1 Light Source

A Nitrogen (N_2) Laser is used as the light source. The Laser produces pulse of light at the wave length of 337 nm when triggered. Produced light passes through an organic dye which transforms the light to the wave length

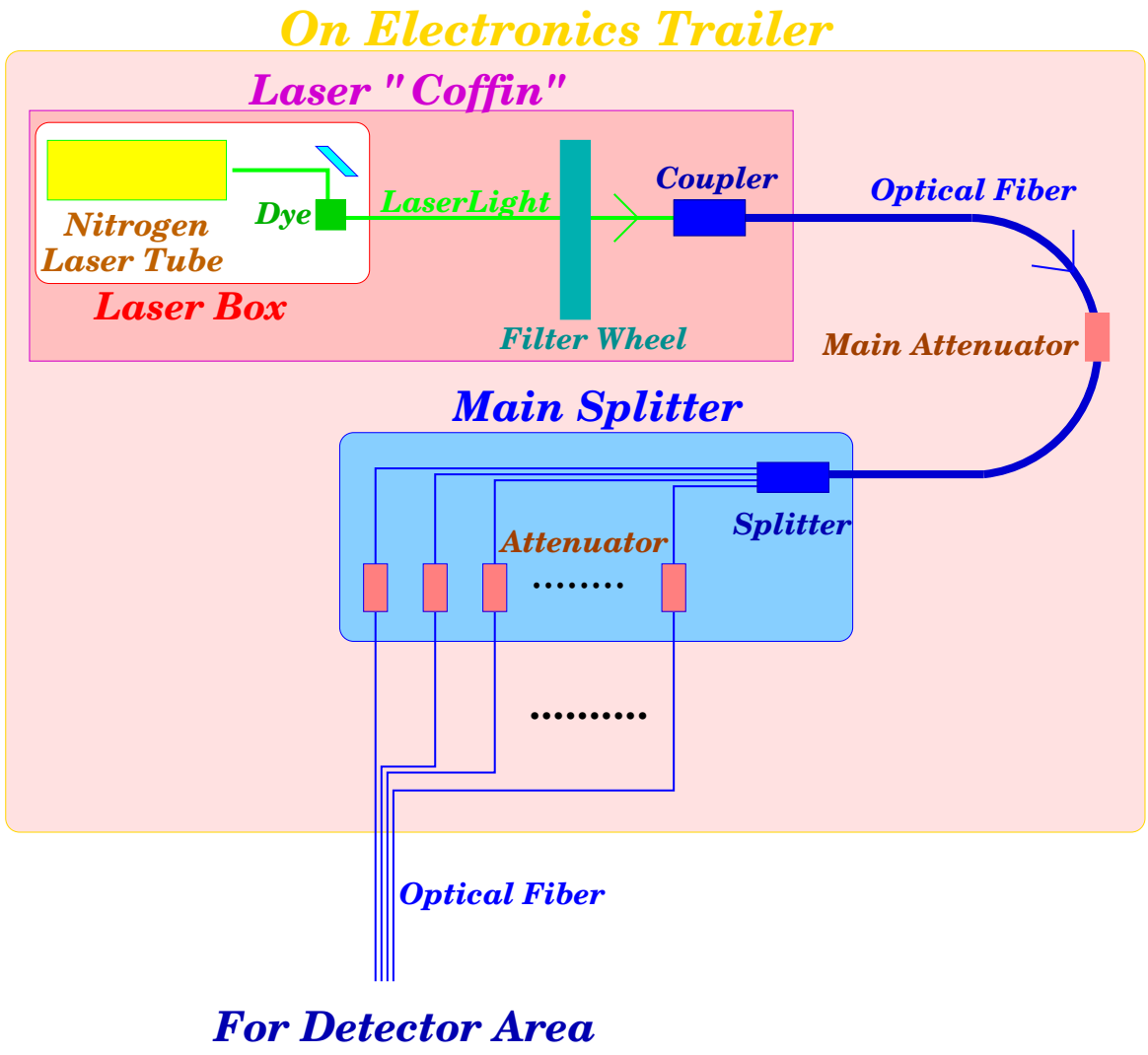

Figure 4.2: The general configuration of the GMS on the Electronics Trailer. The system consists of a N_2 Laser, Dye, Filter Wheel, Attenuator and Splitter.

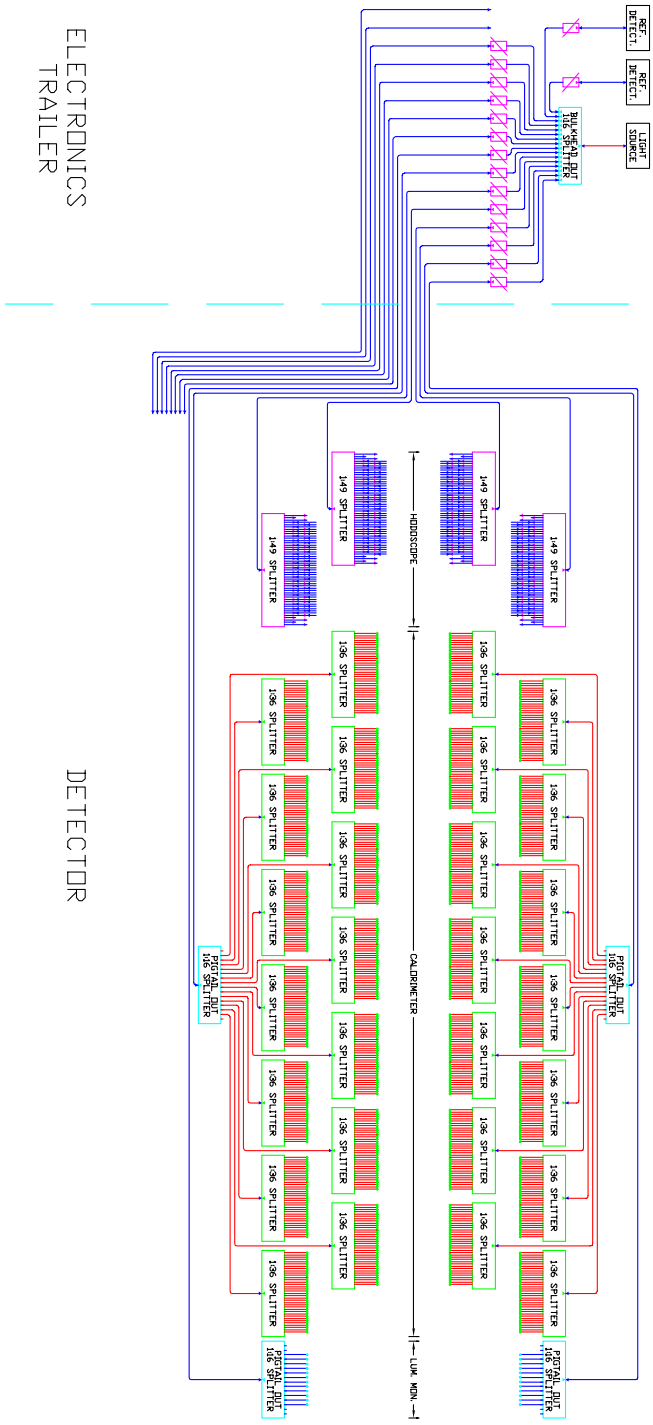

Figure 4.3: Schematic view of the fiber network from the Electronics Trailer to the monitored detectors. This figure shows calorimeter as an example.

of 500 nm. The light is attenuated by the various filters.

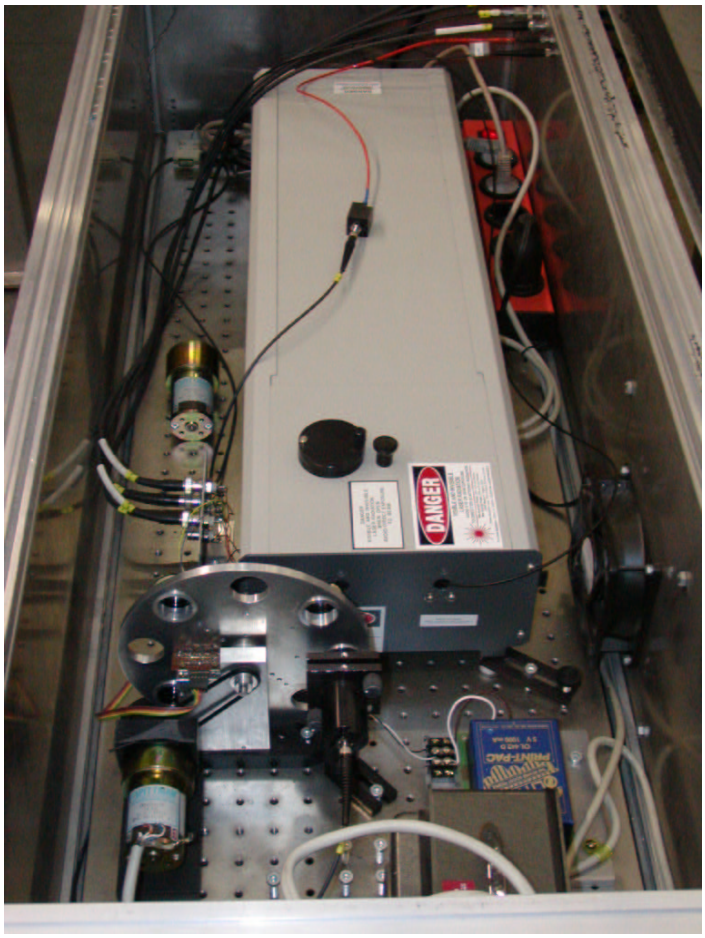

Figure 4.4: The layout inside of Laser "coffin". The white box in the center of this picture is the Laser module (Laser box). The motorized filter wheel is placed in the lower left with the DC-motor.

N_2 Laser

The N_2 Laser (model:LN300C) is a sealed Nitrogen gas type Laser. The Laser was produced by LASER PHOTONICS, Inc (U.S.A). The sealed nitrogen gas Laser tube is loaded in Laser box (Figure 4.5).

Specifications of the Laser are listed in Table 4.1. The values in the table are specification of the direct output before passing through the dye.

Product Name	LN300C
Spectral Output (nm)	337.1
Pulse width (ns)	5
Energy/Pulse (μJ)	250
Beam Dimension(hor. $\times$ ver.)(mm)	9 $\times$ 4
Beam Divergence(hor. $\times$ ver.)(mrad)	1.6 $\times$ 0.7

Table 4.1: N_2 Laser specification. Those are values without dye.

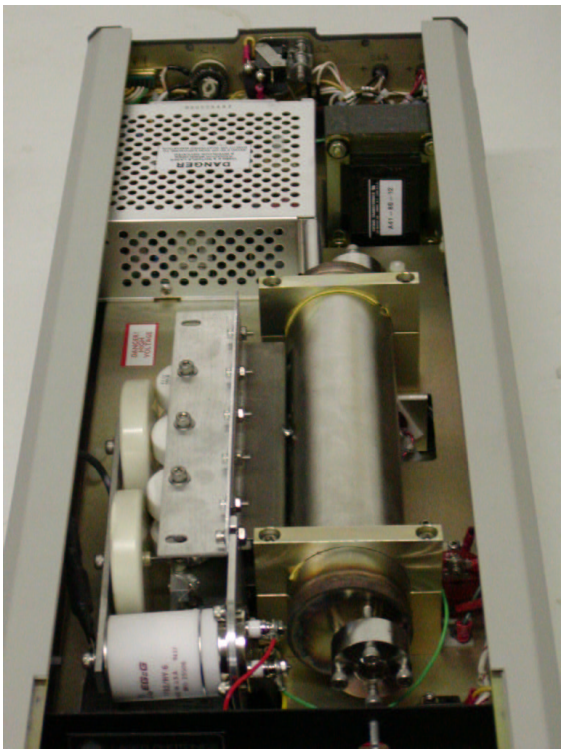

Figure 4.5: The N_2 Laser. Laser Tube is placed at the center of this figure. This is inside view of the Laser box (See Figure 4.4).

Dye

The N_2 excitation state is unique, therefore the wave length is also unique to 337.1 nm. To shift the wave length, a dye, Coumarin 500 (EXCITON LNC. type : 7A500), is used, which converts to 500 nm as shown in Table 4.2.

		Coumarin 500(7A500)
Wave Length (nm)	Peak	500
	Range	$473 \sim 547$
Output Energy (μJ)		≤ 100
Solvent		ethanol

Table 4.2: Specification of the dye (Coumarin 500). The output energy depends on the wave length. The maximum energy is realized at around 500 nm.

The 500 nm Laser light matches well the specifications of the lead glass and the PMT[1] which are used in the calorimeter.

The dye is in a small container which is called "dye cuvette" on the dye module inside of the Laser box. The photo of the cuvette is Figure 4.6.

4.1.2 Light Filtering System

It is important to monitor the response of the detectors to the light of different intensities. This permits to determine pedestals, gains, and possibly non-linear response.

A filtering system is used in order to alter the intensity of the light. Light pulses with 6 different intensities can be prepared with this system. The light filtering system consists of a "filter wheel" and a small DC permanent magnet motor. The "filter wheel" is placed directly in front of the laser light source, and optical filters of natural density are located on the periphery of the wheel. A general view can be seen in Figure 4.7 and 4.8. The wheel rotates continuously at 1 to 10 Hz, powered by the motor.

Until today, the only major breakdown has been associated with brush wear in the motors and breakage of the rubber o-ring-style belt which couples the motor to the filter wheel.

[1]See Figure 3.8, 3.9

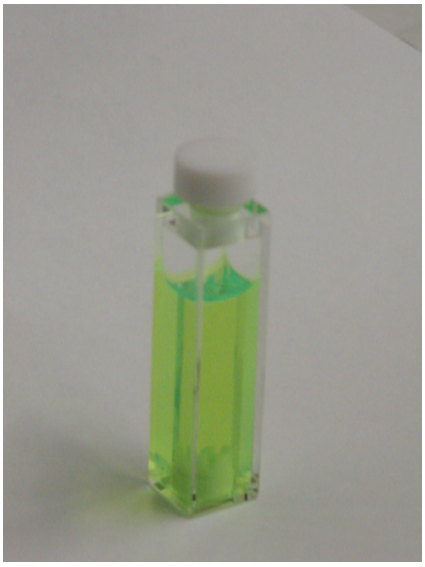

Figure 4.6: The dye is stored in this cuvette on the dye module inside the Laser box. The cuvette volume is 1.2cm×1.2cm×5cm

Filter Wheel

Eight filters positions are available on the wheel, but currently only 5 positions are loaded with filters. The remaining 3 positions are empty and the Laser beam of full intensity pass to the light distribution system.

An additional series of small holes (see Figure 4.7) on the wheel, those are used to identify the filter, currently in position, and the outermost small holes are used for the Laser trigger, which are named "phase ramp" and "trigger lamp".

Phase Ramp

These small holes on the wheel (except outermost small holes) are detected by infrared LED/photo-transistor pairs. The photo transistors are used to read a set of holes, which encode the number of the filter which is currently in position. The position bit and its filter attenuation are listed in Table 4.3. The information of the filter position is included in DAQ data stream. This system is called "phase ramp".

The outermost small holes (see Figure 4.7) are used for the Laser trigger. These are also detected with LED/photo-transistor pairs. This pair produces the signal which triggers the Laser power supply (see Section 4.2.1). This is

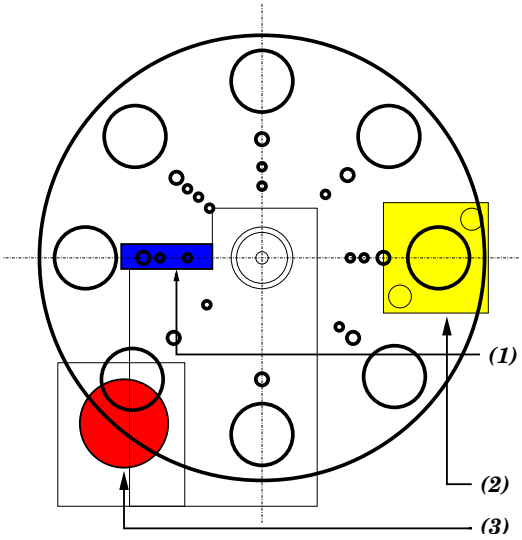

Figure 4.7: Aligned along the filter wheel radii as the filters. (1) is called phase ramp. Some series of small holes are used for laser trigger, and to identify the filter position. (2) is optic coupler for main fiber. (3) is the DC motor.

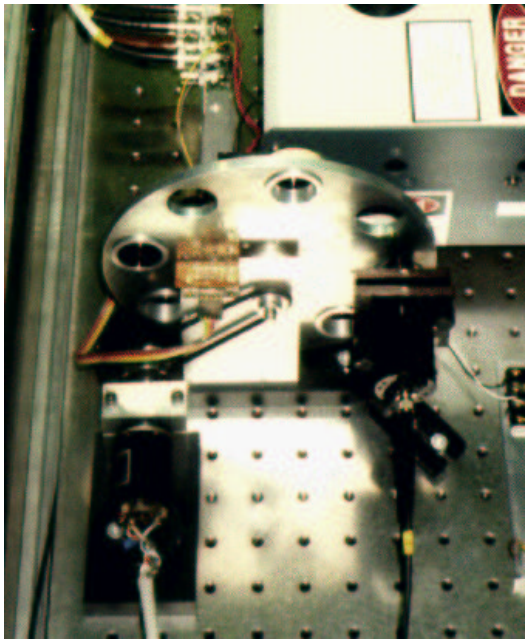

Figure 4.8: Photograph of light filtering system. The holes which are placed on the periphery are for filters.

named "trigger lamp".

4.1.3 Light Distribution System

There are two steps to distribute the Laser light to the monitored detectors. First, the light which directly comes from the light source is divided to 16 with the main splitter. The lights go to the detector area via optical fibers. Then, the lights are split again with sub-splitters at each detector location as shown in Figure 4.3.

Main Splitter

Figure 4.9 shows a photograph of the main splitter. The light from Laser is guided to the leftmost channel of the main splitter, and the other channels are output for the monitored detectors and reference detectors. The detectors connected to each output channels are listed in Table 4.4.

Filter Number	Attenuation (%)	Position Bit
0	50.10	0 0 1
1	20.00	1 0 1
2	No Attenuation	0 1 1
3	No Attenuation	1 1 1
4	39.80	0 0 0
5	No Attenuation	1 0 0
6	31.62	0 1 0
7	10.00	1 1 0

Table 4.3: Position bit and attenuation of optical filters on the filter wheel. The position bit is used as a filter identifier in data flow.

Channel	**Detector Name**
1	Hodoscope 2 (bottom)
2	Now not in use
3	Calorimeter (top)
4	Luminosity Monitor (right)
5	Luminosity Monitor (left)
6	TF block
7	PIN2
8	PIN3

Channel	**Detector Name**
9	PIN4
10	Calorimeter (bottom)
11	Longitudinal Polarimeter
12	Hodoscope H0
13	Longitudinal Polarimeter
14	PIN1
15	NaI
16	Hodoscope 2 (top)

Table 4.4: Main splitter channel usage.

Figure 4.9: The main splitter. This splitter is located at the uppermost of GMS module crate. The splitter divides the main optical fiber to 16 outputs for GMS detectors and reference detectors. See Chapter 4.3 for the GMS detectors, and Section 4.1.4 for the reference detectors.

Light Attenuation

The attenuator in the coffin adjusts the overall light intensity. The other attenuators attached to the output channels inside the main splitter control the light of the corresponding detector systems. In the detector area additional attenuators are installed for each PMT if needed. The attenuation level is tuned to cover the full dynamic range of each PMT with the light pulses of 6 different intensities. Figure 4.10 shows a photograph of the attenuator.

Splitter for Detector Pieces

Figure 4.11 shows a photograph of one of the sub-splitter which has one input and 49 output fibers. The similar type of splitter is installed in the detector area. Actually 14 splitters (in case of calorimeter, 1×36 splitter) are installed for each top and bottom calorimeter half.

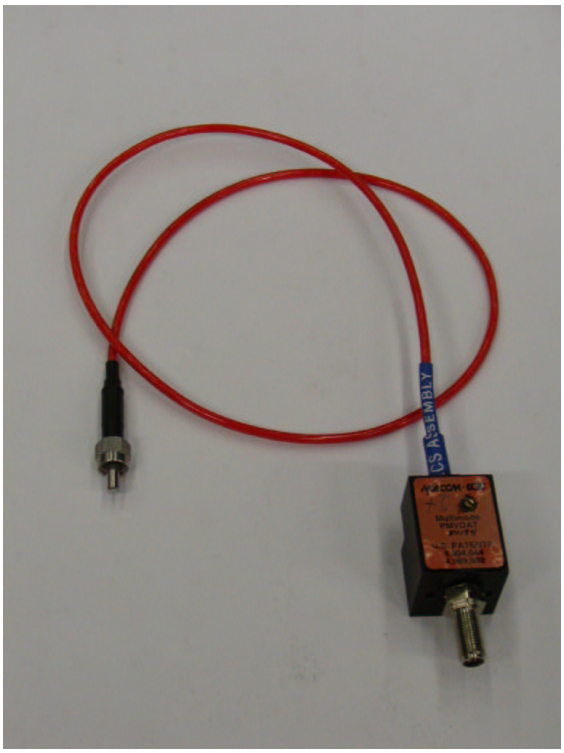

Figure 4.10: The light intensity can be adjusted with this attenuator. The adjustment is done by turning a screw. Turn clockwise : increase intensity, counterclockwise : decrease intensity.

4.1.4 Reference Detector

The GMS has two types of reference detectors, as follows :

1. PIN
2. TF Block

Those two reference detectors have different tasks. The PIN is used to evaluate the detector gain. TF blocks are installed to estimate the radiation damage due to synchrotron radiation of the HERA two beam lines.

PIN

There are 4 “PIN” reference detectors. Each PIN is equipped with a silicon PIN photo-diode. The specification of the photo-diode is shown in Table

Figure 4.11: The sub-splitter. It is used in the detector area to split the light for each detector (directly PMT in some cases). This is 1×49 splitter, the same type as is installed for the calorimeter.

4.5. Those are named simply “PIN1”, “PIN2”, “PIN3”, “PIN4”. All of them are installed in one of NIM modules which are in the GMS electronics module crate in E.T. The lights of 6 different intensities come to these PINs as well as to the monitored detectors. The input Laser intensity is tuned to be different among the PINs, by the attenuator of the main splitter, as shown Figure 4.12 and 4.13. Seven peaks can be seen in each figure. The leftmost peak is a pedestal. Other 6 peaks indicate the detector response to the different intensity light generated with the light filtering system.

The PIN3 is dedicated to the Longitudinal polarimeter. The PIN1, 2, 4 are used to evaluate the gain of the monitored detectors.

The fiber length from main splitter to the detector area is about 50 m. Thus every monitored detector has a 50 m fiber. The fiber which is connected to every PIN has a length of about 100 m. The reason why the fiber length of 100 m is needed for PINs is to synchronize the PIN response with detector response. The GMS needs to take the data (ADC value) of the monitored

Type	Operating Temperature (°C)	Photosensitive Surface			
		Size (mm)	Effective area (mm^2)	Range (nm)	Peak Wave Length (nm)
S119	-40∼+100	1.1×1.1	1.2	320-1100	960

Table 4.5: Specification of the photo-diode for the reference detector PIN.

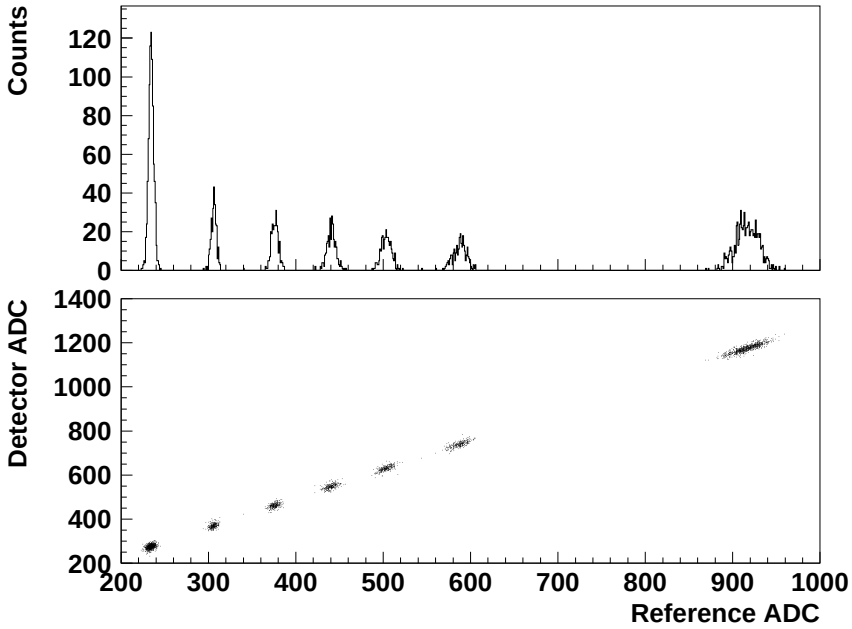

Figure 4.12: Upper figure is a ADC histogram of the PIN1 detector. Lower figure shows a typical correlation between a monitored detector and PIN1.

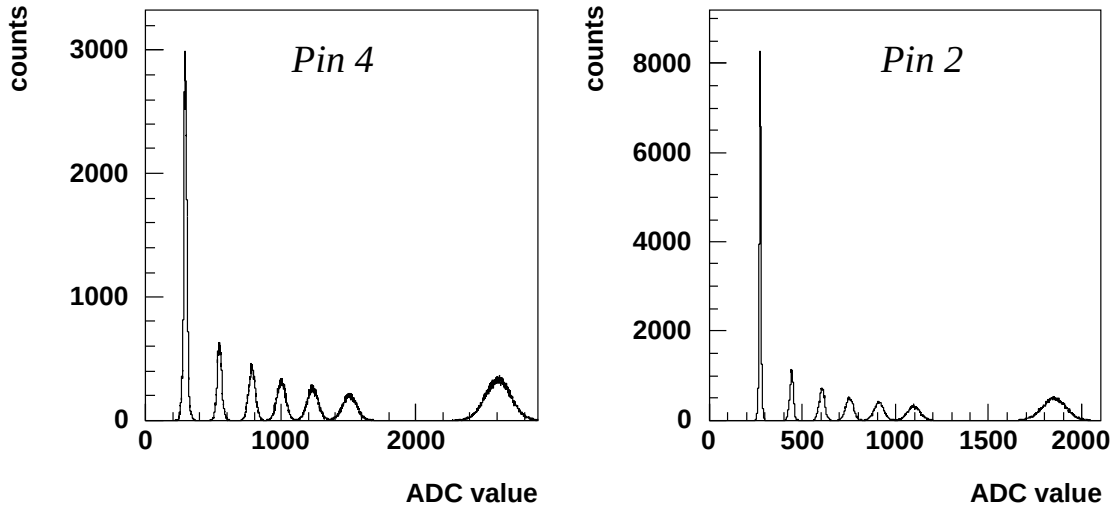

Figure 4.13: ADC histograms for PIN2, 4

detectors and reference detectors in the same GMS event. Namely, the long fiber for the PIN is used for a delay. The details are described in Section 4.2.2.

TF Block

There are four "TF block" reference detectors installed behind the calorimeter, each of them consists a lead glass block with a PMT. The aim is to monitor radiation damage of lead glass due to synchrotron radiation of the HERA storage ring. The possible cause of the radiation is showers produced by beam losses[13] in the HERA proton storage ring. Figure 4.14 shows the location of each TF block for the HERA positron and proton beam pipes.

The TFs are equipped with the same PMTs which was installed in the calorimeter. Each lead glass block is coupled to a 7.62 cm photo-multiplier (Philips XP3461) with a silicon glue (SILGARD 184) with refraction index of 1.41. The TF's lead glass is different from calorimeter's. The TF's lead glass is about 20 times more sensitive to the radiation damage than the lead glass (F101[14]) used in the calorimeter. Therefore, the gain reduction would be seen sooner in these reference detectors.

The lead glass of each TF is listed in Table 4.6.

TF Block	Colour of Lead Glass	Location
TF1	Yellow glass	(1)
TF2	Yellow glass	(3)
TF3	White glass	(4)
TF4	White glass	(2)

Table 4.6: List of lead glass for TF block

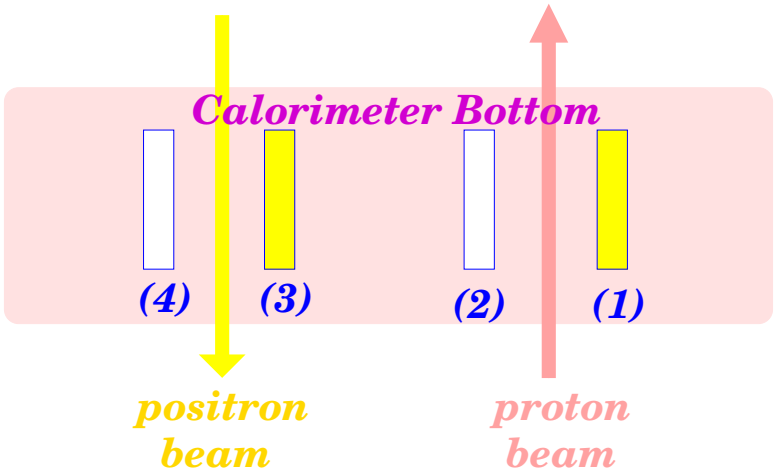

Figure 4.14: TF block location at HERA storage ring. The labeled numbers correspond to "Location" in Table 4.6.

4.2 Trigger

4.2.1 Laser Trigger

The GMS provides the light to the monitored detectors during data taking. But the GMS event has to be separated from the experiment event. For that purpose the Laser trigger is synchronized with "HERA-clock". The HERA-clock is a clock signal with fixed time interval, 96 ns. HERA electron/positron beam is also synchronized with the clock.

There are 220 bunches in the electron/positron beam in the HERA storage ring. Some of them are empty bunches. The number of bunches which are actually filled with the positron is 189. One of the empty bunches is called "Bunch#1". The Bunch#1 appears once in every 21.12 ms (220 bunches $\times$ 96 ns). The GMS sends the light pulse when Bunch#1 is in position.

The Laser is triggered in coincidence with the Bunch#1 signal and trigger lamp signal, which has 100 μs duration with about 3 Hz frequency. The GMS trigger (event) rate depends on the DC motor speed. Figure 4.15 shows the DC motor voltage dependence of the GMS event rate. The detail of the Laser trigger is given in Appendix A.3.

4.2.2 GMS Trigger

Generally in the HERMES experiment, all data from the detectors are buffered in memory, and the data are taken by DAQ when triggered. The data are saved on disk and tape with a tag of trigger types. For example, if some hodoscopes and the calorimeter fire at the same time, a physics trigger condition is satisfied. So, the data is taken and saved with a physics trigger tag.

In the case of the GMS event, the data are taken by the GMS trigger. The GMS trigger is one of the HERMES standard triggers. The GMS trigger is generated by a small PMT which receives the unfiltered light directly from the dye cuvette via an optical fiber of 50 m length. The GMS event is identified with this trigger. The length of the fibers connected to the detector is about 50 m. To adjust roughly the signal timing with the detectors, the 50 m length fiber is also used for the PMT. Additionally, the signal cable delay was installed for the GMS trigger signal to compensate the distance between the detector area and E.T.

On the other hand, the reference detectors have the fiber length of 100 m in order to match the timing of the GMS trigger. In other words, the

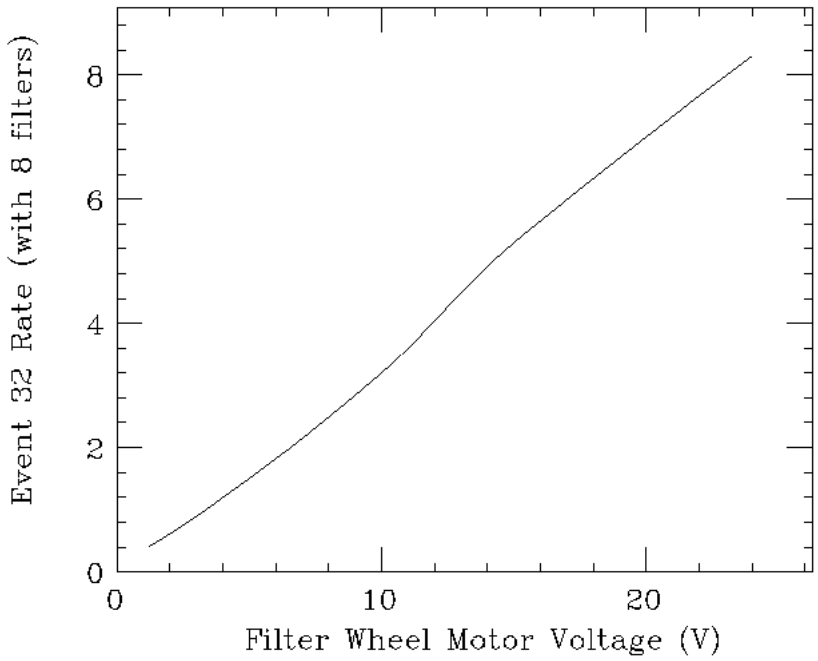

Figure 4.15: The dependence of GMS event rate on motor voltage for the DC motors.

reference detector uses a long optical fiber instead of signal delay cable.

4.3 Detectors monitored by the GMS

The monitored detectors are listed in Table 4.7. Each detectors uses two of the output channels of the main splitter. For example, the calorimeter uses two output for the top and bottom halves. Each outputs is divided to 420 by the splitters for each calorimeter cell. Other detectors are arranged basically in the same way.

4.4 Gain Monitoring

The GMS can provide the relative gain. Roughly speaking, the relative gain is defined as ADC value of a detector divided by PIN's ADC value for

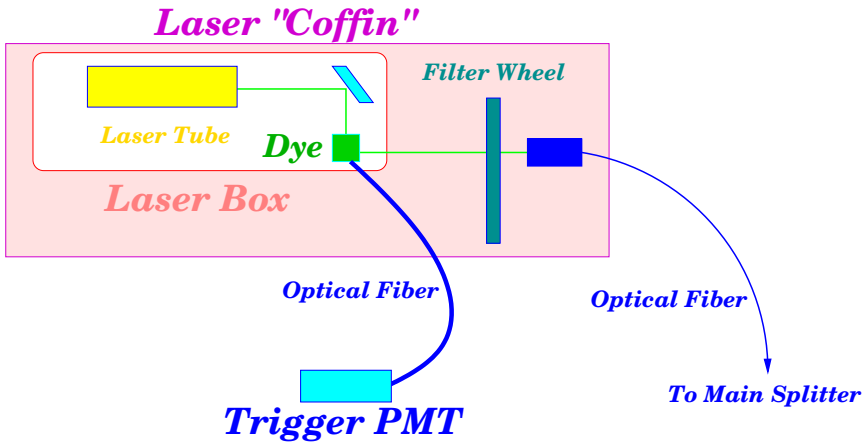

Figure 4.16: The trigger PMT receives the unfiltered light directly from the dye cuvette via optical fiber.

GMS event. The exact definition is given in Section 5.2.

There are two types of the detector gain monitoring. One is online monitoring, which tells the detector condition almost in real time. Another is offline monitoring which is done for each run. In addition to these gain monitoring, the GMS has a system to check the GMS hardware conditions, which is called private decoding system.

The relation between the GMS monitoring software, the HERMES general software, and data handling for GMS can be seen in Figure 4.17. The detail of the data handling for the online and offline monitoring are explained in following section.

4.4.1 Online Monitoring

One of the GMS task is to check the detector responses in real time. For that purpose, the full data flow is not needed. Actually, GMS uses 2∼5% data of the DAQ data stream for online monitoring, and evaluates the detector gain about once per 10 sec. Therefore, the online gain monitoring has proven to be very useful for monitoring the detector "trip" and the high voltage supply status.

The GMS has the online monitoring display which is called "GMS Pink window". The Pink window, Figure 4.18, is actually used in the HERMES experiment control room.

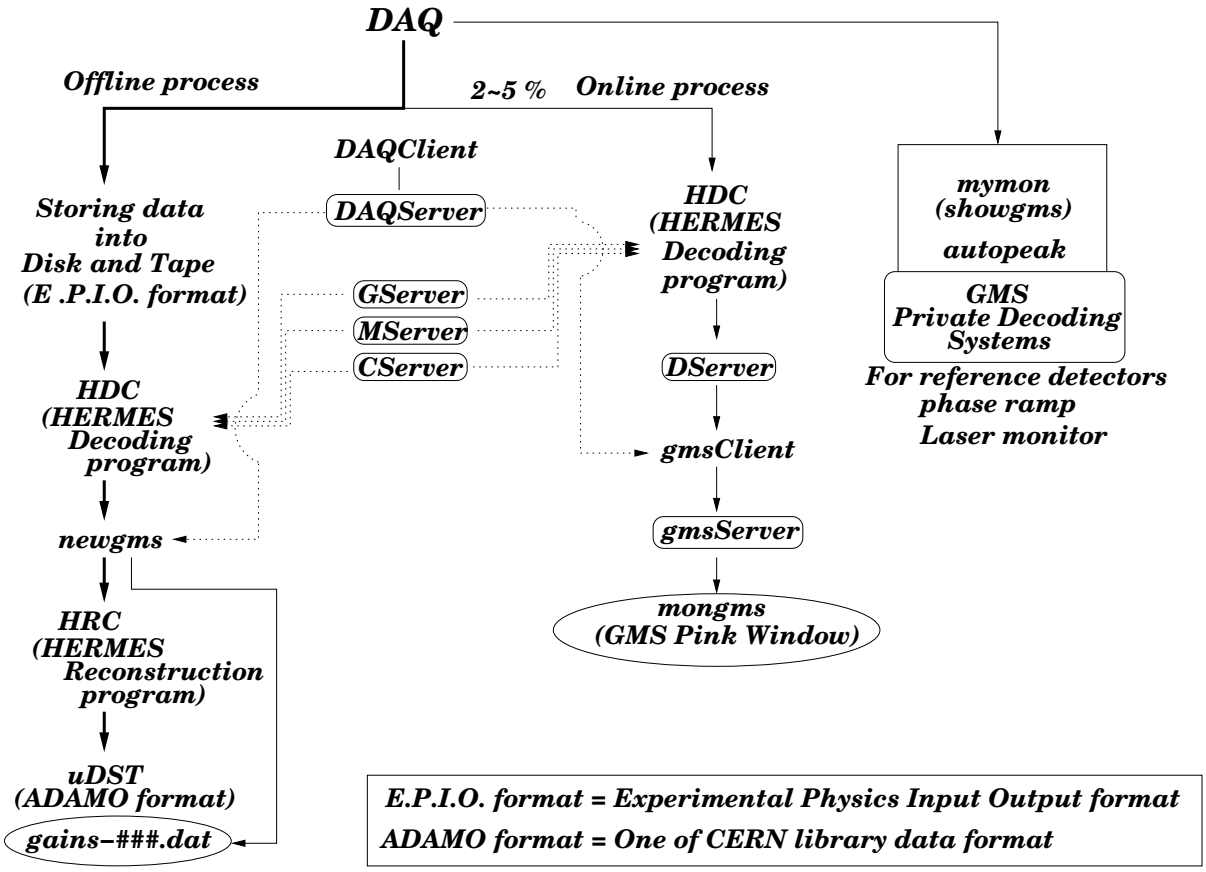

Figure 4.17: Flow of data handling. The GMS data are taken by DAQ. For GMS, data handling has three types. One is used for online monitoring. The second is for offline analysis. The third is private decoding system. The private decoding software decodes without using HDC.

Detector Name		Number of Channels
Calorimeter	Top	420
	Bottom	420
TF block	TF1, 2, 3, 4	4
Luminosity Monitor	Left	12
	Right	12
Longitudinal Polarimeter	Crystal Calorimeter	4
	Scintillation Fiber Counter	32
	Sampling Calorimeter	1
Preshower Counter	Top	42
(Hodoscope 2)	Bottom	42
H0	Top	2
(Hodoscope 0)	Bottom	2

Table 4.7: The detectors monitored by the GMS.

The online data of the monitored detector are taken by DAQ. The HERMES decoding program (HDC) decodes the data, and the decoded data are stored in data sever (DServer) temporarily. Then GMS client (gmsClient) software evaluates the detector gain using the data of the detector and reference detector. The evaluated gain is stored in the GMS server (gmsSever). The gains are picked out and visualized on the GMS Pink window. The flow of the GMS data is summarized in Figure 4.17. Those servers perform as follows :

1. **DAQ**
   Buffered data are taken from Fast Bus by DAQ. Then a part of data is put into HDC for online monitoring.

2. **HDC** (HERMES decoding program)
   The HDC is HERMES raw data (E.P.I.O format) decoding program. This program converts the raw data to ADAMO format data files or pipe. Generally, all online and offline software access the ADAMO file (pipe) and work for each task.

   The HDC decodes the data which come from DAQ. This is necessary to define the relationship between detector name and ADC channel using a mapping server (MServer).

3. **DServer**
   The decoded data which come from HDC are saved and updated when the HDC updates the data.

4. **gmsClient**
   The gmsClient picks up the data of the monitored detectors and the reference detectors from DServer. The gain evaluation is done using the reference detector PIN1's ADC value. This client is related to the DAQ server.

5. **gmsServer**
   The gmsServer stores the evaluated gain which is named "fast gain".

6. **Pink window**
   The gains are normalized using "nominal value" which is defined in an external file, and displays the normalized gain.

The processes "4∼6" are managed by the GMS specific software. Table 4.8 shows several functions of the HERMES servers on which the GMS depends.

Server Name	Program Name	Action
Geometry Server	GServer	Define the relationship between detector location in D.A. and its detector name
Mapping Server	MServer	Define the relation between ADC channels and detector pieces
Calibration Server	CServer	Transform the ADC values to physical values
Data Server	DServer	Store the decoded data
DAQ Server	daqServer	Provide event informations (For example, event trigger etc)

Table 4.8: This table is HERMES general servers which GMS client and sever depends on. See Figure 4.17 for details on the dependence.

Pink Window

What the GMS Pink window shows is the normalized relative gains with color. The colour changes if the detector response changes. The "relative gain" means that the sum of detector ADC value divided by the sum of PIN ADC value. This calculation is done by "gmsClient". To normalize the

detector gain, the "nominal value" is used. The nominal values is a gain which is evaluated before starting the experiment. Thus, by comparing the initial response of a detector to these calibrated light pulses with the response of the detector later in the experiment the response of the detector can be monitored. So, that is 1.0 if relative gain is the same as the initial gain of the detector. In short, the normalized relative gain is displayed with "light green" in the Pink window if in the normal condition.

Usually the Pink window is updated about once a minute. So, the Pink window is a very useful tool to check the current status of the monitored detectors.

Private Decoding Systems

The GMS has two private decoding codes. Those are named as follows :

1. mymon
2. autopeak

Those private decoding softwares are used to extract and decode the data directly from the DAQ data stream without using HDC. Then the extracted data are stored in memory space as histogram.

This system is used only for the GMS reference detector, phase ramp and Laser monitor which is described in the next section, and used for daily checks of the GMS equipment. So, if some parts of the GMS need maintenance, this private decoding system can be used.

4.4.2 Offline Analysis

In the HERMES experiment, the data are saved on disks and tapes. The saved data format is E.P.I.O. format (Experimental Physics Input Output format). Generally, to make the data files for physics analysis, the E.P.I.O. raw data are decoded by HDC, and then reconstructed event by event with HRC (HERMES Reconstruction program). The physics analysis data files which are called μDSTs (DST = Data Summary Tape, ADAMO format) which are made from the outputs of HRC.

The GMS event data are not included in μDSTs, but the gain which is calculated in the offline and online processes are used as one of data quality parameters. The gain that is calculated in the offline process is used as a correction factor of monitored detectors to transform the detector ADC

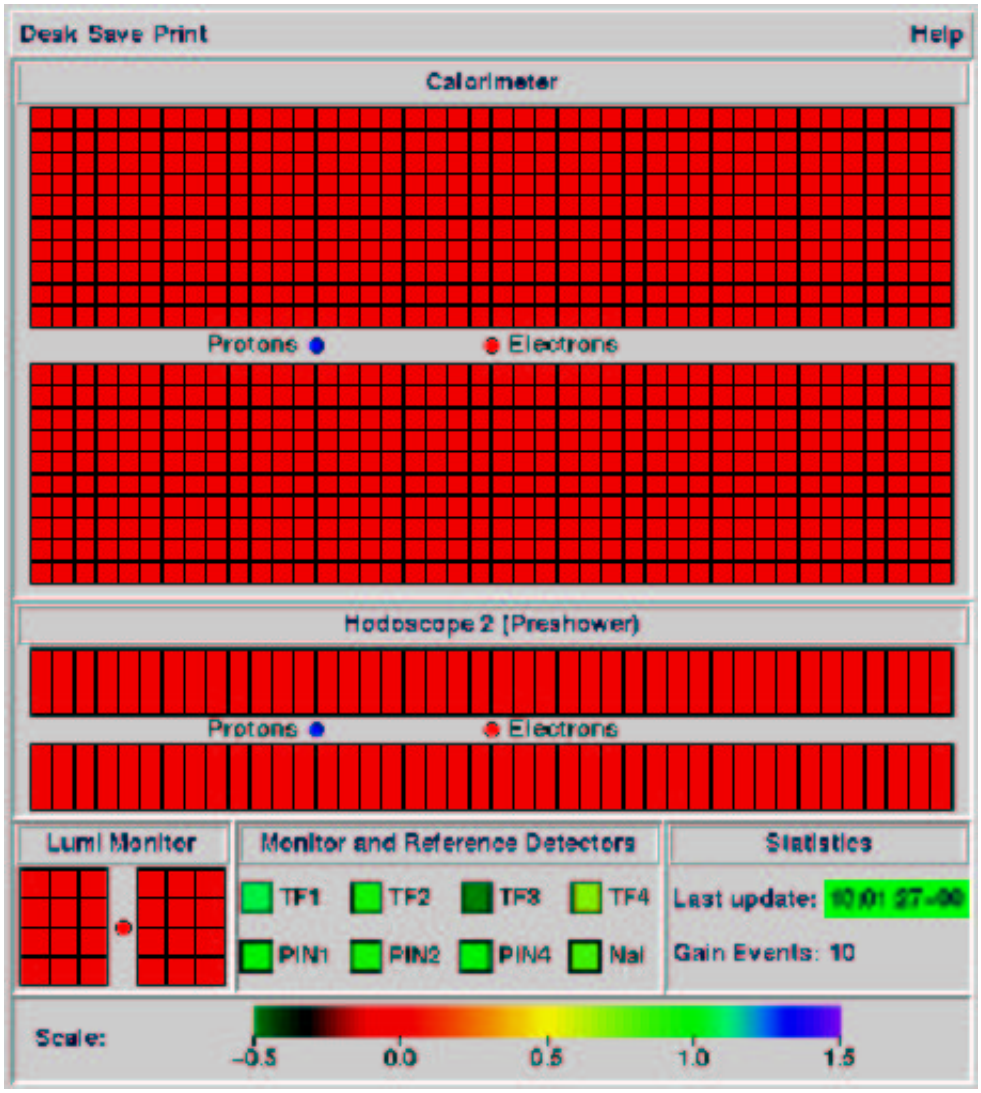

Figure 4.18: GMS Pink window. This window is actually used in HERMES experiment control room.

values to physical values. The farther details of the offline analysis will be given in Chapter 5.

4.5 Laser Monitoring System

Laser monitoring system has been added to the GMS components newly. Earlier, the GMS did not have a system to monitor the Laser output itself.

The GMS calculates the gain using the ratio of the detector ADC value and reference detector "PIN" ADC value. The reason to use the ratio of those is to cancel the apparent fluctuation of detector response which is caused by the Laser output fluctuations. Thus it is important to estimate the reference detector performance. The Laser monitoring system can be used for the estimation of the performance. The reference detector performance is discussed in Section 5.1.

The structure of the Laser monitoring system is shown in Figure 4.19. To detect the Laser intensity, this system uses the same PMT as used for the GMS trigger. The PMT signal is divided for the DAQ trigger (digital signal) and the Laser monitoring system. For the Laser monitoring, the Laser light comes directly from the dye cuvette is used, the light is unfiltyered.

The signal of the Laser monitor is sent to an ADC, and put into the DAQ data stream as well as the reference detectors. The data can be used for the online as well as for the offline monitoring. The GMS Laser output condition can be checked using GMS Pink window, private decoding system and offline analysis in the same way as PINs. Figure 4.20 is a histogram of actual Laser monitor ADC value.

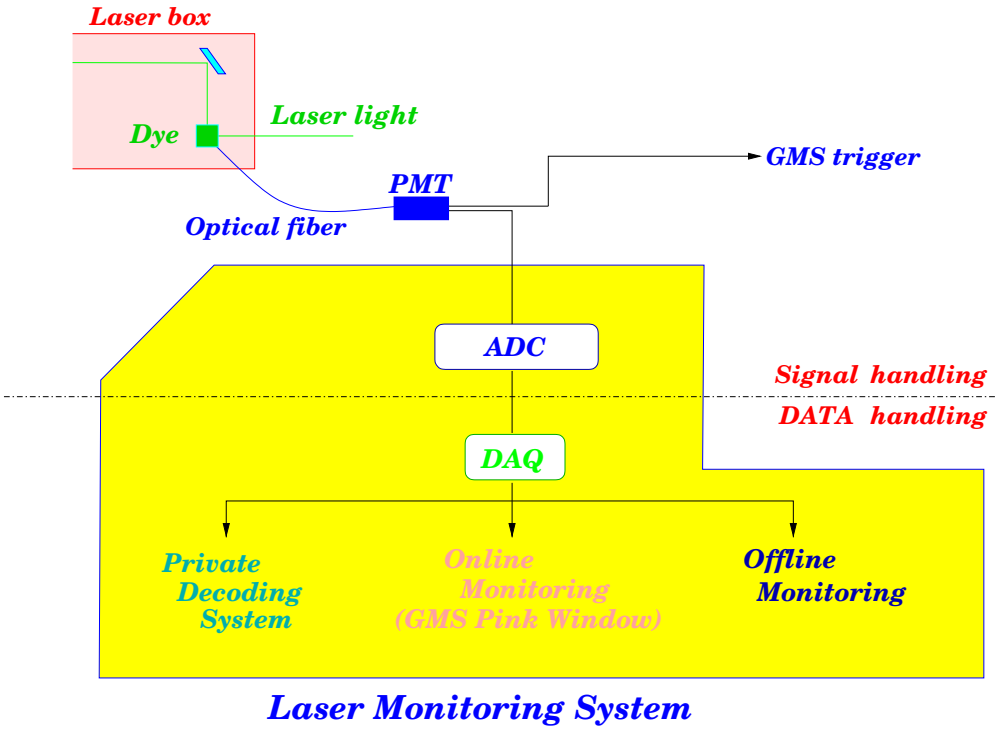

Figure 4.19: Schematic view of the system structure.

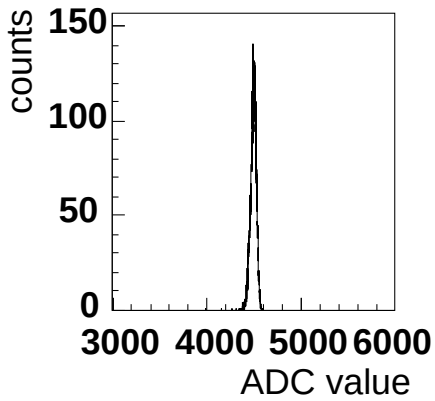

Figure 4.20: Histogram of Laser monitor ADC value. This is plotted using private decoding system.

Chapter 5

GMS Analysis

There are two types of the detector gain monitoring. One is the online monitoring which is done once a minute and visualized on the GMS Pink window[1]. The monitored detector conditions can be found in real time. The other one is run level offline monitoring. One run takes about 4∼10 minutes. This monitoring is done run by run. Thus the offline monitoring is useful to evaluate the PMT gain changes in a longer term.

The GMS provides 6 different light intensities for the monitored detectors. GMS has, in addition, reference detectors to which light with 6 different intensities are sent[2].

To evaluate the detector (PMT) gain, the GMS defines a relative gain. The reason why GMS defines the relative gain is to subtract any gain changes which is caused by the Laser output fluctuation. For this purpose, the following points are required for the reference detectors :

- The reference detector is sensitive to the Laser output changes
- The gain of the reference detector itself is stable.

These points are discussed in the following section. After that the detector gain monitoring will be discussed.

5.1 GMS Stability

Laser Stability and Reference Detector Sensitivity

[1]See Section 4.4.1
[2]See Section 4.1.4

Because the GMS calculates the detector gain as a ratio of the pedestal-subtracted ADC values to the reference detectors, it is important for the reference detector to be sensitive to the Laser. The purpose of the Laser monitoring system is to check it.

In Figure 5.1, the uppermost figure shows pedestal-subtracted and averaged ADC values of Laser monitoring system readout. The middle figure shows the same for the PIN detector. In the bottom, the ratio is plotted. Here, the average ADC value for the two hours is calculated as the center of the ADC distribution by fitting Gaussian to it.

For the PIN's plots, the mean value for the no attenuation light was used.

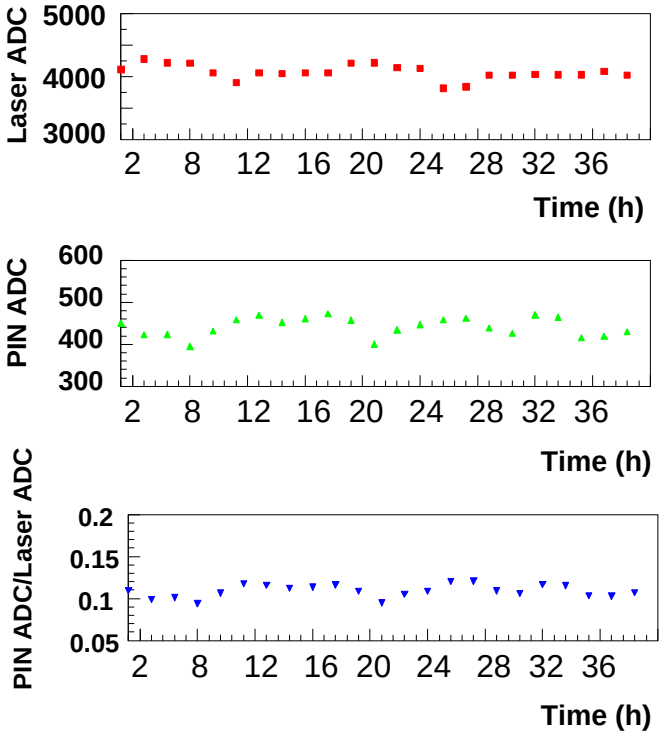

Figure 5.1: The Laser output and the corresponding PIN response. Upper figure shows the pedestal-subtracted and averaged ADC values of Laser monitoring system read out. The middle figures is averaged PIN ADC values where the pedestal is subtracted. The light with no attenuation was used. The lowermost figure is the ratio of between the two.

The average and its relative error for about 40 hours (about 20 times measurements) in Figure 5.1 are tabulated in Table 5.1. The Laser output

fluctuation was less than 5.2%. The PIN readout changed less than 6.6%. Then the standard deviation (S.D.) of the lowermost figure was about 0.01, the relative error (S.D. / Average) was 8%.

	Average (ADC)	1σ (S.D.)	Relative Error (%)
Laser Monitor	4253	222.0	5.22
PIN	461	30.4	6.59
PIN ADC/Laser ADC	0.1	0.01	8.01

Table 5.1: N_2 Laser and reference detector fluctuation

This result indicates that the reference detector is insensitive to the small Laser fluctuation ($\sim$5%). Next, we discuss the reference detector response changes in a longer term.

Figure 5.2 shows the pedestal-subtracted and averaged ADC value of PIN detector for 100 days. This calculation is done in the same way as used for Figure 5.1. In the present case, the measurement is done once a day.

Around 60th day, the ADC value rapidly changed. The reason was exchange of dye. The dye used for light source has to be exchanged periodically because the dye degrades. In the figure this can be seen as a gradual decrease of the ADC value with time.

This result indicates that the reference detector is sensitive to the large change of Laser output.

Here, what we have to consider is how Laser and PIN fluctuation affects the gain monitoring. Both the reference and monitored detectors are insensitive to the small fluctuation, since the reference detectors were connected to the Laser with 100 m optical fiber to have the same condition as the other detector. The injected light could be distorted. So the PIN's is not sensitive any more to such small Laser fluctuation as shown in Figure 5.1. However to evaluate the detector gain, it is sufficient because the input light to the detector also could be distorted. For the large changes of Laser output, the reference detector reflects the changes. One of the conditions which the reference detector has to satisfy is that it can reflect large Laser output changes.

So, in this sense, it can be said that our reference detectors satisfy the requirements.

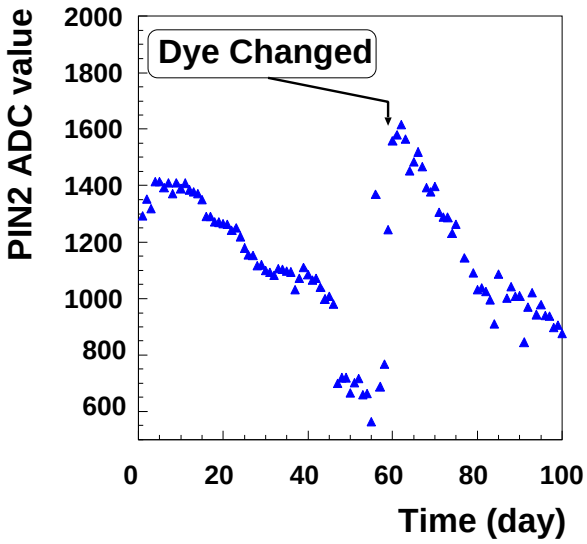

Figure 5.2: Reference detector response for about three months. Data were taken once per day with GMS private decoding system. Each point is PIN ADC value for no-attenuation light.

Gain Linearity of the Reference Detector

Here, the linearity of the reference detector gain is discussed. If the reference detector does not have the gain linearity, gain evaluation of the detector which is done by the GMS becomes meaningless. Therefore this linearity is very important.

Figure 5.3 shows a histogram of the value ith peak divided by the 6th peak in PIN ADC histogram (i = 1, 2, ...,5). The ith peak can be seen in Figure 4.12. For example, for the first peak :

$$\frac{< 1st\ peak\ ADC\ value >}{< 6th\ peak\ ADC\ value >} \quad .$$

The first peak is generated with the 10 % attenuation filter on the light filtering system. It is leftmost peak in Figure 4.12. If the reference detector keeps the gain linearity, the peak position of the first peak in Figure 4.12 is consistent with the attenuation factor of the filter. Actually, the first peak position is consistent with the 10% attenuation.

Other peaks in Figure 4.12 are obtained in the same way. All of them is also consistent with each attenuation factor of the filters (see the attenuation

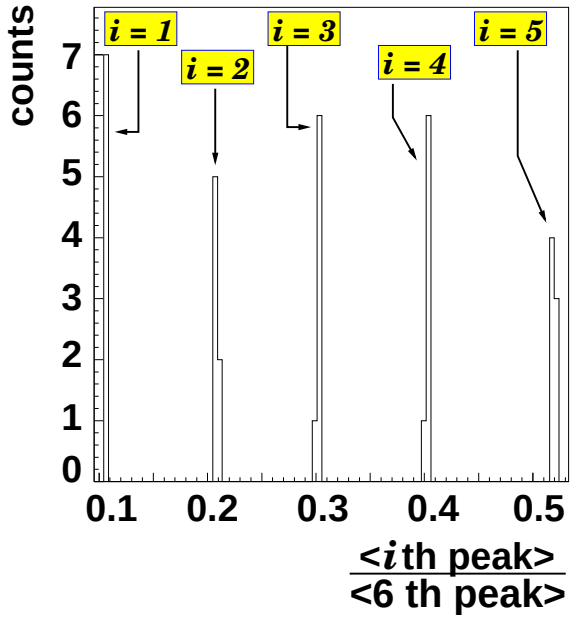

Figure 5.3: PIN gain linearity. Compare the peak positions of this histogram with the attenuation factor of each filter in Table 4.3.

in Table 4.3). For this analysis, data from run26225-26375 have been used. The time span for these runs is about 12 hours, so at least for that period the PIN keeps a gain linear. As a conclusion, we are confident that during the usual time scale for one single run[3] (4∼10 minute) the GMS system has a linear response.

5.2 Analysis Gain

Basic Idea of Gain Measurement

Generally, photo-sensitive detectors, such as PMT and photo-diode, linearly transform the number of incident photons (N^{photon}) to an electric signal (pedestal subtracted ADC value : ($ADC\ value$)) :

$$(ADC\ value)_{det=i} = \ G_{det_i} \ \cdot N^{photon}_{det=i},$$

If the photo sensitive detector gain does not change, then G_{det_i} is constant. However, in case when the photo sensitive detector has some problems, the

[3]GMS offline analysis is done once per run.

linearity of the transformation (gain) from photons to electric signal changes, for example G_{det_i} might decrease, or in more fatal case, looses the gain linearity. In experimental physics for certain measurements it is necessary that detector gains are constant. Thus it is very important to monitor the detector gain changes.

The GMS uses a reasonable method : The method uses the reference detector response as the standard for the monitored detector gain. The concrete idea of the method is following.

If there is a photo-sensitive detector which has a fixed gain without any changes,

$$\begin{aligned} (ADC\ value)_{ref} &= G_{ref} \cdot N_{ref}^{photon} \ , \\ \delta G_{ref} &= 0 \ , \end{aligned} \tag{5.1}$$

where $(ADC\ value)_{ref}$ is the reference detector ADC value, G_{ref} is its absolute gain (amplification). Generally, for the same incoming light, the photo-sensitive detectors have a relationship as :

$$(ADC\ value)_{det=i} = \alpha_{ij} \cdot (ADC\ value)_{det=j} \ . \tag{5.2}$$

Here $(ADC\ value)_{det=i}$ is the ADC value of the detector i, and α_{ij} is basically a constant value. This relation should also be correct for the reference detector :

$$(ADC\ value)_{det=i} = \alpha_{ij} \cdot (ADC\ value)_{ref} \ . \tag{5.3}$$

In this relation, the index j corresponds to the reference detector. From the above, the detector gain (absolute), G_{det_i}, is expressed as :

$$\begin{aligned} (ADC\ value)_{det=i} &= \alpha_{ij} \cdot G_{ref} \cdot N_{ref}^{photon} \ , \\ G_{det_i} &= \alpha_{ij} \cdot G_{ref} \cdot \beta_i \ , \\ & \quad (j = \text{reference detector}) \ . \end{aligned} \tag{5.4}$$

Here β_i is a proportional factor, as follows :

$$N_{det=i}^{photon} = \beta_i \cdot N_{ref}^{photon} \ ,$$

β_i is originated from the fact that the number of incident photon (intensity) to the monitored detector is different from that to the reference detector

PIN. This factor does not change with time. It is fixed by the GMS hardware components, sub-splitter and attenuator etc. Hence, the detector gain changes can be expressed as :

$$\delta G_{det_i} = \delta\alpha_{ij} \cdot G_{ref} \cdot \beta_i \ . \tag{5.5}$$

Therefore the detector gain change can be monitored by checking the proportional factor α_{ij} of Eq. 5.3. So principally the GMS defines the relative gain as

$$Gain^{det=i} \equiv \alpha_{ij} \ . \tag{5.6}$$

(j = reference detector, i the monitored detector)

Consider the concrete way to evaluate the detector relative gain $Gain^{det=i}$. A typical figure of the detector response for GMS events is shown in Figure 5.4. As you see, the six intensities are separated as well as reference detector PIN (lower figure of Figure 4.12).

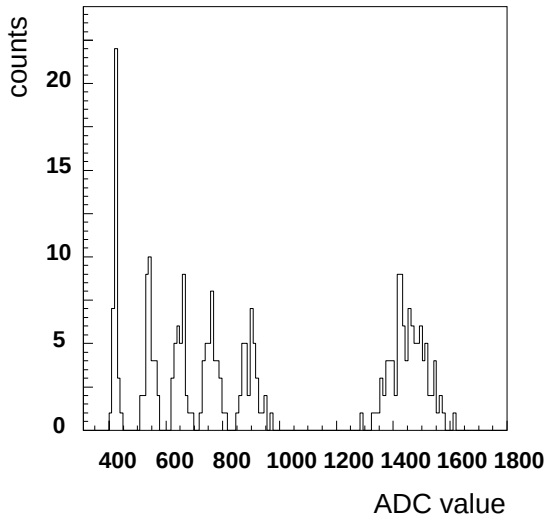

Figure 5.4: Histogram of detector ADC value. The six peaks are generated by the light filtering system.

Then, comparing the monitored detector response with reference detector PIN, result in a figure like Figure 5.5 is obtained. If the detector absolute

gain (G_{det_i}) decreases, then the slope of the Figure 5.5 is going to decrease. Conversely, if this slope changes, it indicates that the detector absolute gain, G_{det_i}, has changed. This slope corresponds to the α_{ij} in Eq. 5.3.

In a scatter plot (Figure 5.5) the detector ADC value versus PIN ADC value shows a straight line. In this case, we can obtain a histogram as Figure 5.6. This is histogramed obtained from the detector ADC value divided by PIN ADC value for each GMS event. The mean value of the histogram corresponds to the slope in Figure 5.5. That is to say, the relation Eq.5.3 is correct for the reference detector, at event level.

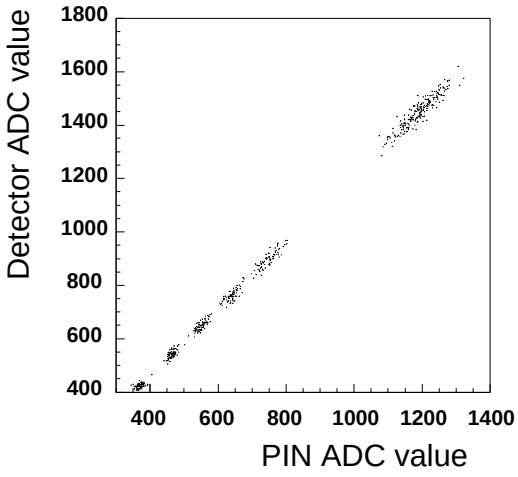

Figure 5.5: Scatter plot of Detector ADC value versus PIN ADC value. Normally detector shows complete linear response like this.

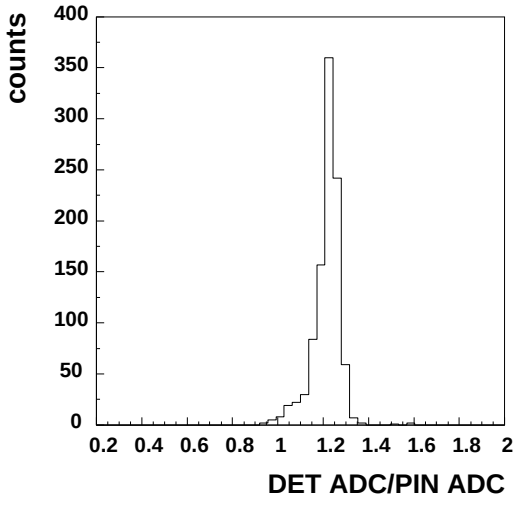

Figure 5.6: Histogram of detector ADC value divided by PIN ADC value for event by event. This peak's mean value correspond to the slope of Figure 5.5.

Figure 5.7 shows a scatter plot and linear fit to it, the pedestal has been subtracted. The triangle point is computed as the mean value for each peak. In this example data from calorimeter cell 440 has been used. The six peaks are not Gauss distributions because of low statistics, thus, as a mean value the simple average was used. For the error in x-, and y-axis (PIN ADC, and cell440 ADC-axis), 1σ is used. The linear fit $y = ax$ has been applied. The fit function is decided from the relation between detector ADC value and PIN ADC value (Eq. 5.3) as :

$$(Detector\ ADC\ value) = Gain^{det=i} \cdot (PIN\ ADC\ value)\ ,$$

so it is a linear function which starts at the origin. In this case, there are errors for x- and, y-direction for each point. To find the best linear fit, chi

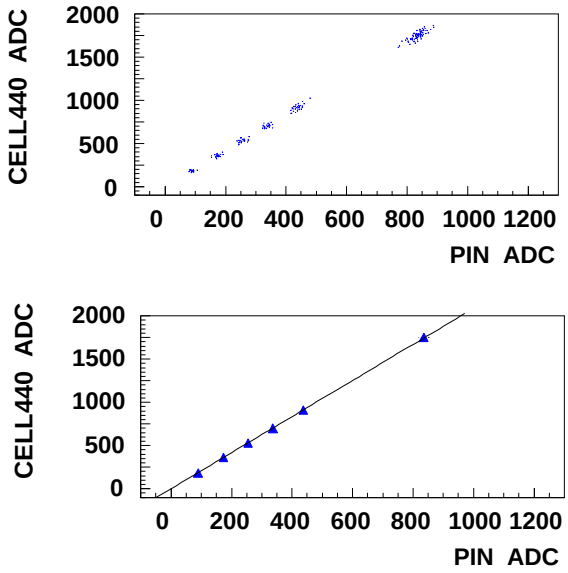

Figure 5.7: Linear fit for the calorimeter cell 440 ADC value versus PIN ADC value. Upper figure is used the scatter plot of the cell 440 vs PIN. Lower figure is fit to mean value for the six peaks, and $y = ax$ is used as fit function. For this plot run26225 of the year 2000 data are used.

square (χ^2) is defined in Eq. 5.7. The chi-square is then minimized.

$$\begin{aligned} \chi^2 &\equiv \sum_i \frac{(< y > -y_i)^2}{\sigma_i^2}, \\ \sigma_i^2 &= \delta y_i^2 + a^2 \delta x_i^2, \\ y &= ax \ \cdots \text{ fit function}, \end{aligned} \tag{5.7}$$

y is equal to the cell 440 ADC value, x corresponds to the PIN ADC value.

The quality of the fit can be seen in Figure 5.8 where the chi-square value for each intensity is shown. The horizontal axis is the peak position, the vertical axis is the chi-square value.

We can see from Figure 5.8 that the linear fit has a very good precision. Therefore this detector gain is clearly linear.(The PIN gain linearity was already shown in Figure 5.3)

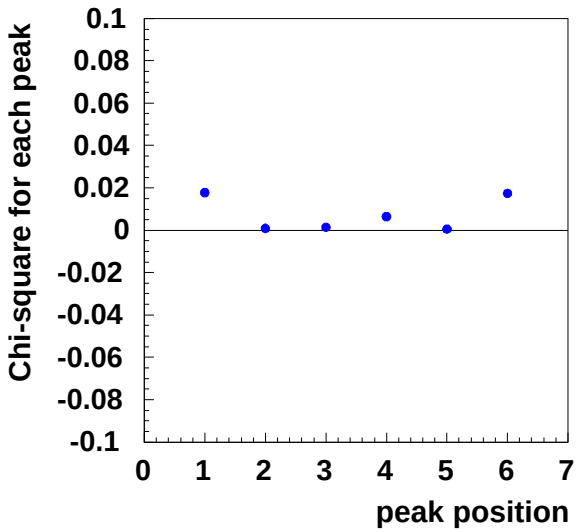

Figure 5.8: Chi-square of the linear fit result for each peak.

Gain Definition and Estimation

As mentioned above, the monitored detectors show a linear response and the linear fit can be done with a good precision. Therefore, to compute the detector gain which follows the definition Eq. 5.6, GMS actually uses a function as follows :

$$Gain^{det=X} \equiv \frac{\sum_i^{N_{gms}} (ADC_i^{det=X}) - N_{gms} \times Ped^{det=X}}{\sum_i^{N_{gms}} (ADC_i^{det=PIN}) - N_{gms} \times Ped^{det=PIN}} \ , \tag{5.8}$$

where $ADC_i^{det=X}$ is "detector X" ADC value for GMS event, $Ped^{det=X}$, $Ped^{det=PIN}$ are "detector X" and PIN ADC value of pedestal event, the N_{gms} is the number of GMS events. The index i is for GMS event in a run.

Especially, the ADC value of $Ped^{det=X,PIN}$ is defined as :

$$Ped^{det=X,PIN} = \sum_j^{N_{ped}} \frac{1}{N_{ped}} \ ADC_j^{det=X,PIN} \ . \tag{5.9}$$

Here the sum of Eq. 5.9 runs over all the pedestal event in a run. N_{ped} is

number of pedestal events, the $ADC_j^{det=X,PIN}$ is ADC value which is identified as pedestal event with pedestal trigger. The $Ped^{det=PIN}$ in Eq. 5.8 is the average over ADC values for pedestal events. Then N_{GMS} times $Ped^{det=PIN}$ is subtracted from the sum of GMS event ADC values.

The gain definition (Eq. 5.8) is based on the Eq. 5.6. In short, the gain definition (Eq. 5.8) is the ratio of detector ADC value to PIN ADC value. This means the $Gain^{det=X}$ is basically constant at event level. This is evident from the Figure 5.6. Then GMS gain evaluation of the monitored detector is done once per a run.

It has to be checked whether the gain definition from Eq. 5.8 is consistent with the gain which was obtained by linear fit like in Figure 5.7. As an example, we compare the gains for cell 398 which is one of blocks of the calorimeter.

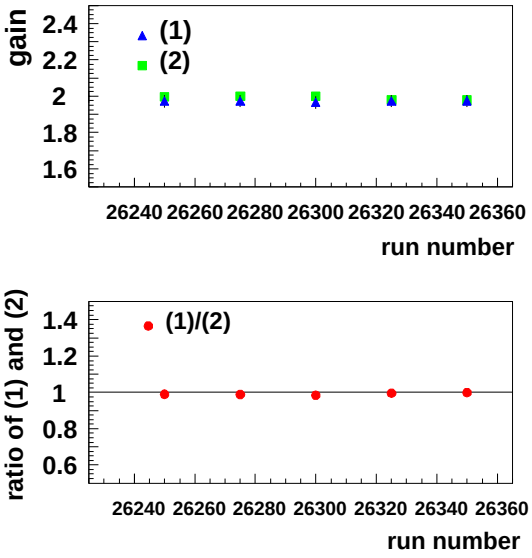

Figure 5.9: Gain comparison between linear fit and calculated with the definition Eq. 5.8. The mark "(1)"(triangle) is obtained using linear fit, "(2)"(square) is by the definition.

Figure 5.9 is the comparison of the gains for run26225 $\sim$ 26365 of year 2000 data, especially run26250, 26275, 26300, 26325, 26350, 26365 are picked up. The mark "(1)"(triangle) in upper figure is the gain which is obtained using linear fit, and "(2)"(square) is calculated with the definition of gain (Eq. 5.8). Then the lower figure is ratio of "(1)" and "(2)". The two methods are completely consistent in the runs (actual duration of those runs is about 12

hours). Therefore, the gain definition is equivalent to linear fit. Thus in the following, Eq. 5.8 is used for the gain calculation.

The gain is calculated (Figure 5.10) for the calorimeter cell 398 for all the run numbers mentioned above. The result is plotted in Figure 5.10. The calorimeter cell 398 is one of the cells near the positron (electron) beam pipe. It can be seen from Figure 5.10, the cell 398 is very stable. This gain is used to check detector stability during data taking. Of course the gain calculation is done for all the monitored detectors. Figure 5.11 and 5.12 show gain plots for some of monitored detectors using the year 2000 data (run23000-30530).

In Figure 5.12, the preshower counter gain changes periodically. The periodical changes are seen not only for the preshower counter but also for other detectors. As the time distance between the last bunch with electrons and the empty bunch which is used for the GMS measurement is only a few hundred nanoseconds, it is possible that due to high rates during injection and at the beginning of a fill, the response of the PMTs to the GMS laser light is not absolutely linear and depends to some extent on the positron beam current. For example in the gains of the calorimeter, an increase of the gain with the increase of the beam current can be seen in Figure 5.13.

A blank of the gain for each period can be seen like in Figure 5.13 (c). The blank (gap) is caused by "LPol run[4]" which is done before turning on the high voltage of all the detectors. During a LPol run, all detectors are off, although the DAQ is running. The GMS does not stop the gain computing during that time. Thus a gap seen in (c) in Figure 5.13 appears once at the beginning of every fill[5].

The gain change measurements have to be done within each fill since all the detector gains are recovered by turning off the high voltages. Also the LPol run should be cut out as the detectors are off in that period.

To discuss the detector gain, it is useful to use the "deviation". The detector gain does not always change continuously in a fill, for example because of high voltage trip. Therefore, we defines as follows :

$$Gain\ deviation_i \equiv \sum_{j}^{N_{run}} \sqrt{\frac{1}{N_{run}} (gain_j - < gain >_i)^2} \ . \qquad (5.10)$$

The sum runs over all the run numbers in a fill, thus the index i is for a fill, then index j is for a run. N_{run} is the number of runs in a fill. In short, the

[4]See Figure 3.4 about LPol run

[5]The gain during the LPol run is so small, usually the value close to zero. So in the figure, the gain is out of range.

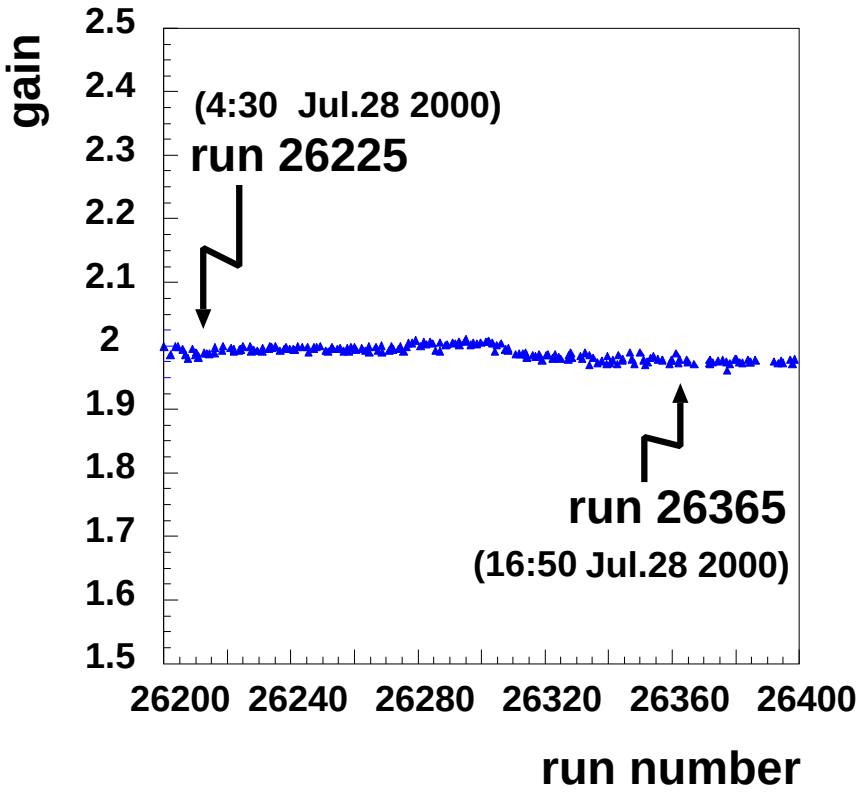

Figure 5.10: Gain from the run26225 to 26365. As an example, the gain for calorimeter cell398 is shown here. This is evaluated with Eq. 5.8.

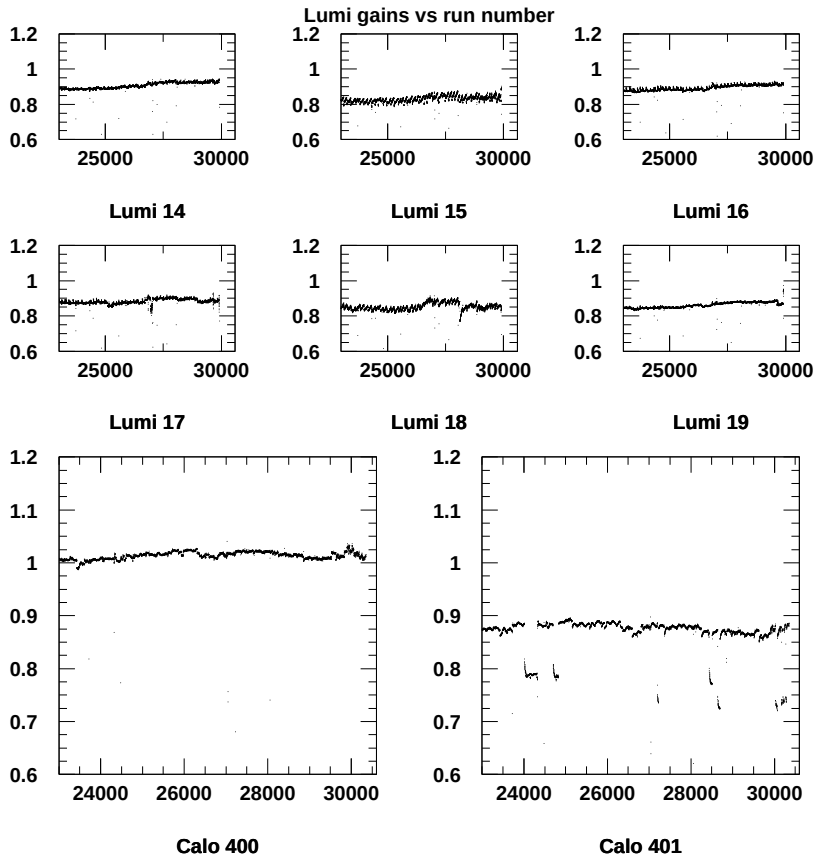

Figure 5.11: Gains in the run23001-30530. Those are evaluated with Eq. 5.8 and are normalized. The six upper figures are Luminosity monitor, channels 14 $\sim$ 19th. The two lower figures are calorimeter cell 400, 401, which are two of the nearest cell to the the positron beam pipe.

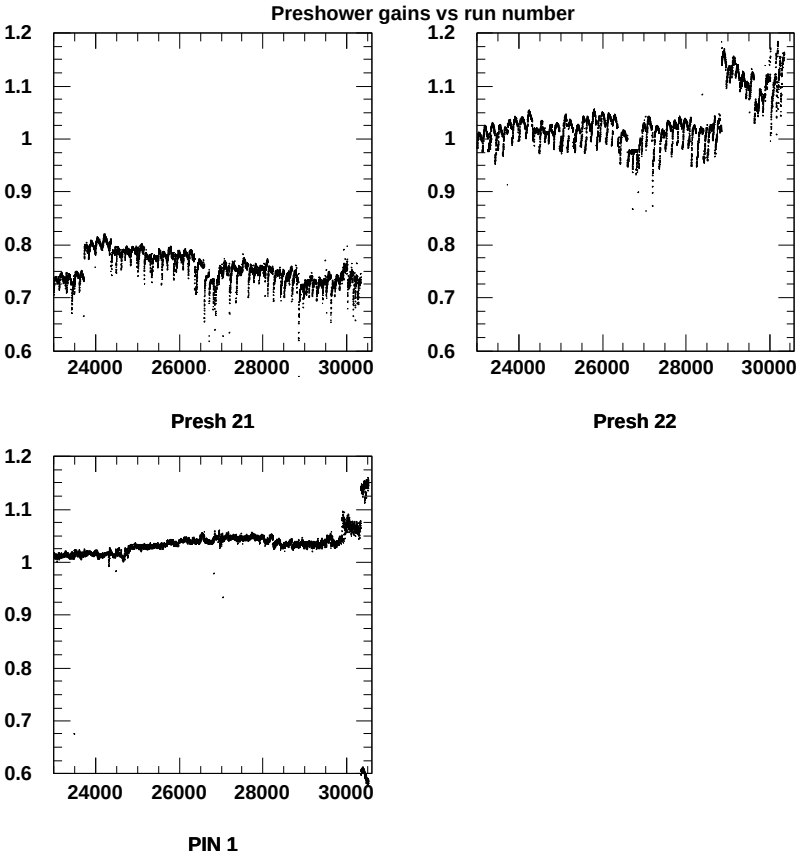

Figure 5.12: Gains from the run23001-30530. Those are evaluated with Eq. 5.8, and are normalized. Two upper figures are preshower counters, which are the two nearest to positron beam pipe.

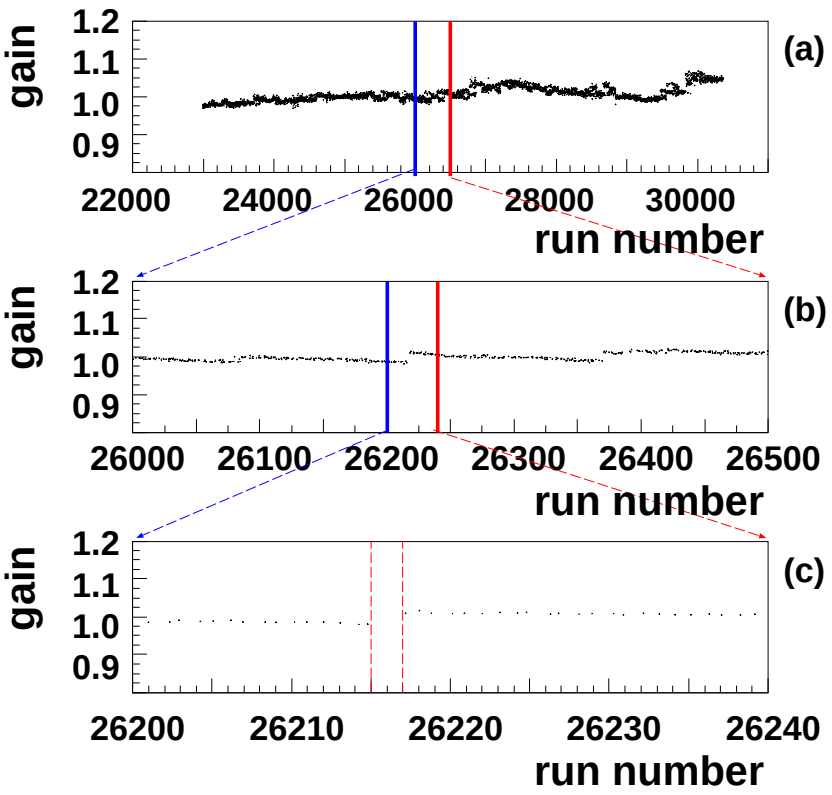

Figure 5.13: Magnification of the gain for one fill. Uppermost figure (a) shows the gain plot for run23000-30530 of the year 2000 data. (b) is enlarged figure for run26000-26500 of (a). (c) is once more enlarged for run25550-25600 of (b).

Gain deviation$_i$ is the square root variance of the gain in a fill.

Figure 5.14 shows a distribution of the gain deviation. The vertical axis is the *Gain deviation*. If the detector gain has large dispersion, the *Gain deviation* becomes large. That means that the detector has large gain changes in that fill. In Figure 5.14 there are a few points which have large values. The reason for that changes is understood and listed in Table 5.2.

Basically, the detector gain measured by GMS is very stable if experimental systems such as DAQ and HERA-beam are working normally. This can be seen in Figure 5.15 which shows a distribution of the gain deviation. A couple of points show problems and have been reported in the the HERMES experiment shift reports (for example the Table 5.2) in order to pass the information to offline analysis.

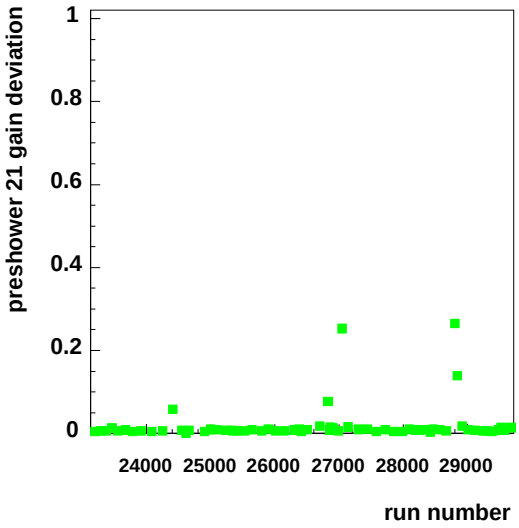

Figure 5.14: Gain deviation per a fill. The value calculated with Eq. 5.10 for a fill is plotted . This shows distribution of the gain deviation for each fill. The same data and the same channel of the preshower counter 21st block is used as in Figure 5.12.

Figure 5.15 shows the same plot as Figure 5.14 but with a different scale for the vertical axis. There, only fills with normal gain deviation were ploted and the gain change observation was less than 4% relatively.

Calorimeter

In this section, the electromagnetic calorimeter will be discussed. The calorimeter is one of the detectors which require good gain linearity and sta-

Run Number	Fill Number	Cause
24339 - 24484	2131	There is a dummy run to test message system
24701 - 24830	2138	GMS software trouble
26808 - 26839	2164	High proton background
27039 - 27046	2170	Not all detectors actually switched on
28812 - 28860	2198	stop run to re-set prescale factors

Table 5.2: List of causes of large gain changes.

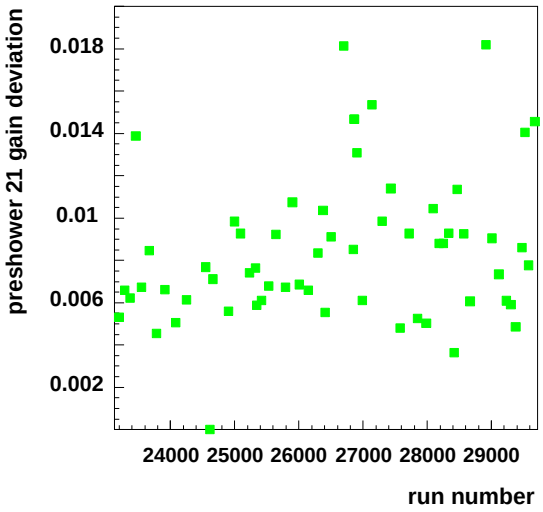

Figure 5.15: Gain deviation of preshower counter 21st block. This is the same as Figure 5.14, but the scale of the axis is evaluated.

bility. Thus it is important to detect the gain changes and also to check GMS monitoring accuracy for the calorimeter gain. GMS has been monitoring all calorimeter channels. The GMS N_2/dye Laser wave length is suited to the PMT's high quantum efficiency region and the low light attenuation region of the lead glass[6].

From the calorimeter data the energy of an incident charged particle is calculated with Eq. 3.3. The variable x of the equation is sum of the corrected ADC value (pedestal subtracted ADC value) for 9 cells. To see the energy region where GMS monitors, assume the following :

- An incident particle deposits its energy mainly in one lead glass block. Then we can express Eq. 3.4 as following :

$$x = \sum_{i=1}^{9\text{cells}} (\text{ADC}_i - \text{pedestal}_i) \tag{5.11}$$

$$\equiv \sum_{i=1}^{9\text{cells}} (\text{ADC}_i)_{corr}$$

$$\simeq (\text{ADC}_j)_{corr} \ , \tag{5.12}$$

[6]The calorimeter hardware components and its specification are explained in Section 3.3.2. The specification of the lead glass and PMT can be seen in Figure 3.8 and 3.9.

where $(\mathrm{ADC_i})_{\mathrm{corr}} \equiv (\mathrm{ADC_i} - \mathrm{pedestal_i})$. In this case, we can evaluate the energy region for the six light intensities which GMS provides. Figure 5.16

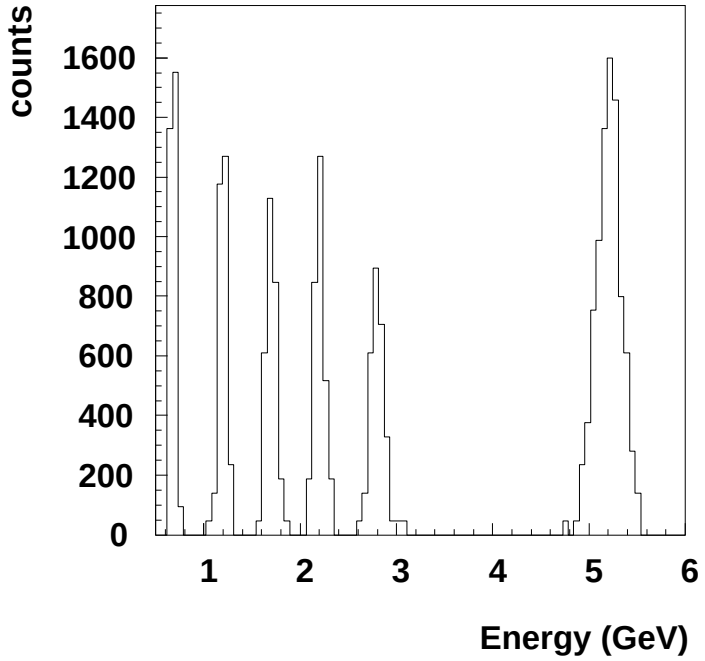

Figure 5.16: Energy region coverage of the GMS lights.This is computed with the assumption : Eq.5.12. This is for calorimeter cell 400.

shows the calculated energies for the six light intensities from Eq.5.12. This figure indicates that the light which GMS provides corresponds to an energy range of 0∼6 GeV for incident particles. However, the energy is different for each cell because the Laser light intensities are not completely equal : it depends on the sub-splitter. Roughly speaking the GMS covers energy region of 0∼10 GeV for each cell. To check the GMS monitoring accuracy for the calorimeter gain, we obtain from Eq. 3.2,

$$y \equiv (ADC^{det=calo})_{corr} \quad ,$$

$$E \simeq C_0 + C_1 \cdot y \quad , \tag{5.13}$$

$$\delta E \simeq C_1 \cdot \delta y \quad , \tag{5.14}$$

($\because C_0 = 0.19169,\ C_1 = 0.0043086 \gg C_2 = -1.02 \cdot 10^{-7},\ C_3 = 1.02 \cdot 10^{-11}$).

From the above equation and together with Eq.5.5, 5.6, we obtain a relation ;

$$\frac{\delta E}{E} = \frac{\delta Gain}{Gain} \tag{5.15}$$

This relationship is based on the assumption Eq. 5.12. Then one can compare the GMS resolution with Eq.3.2 in term of the energy resolution as shown in Figure 5.17.

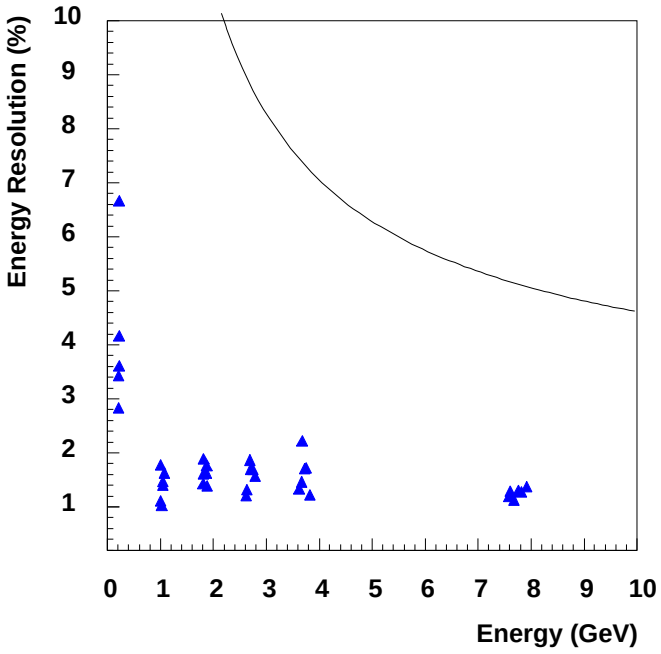

Figure 5.17: Comparing energy dependence of the GMS resolution and calorimeter energy resolution. The triangle is the evaluated GMS resolution for each peak, which means energy dependence GMS resolution. The value of the resolution is evaluated for calorimeter cell 398, 399, 400, 406, 407, 408, 409, 440, 441, 443, 448, 449, 450, 451. The curve in the figure is ploted with Eq. 3.2.

In Figure 5.17, the solid curve is Eq.3.2, the triangles are the relative error of the gain (right side of the Eq.5.15) for each peak.

Since the relation between ADC value and energy is almost linear and the GMS gain resolution also does not change as shown in Figure 5.17, this energy resolution comparison can be judged as fairly reasonable.

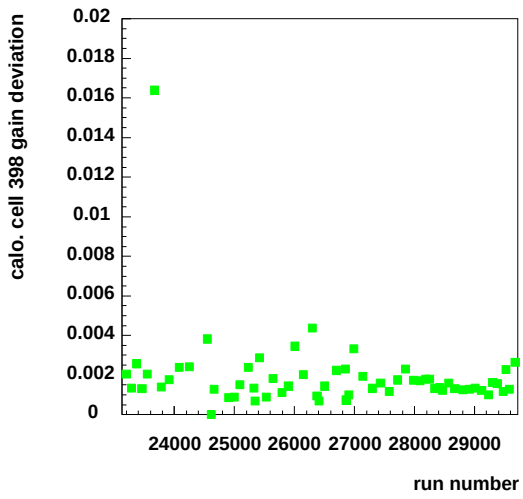

Figure 5.18: Gain deviation of calorimeter cell 398.

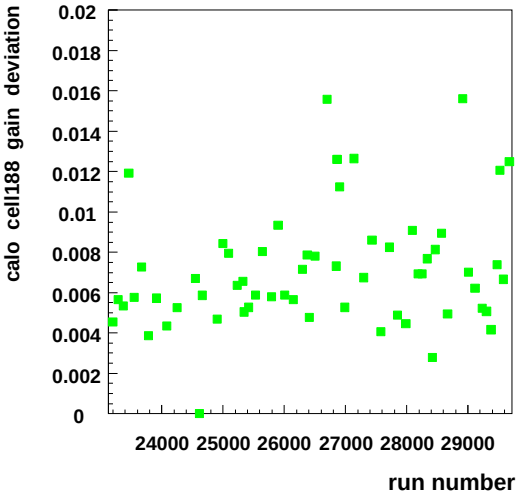

Figure 5.19: Gain deviation of calorimeter cell 188

The calorimeter gain deviation can be seen in Figures 5.18 and 5.19. The Figure 5.18 is for the calorimeter cell 398, Figure 5.19 is for the cell 188. Those cell positions are shown in Figure 5.20. Here, the cell 398 is one of the cells which are nearest to the positron beam pipe, and the cell 188 is in the center of the calorimeter. Comparing those gain deviations, they are clearly different. The cell 188 gain changes are larger than cell 398. This difference is not only between cell 398 and 188, but also for cell 189∼191, 230∼233 and cell 399∼401, 407, 408. For the cells which are in the center of calorimeter half, its gain deviation are generally larger than at the edge of the calorimeter. The reason for that differences is not clear yet and requires detailed investigation.

Next, we discuss long term gain changes. Figure 5.21 shows a histogram of gain for all of the year 2000 data.

The uppermost histogram is for run00001-15000 and labelled (a), histogram (b) is for run15000-23000, and histogram (c) for run23000-30530. There are two or more peaks in the histogram (a), this is caused by some detector problems and tests at the beginning of the experiment. In the histogram (a)∼(c), the gain is shifted to lower value. That is to say this PMT gain showed about 2% decrease. However this is not common for all of the cells of the calorimeter. The changes are different in each cell.

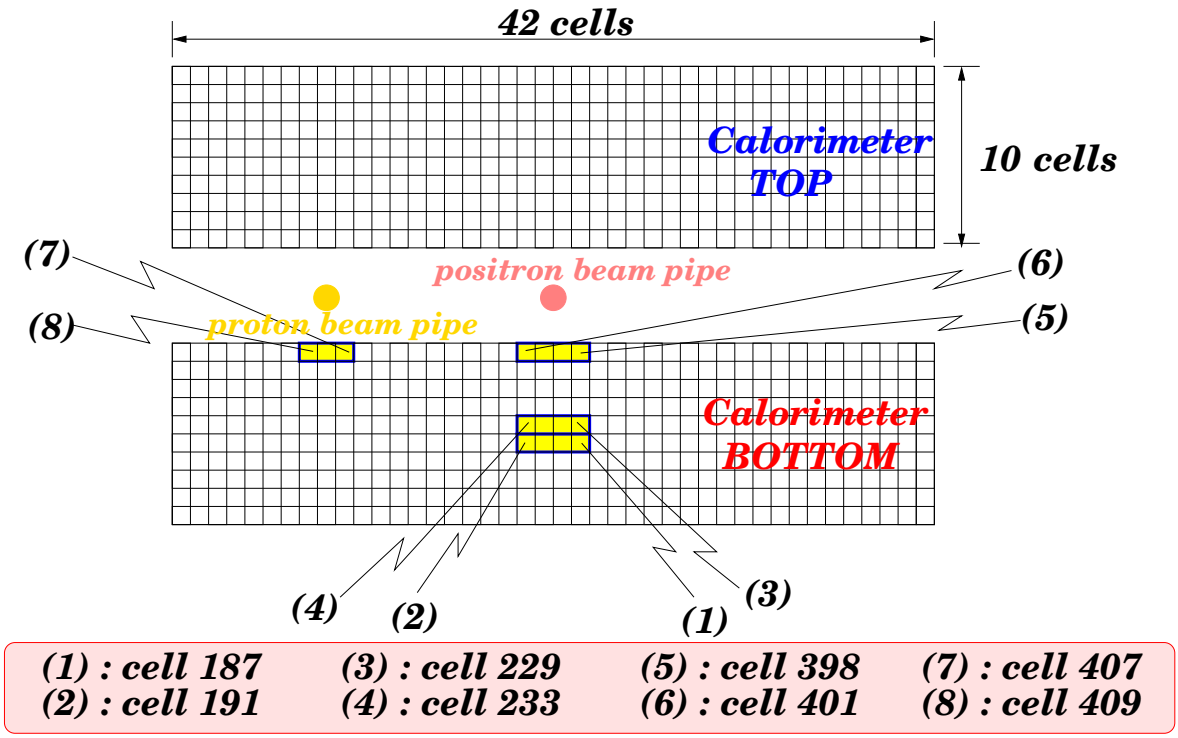

Figure 5.20: Calorimeter cell position. This position corresponds to the Pink window.

Detail of Gain Analysis and Prospect of GMS

Above, we dealt with the case where the detector gains are linear. However, PMTs don't always respond linearly. A typical example of non-linear behavior is the saturation of the PMT gain. In a high ADC range, PMT can not transform from photon to electric signal linearly.

Basically any detector is designed to satisfy the requirements for its special task. For example, HERMES electromagnetic calorimeter is built to detect a charged particle with up to 30 GeV, and the calorimeter actually satisfied the requirement. On the other hand, the PMT gain can be saturated by a high event rate. Then, in the worst case, the linearity is broken in the high ADC region.

In case where the detector is saturated, it shows a behavior like in Figure 5.22. Slope changes can already be seen in Figure 5.22. If the slope is

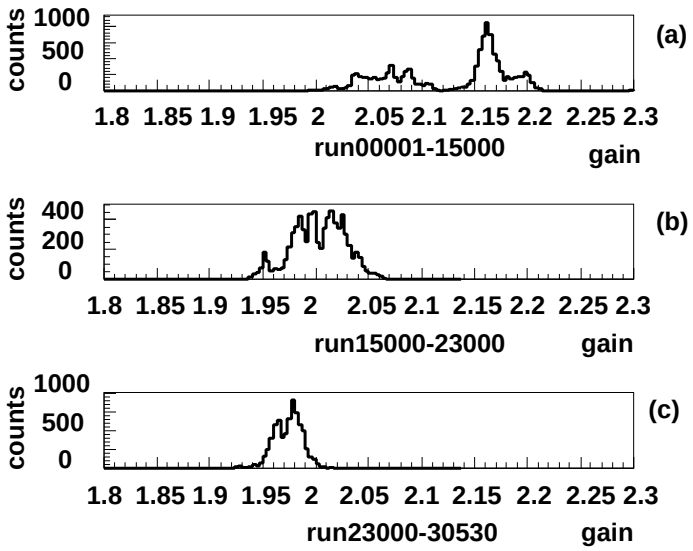

Figure 5.21: The cell 398 gain histogram for all run in year 2000 data.The uppermost figure(a) is run00001-15000, the next figure(b) is run15000-23000, and next lowermost figure(c) is run23000-30530. Then the lowermost figure(d) is the superposition of the above histogram. The red histogram is (a), green is (b), blue is (c).

calculated like Figure 5.6, the resulting Figure 5.23 shows a broad distribution with several peaks. This is not due to statistical problem. The slope for each intensity calculated in the same way shown in Figure 5.24. It indicates that the $[(Detector\ ADC\ value)_i/(PIN\ ADC\ value)_i]$ (i is event number) are not on a straight line in Figure 5.22. Actually the peaks of high intensity (lowermost figure in Figure 5.24) are shifted to lower side on the horizontal axis. In the gain definition of Eq.5.6 and 5.8 the gain linearity is assumed. However, what we have to know is at which ADC channel the PMT becomes saturated. If the gain definition is used in the region where the detector is saturated, then the calculated gain with the definition is simply too low.

Here we can test the linear fit of the detector ADC values in the same way as used in Figure 5.5. The result can be seen in Figure 5.25. Figure 5.26 shows the chi-square for each peak after the linear fit. The vertical axis is the ADC value of each peak.

The chi-square value decreases from the first to fifth peak, and there is a large chi-square for the sixth peak. Here in the linear fit, the value of the sixth peak is low. By the way the second peak has large chi-square value.

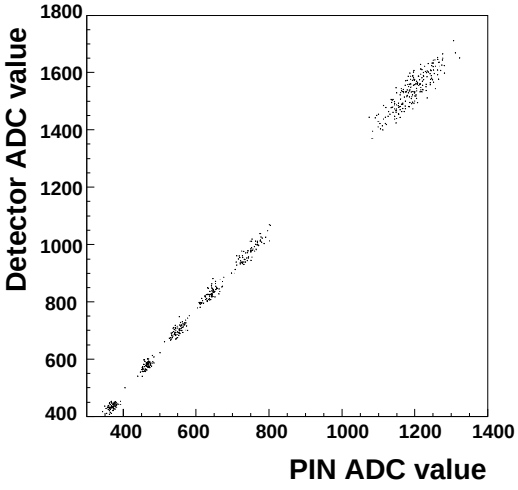

Figure 5.22: Scatter plot of Detector ADC value versus PIN ADC value. The detector is different from Fig. 5.5.

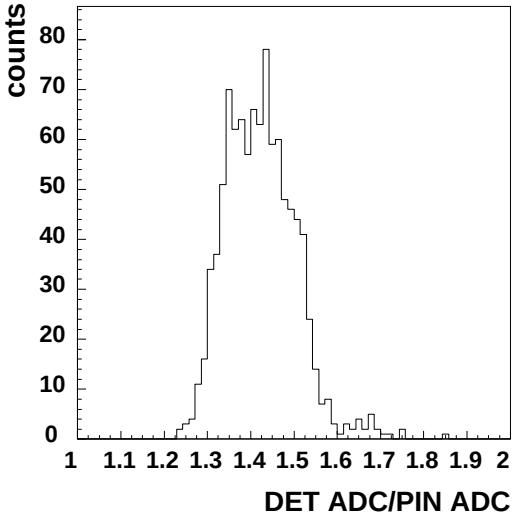

Figure 5.23: The detector ADC divided by PIN ADC value. This is for different detector from Fig. 5.6.

This is caused by very small error (error $\equiv \sigma$). From this figure, it is possible to know that at least the sixth peak is saturated. However we cannot obtain any information of the ADC region where the saturation starts. There are about 440 ADC channels between the fifth peak and the sixth peak. Thus, to obtain exactly the information of the detector saturation, it is necessary to cover this ADC channels. So more optical filters have to be installed to cover this region with a smaller attenuation step. The existing optical filter of light filtering system is listed in Table 4.3. There are two available positions on the wheel to install new ones. In the future, I plan to install new filters to be able to study the gain linearity in more detail.

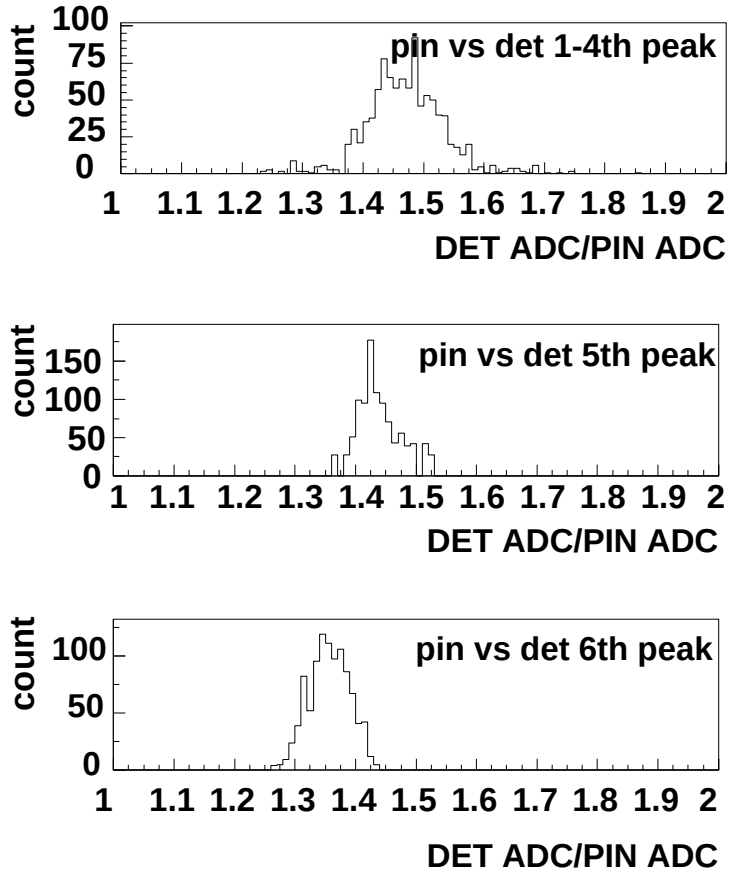

Figure 5.24: Histogram of $(Detector\ ADC\ value)_i/(PIN\ ADC\ value)_i$ for each peak. The uppermost histogram is for 1∼4th peaks. The middle figure is for 5th peak, and the lowermost is for 6th peak. These histograms are made in the same way as used for Fig. 5.23 etc.

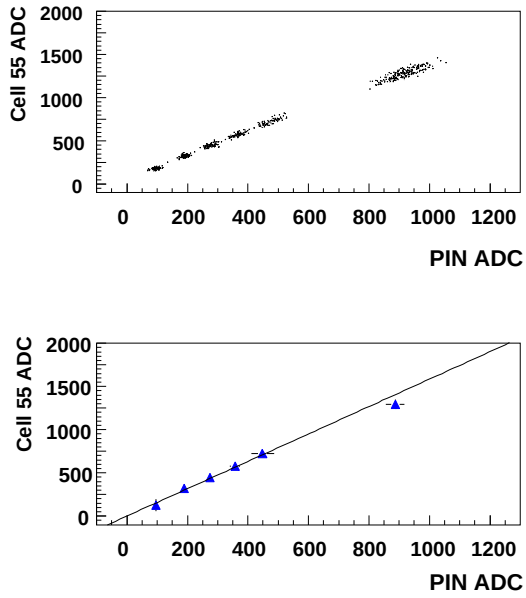

Figure 5.25: Linear fit in case where the detector is saturated.

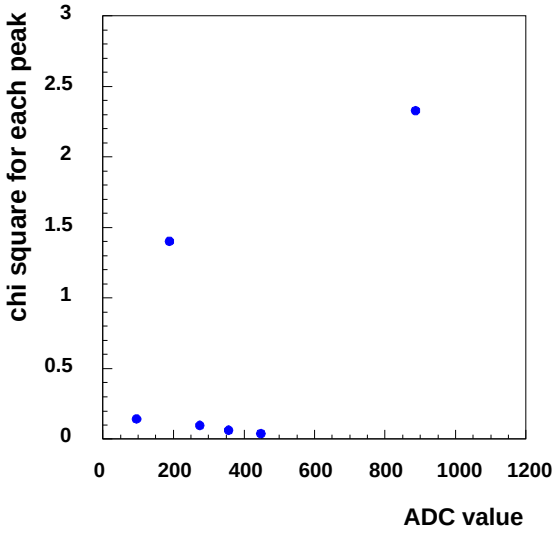

Figure 5.26: chi-square for linear fit.

Chapter 6

Summary

The main subject of this thesis is the study of the detector gain by using the HERMES Gain Monitoring System (GMS), and to prove the GMS stability, which the detector gain measurement is based on, with a newly built Laser monitoring system.

The GMS has been operating since the HERMES experiment was set up in 1995. The GMS is designed to measure the stability of the response of experimental detectors. Especially, the measurement is done for detectors which use photo multiplier tubes. Generally, the physics value extracted from experiment is based on the detector gain linearity and stability. Therefore it is very important to measure the detector linearity and stability.

The operation of the GMS is done with the following procedure :

1 Generate the light pulses of different intensities by combination of nitrogen/dye Laser and a light filtering system.

2 The generated light pulses are split and distributed to all the monitored detectors as well as to a series of reference detectors.

3 By comparing the initial response of the detector with the response of the detector later in the experiment time-dependence of the responses of the detector is monitored.

To evaluate the detector gain (amplification), GMS uses a series of reference detectors. It is most important to estimate the reference detector performance. The conditions which the reference detector should satisfy are
1. Constant gain as a function of time
2. Gain linearity
3. To reflect the Laser light fluctuation

In this work, the performance of the HERMES GMS has been tested first. For that purpose, the Laser monitoring system was newly added to the existing GMS components. With this system it became possible to exactly evaluate the reference detector performance. As the result it was proven clearly that the reference detector satisfies the conditions during the standard operation.

Secondly, the monitored detector gain for the year 2000 data was analyzed. The detector gain fluctuates about 4% in worst case. The gain of some detector decreases about 2% over 7 months. The uncertainty of the gain determination is less than 2%. For the electromagnetic calorimeter the GMS monitored the energy region about $\leq$10 GeV for each cell.

The detector gain becomes non-linear when the detector is saturated. The method to identify the non-linearity was demonstrated. The non-linear response cannot be handled well with present GMS. As a future plan, the following improvement can be considered. The idea is that two optical filters are added to the light filtering system. Then using a parameter fit, the ADC region where the detector is saturated can be found. This information will be useful. So, even in the case when the detector is saturated, the GMS will be able to provide a correction factor to the detector response.

Appendix A

Electronics

A.1 The GMS Electronics Modules

Very briefly, an outline of the electronics in the NIM crate near the GMS laser (on top of the electronics trailer) is described below. Modules are listed from left to right.

1. HV Power Supply. Settings (labelled on module):
   (a) Light Trigger -750V
   (b) NaI -1650V
2. Cable Delay for NaI. Currently set at 28 ns.
3. Cable Delay for Light trigger. Currently set at 58 ns.
4. PIN Cushion. Houses the PIN Photodiodes; 1-4, from top to bottom. Optical fiber input on left (fibers B, M, N, O, respectively) and BNC output cables (cables 10, 15, 16, 17, respectively) to ADC (first floor of ET) on right.
5. Pegel Converter (Type L49A, Nr:111).
   (a) TTL in / NIM out – 4 slots, from top to bottom:
      i. Lemo cable 6 in (from laser, it tells when a filter is in place); output to Quad Coincidence slot 2
      ii. Lemo cable 0 in; output to ADC

iii. Lemo cable 1 in; output to ADC

iv. Lemo cable 2 in; output to ADC Note: cables 0, 1, and 2, together encode which filter is in position.

(b) NIM in / TTL out – only one slot used: Lemo cable 10 in (from Gate Generator); Lemo cable 4 out (to laser, tells laser when to fire)

6. Quad Coincidence (LeCroy Research Systems LRS Model 622) 4 slots, from top to bottom:

(a) Not used

(b) AND of Pegel converter NIM out slot 1 (Filter wheel) and output of slot 3 of Quad Coincidence. Output to Walter Delay Box.

(c) AND of BNC B1 (Bunch one signal; BNC cable 14, further labelled "B1") and L-bar output of Gate Generator. Output to slot 2 of Quad Coincidence.

(d) OR of inverted Hera Clock signal (BNC cable 5, converted to lemo; this signal comes from TOM electronics, also on 2nd floor of ET) and nothing. Output is inverted and sent to Walter Delay Box.

7. Gate Generator (Type: G43, Nr: 203) Two slots:

(a) Not used

(b) START comes from Walter Delay Box. Output: L goes to Pegel (Nim in / TTL out) slot 1 L-bar goes to Quad Coincidence slot 3

8. Walter Delay Box. Only first of 4 slots are in use. There is a number on display, it reads 802 now. There are four lemo connections below it.

(a) Inputs

i. Upper left: Inverted OUT of Quad Coincidence slot 4. This is essentially just HC (Hera Clock).

ii. Upper right: OUT of Quad Coincidence slot 2. This is essentially an AND of Filter Wheel, B1, and Gate Generator's L-bar.

(b) Outputs

i. Lower left: to START of Gate Generator.

ii. Lower right: Same signal, but to Cerenkov, so they can trigger their LEDs when we trigger our laser.

(c) How the module works:
The module takes the upper-right signal (in our case Filter_wheel&&B1&&L-bar) and delays it by 1000-x (where x is the number on display, for us 802) periods of the upper-left signal (HC). It puts two identical outputs in the lower two slots.

9. H1-Z Octal Discriminator (LRS Model 623Z)
The thresholde voltage is -337 mV. Then the small PMT output is around -890 mV (not divided for Laser monitroting system)

Only 4th slot used. Input from Light trigger (which lies on top of Blue 1x16 splitter). Output to Cable Delay Box (documented in part (c) above).

A.2 Phase Ramp

The series of phase ramp which are coupled with LED/photo-transistor pair readout the TTL base signal, then the filter identification is don with phase ramp signal. The logic can be seen in Figure A.1.

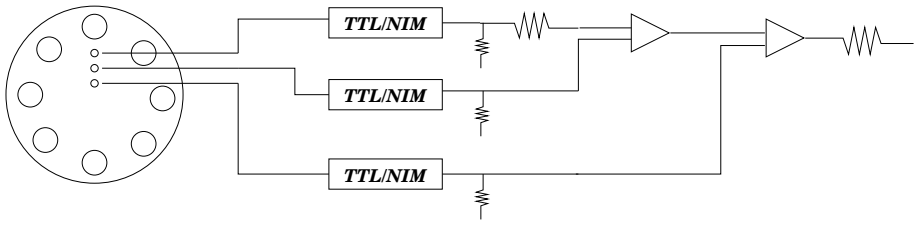

Figure A.1: Phase ramp logic.

Each modules is detailed previous section. The phase ramp signal can be accessed by private decoding system.

A.3 Laser Trigger

The Laser trigger depends on the trigger lamp and Bunch#1 signal. The Bunch#1 signal is prescaled signal of HERA-clock. The signal handling of the Laser trigger can be seen in Figure A.2. Each modules is detailed previous section.

The uppermost signal in Figure A.3 is Laser light signal. The second figure from uppermost is Laser trigger signal. The lower figures (labeled (a)

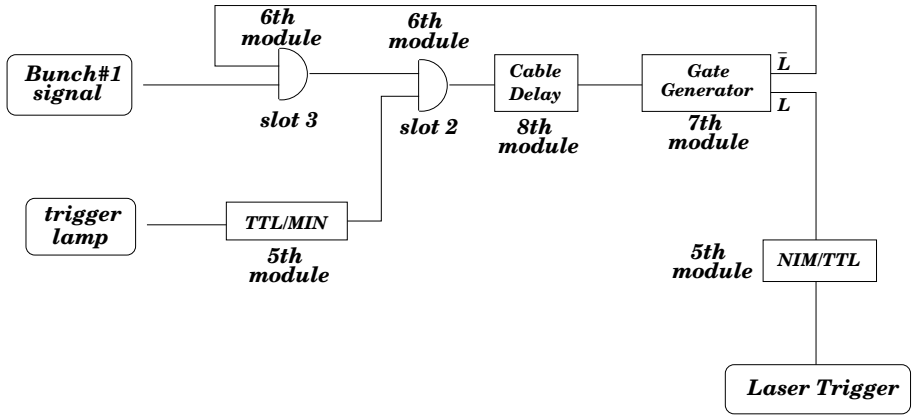

Figure A.2: Laser trigger logic.

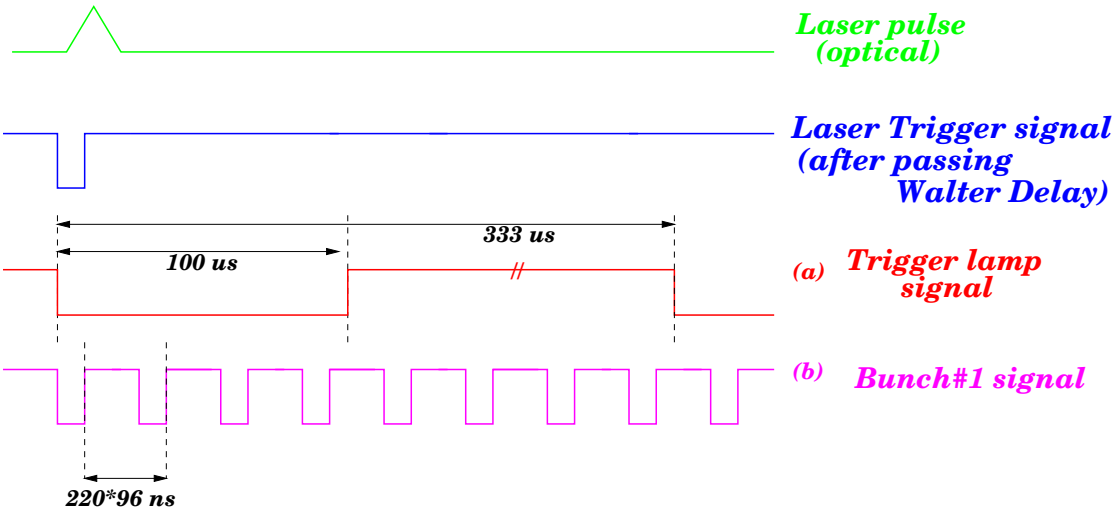

Figure A.3: Laser trigger signal production.

and (b)) are "trigger lamp" signal and "Bunch#1" signal. The Bunch#1 signal is simply prescaled signal of the HERA-clock signal. Basically, the Laser trigger is coincidence signal of Bunch#1 signal and the trigger lamp signal. Naively, the coincidence signal can be about 12 Hz. However the coincedence signal is transformed by a module which is called "Walter Dealy Box[1]". With this module, the coincedence signal is tuned to the Laser trigger signal (second figure from uppermost Figure A.3). As the result, the Laser trigger is about 3 Hz at usual operation. On the other hand, the Laser trigger is sensitive to the DC motor voltage, as mentioned above. The DC motor dependence GMS event rate can be seen in Section 4.2.1.

[1]See A.1

Appendix B

Software for Gain Monitoring

The description in this section largely owes to the documentation on HERMES web[16] which was prepared by Illinois group.

B.1 Online software

mymon

"mymon" performs private decoding of the incoming datastream. Values read from channels of an ADC or a TDC fastbus module are histogrammed in a global section, which can be accessed with PAW. mymon provides a simple direct way to view the performance of the GMS hardware, which is independent of much of the other machinery associated with Hermes data acquisition. It is particularly useful for a quick look at the behavior of ADCs and TDCs for detectors monitored by the GMS.

The temporary version, March.2002, of the program can be found in the directory (this is not final version but it can be run on the PC-farm);

PC-farm :/group01/gmsgrp/common/mymon/

The only requisite files there are Makefile, mymon.f (the most recent Fortran source), and mymon help (a help file). Also required is the wlib library found in /group01/gmsgrp/common/lib/ and named libwlib.a. Given these components one can compile a private version of the program by typing make. Note that source code for the wlib library is located in /group01/gmsgrp/common/wlib/. The most up-to-date version is always called mymon.f.

To run the program, simply type mymon. You will then be given a mymon prompt (MYMON), from which you can issue various commands. Some of the important commands are:

1. BIN-SIZE $<$ *number of channels* $>$:
   Allows one to group together adjacent ADC or TDC channels in a single bin in the output histograms (by default mymon does no binning, ie the number of channels binned together is 1).

2. FASTBUS-SLOT $<$ *slot number* $>$:
   Used to define the slot address of the fastbus module that will be considered by mymon. By default, this is slot 17, which contains and ADC attached to, among other things, the PIN photodiodes, NaI and TF1 radiation damage detectors, phase ramp and newly built Laser monitoring system.

3. MODULE-TYPE $<$ *ADC or TDC* $>$:
   Defines whether the module to be considered is an ADC or a TDC (by default, an ADC is assumed).

4. TRIGGER-CLEAR $<$ *trigger designation* $>$
   $<$ *trigger designation* $>$ ... and TRIGGER-SET
   $<$ *trigger designation* $>$
   $<$ *trigger designation* $>$ ... :
   These commands are used to define bits that must be clear and bits that must be set in the trigger mask for an event to be considered by mymon. By default, no bits are required to be set, and all bits except the GMS bit and the PEDESTAL bit are required to be clear. This means that mymon will consider events in which only the GMS and PEDESTAL bits may (but need not be) on.

5. GO :
   Starts data collection.

6. HELP $<$ *command* $>$:
   Provides a description of the use of a particular mymon command. If no command is entered, a list of available commands is made.

7. QUIT :
   Terminates mymon and returns to the system.

Most commands requiring arguments will print the currently selected values of their arguments if none are entered.

After defining the module and module type, the binning for histograms, and the trigger bits, and after entering GO to begin data acquisition, a PAW session can be opened to view histograms. The first command entered to PAW should be "`glo gmso`" to establish a mapping to the mymon global

section. Note you must open the PAW session on the same machine that is running mymon. A listing of histograms will show that 64 are defined, one for each channel of the fastbus module.

Data acquisition can be halted at any time (after GO or CONTINUE has been entered) by typing "control-C" to mymon. Parameters for the acquisition can then be altered by entering more mymon commands. GO can then be entered to restart acquisition, clearing all histograms, or CONTINUE can be entered to restart without clearing histograms.

The autopeak program

"autopeak" was written by Brynnen Owen to facilitate the measurement of GMS PIN diode peak positions.

The most current version of the source is on the "lxher4" machine or the gms group disk on PC-farm. The files Makefile, autopeak.f, and autopeak.inc are required to make the autopeak executable (using "make autopeak"). To fully realize the capabilities of autopeak, the additional files subpeaks.f, makepeaks.scr and autopeak.scr are needed. The subpeaks program executable must be generated using "make subpeaks". In order for script procedures to operate correctly, all files must be installed in a directory /home/gmsgrp/packages/autopeak on the machine.

The heart of the autopeak package is the autopeak program. It can be called from the command line with the following syntax:

autopeak [+/ − f] [−p#] [−n] [−o] [−t{g|p|a}] [−F{n|o}{file}] [−N#]

If autopeak is invoked without any options, it collects 300 unfiltered laser pulses and fits them to a Gaussian for each PIN diode. It then prints the results to stdout. autopeak has several command line options.

-f Fit the PIN data to Gaussians. This is the default if the trigger mask and filter positions are left unchanged. If a filter or (non GMS) trigger is specified, then peak fitting is turned off.

+f Turn off Gaussian fitting. Useful if you just want to make an n-tuple and not fit anything.

-p# This allows filter wheel position # to be included. If any -p's are given, then only the filter positions typed on the command line are processed. If no -p's are given, autopeak looks at either unfiltered wheel positions or all events based on the trigger mask. If the trigger mask is set to

GMS, then only unfiltered peaks are accepted. If the trigger mask is set to either PEDESTAL or ALL, then all filter positions are processed.

-n This option creates an n-tuple of all of the events processed. The n-tuple has an ID of 20 and it contains 5 entries.

IWHEEL	the calculated filter wheel position
ADCWHEEL	the wheel ADC output used to generate IWHEEL
PIN1	data from PIN1
PIN2	data from PIN2
PIN4	data from PIN4

-o Create summary output file. This information is only printed if peak fitting is turned on. The summary output file contains 6 fields as follows:
date time pin1peak pin2peak pin4peak numpts_used

-t(g—p—a) Set the trigger mask. -tg is the GMS trigger only. -tp is the PEDESTAL trigger mask only. -ta is both.

-F(?) {name} Set the name of either the summary file or the n-tuple file to {name}. (?) is either 'o' or 'n' for summary file or n-tuple. The default file name for the n-tuple is autopeak.rz. The default file name for the summary file is autopeak.dat.

Examples: To create the n-tuple and name the file ntuple.rz, type:

autopeak -n -Fn ntuple.rz

To create the summary file called summary.dat, use

autopeak -o -Fo summary.dat

-N# Sets the total number of events to process before exiting to #. This is the total number of events that are actually counted. If autopeak looks at only filters 1, 2, 3, and 4, and the option -N1000 is given, autopeak will process ∼2000 events, since half will be for filters 5, 6, 7, or 8.

autopeak examples

If you want to create an n-tuple that resembles the paw global session created by mymon with both GMS and PEDESTAL triggers, and you want the n-tuple named data.rz, type: (it will default to 300 events since events aren't

specified. Since the trigger has changed and no filter positions have been specified, it will look at all filters.)

autopeak − n − Fn data.rz − ta

If you want to look at the pedestals on filter 6 (which is slightly misleading, since during a pedestal the wheel position is undefined) and just see the fitted peaks on the screen type: (once again, it will default to 300 events and all filter positions.)

autopeak − tp − p6 − f

To generate a summary file called autopeak.out of 1000 events of the unfiltered positions using only the GMS trigger type

autopeak − N1000 − o

To generate a summary file called filter5.peaks of 200 events of the GMS trigger of filter 5 type:

autopeak − N200 − o − Fo filter5.peaks − p5

To generate an n-tuple of GMS triggers of the unfiltered positions without fitting the peak, type:

autopeak + f − n

The makepeaks.scr script and subpeaks

makepeaks.scr is a script for running autopeak to find pedestal subtracted peak positions. It runs autopeak twice: once to get the unfiltered peak position and once to find the pedestal. makepeaks then runs a special purpose program called subpeaks to subtract the pedestal from the unfiltered peak position. Note that subpeaks is designed to be used only from the script makepeaks.scr.

The makepeaks script concatenates its output (using cat) to the end of peakpos97.dat. That file is in the format defined by Balijeet Bains for the 1996 data. A comment may optionally be added to the output of makepeaks. This is taken from any characters that follow the call to makepeaks.scr

The following will cause a measurement of the peak positions to be done and a commented line to be added to peakpos97.dat.

makepeaks.scr reattenuated laser

The line in the peakpos97.dat file will be

(date) (time) (peak1) (peak2) (peak3) : reattenuated laser

For GMS expert, if you do for GMS hardware (for example, change the dye , re-alignment or change the attenuation etc), everything what you did have to be written in the GMS logbook and the peakpos##.dat in line of the day.

The autopeak.scr script and cron

makepeaks.scr can be called interactively as described above. It can also be called automatically at regular intervals using the "cron" facility of Unix. The results of makepeaks are then e-mailed to you. This is accomplished using yet another "wrapper" script called autopeak.scr as described below. It is assumed here that you are **not** already running jobs using the cron facility.

In order to set up automatic running of autopeak.scr, you must first create (edit) a file containing a single line. Call the file autopeak.crontab and keep it in your ~/gms/autopeak directory. The single line in the file should be of the form:

min hour * * * /yourdisk/yourname/gms/autopeak/autopeak.scr

Here, min and hour specify the time of day when you want the peak measurement to be performed. Note that, typical of Unix, the order of min and hour is the reverse of the normal logical order. The three asterisks specify that the task is to run every day. The final item on the line is the shell command to run the autopeak.scr command. You may not use õr $HOME in the path specification. You must spell out the path with no abbreviations. In particular you must fill in the disk name (yourdisk) and user name (yourname) appropriate to your account on the "r" machines. To determine full path required in this shell command use the pwd command in your ~/gms/autopeak directory. As an example, Steve Williamson uses the following line in autopeak.crontab:

45 7 * * * /us0/willy/gms/autopeak/autopeak.scr

This causes autopeak.scr to run at 7:45 AM everyday. **But do not use this example**. Running autopeak more than once at the same time may cause problems. Please use a different time.

gmsClient and gmsServer

A brief description of the GMS slow controls software and descriptions of the software components is provided below.

There are three pieces of code that make up the GMS slow control software: gmsClient, gmsServer, and mongms.pink. An online version of the HermesDeCoder (HDC) runs under jobctrl (a watchdog which makes sure programs are continually running, and restarts them if need be) and sends decoded events to a server called DServer. (NOTE: all software involved in the slow controls - clients, servers and Pink scripts- runs under jobctrl - for details on jobctrl, see Vitaly Shutov). The gmsClient reads updates from DServer and processes them. gmsClient then performs two kinds of calculations. One is performed every 10 events (GMS and pedestal events only) and is a very crudely calculated gain (called a fastgain). The other is a more sophisticated calculation of the gain and is performed at the end of each data-taking run or when DAQ is stopped or every 20000 events. The gains generated by the two types of calculations are sent via two different dataflows to the gmsServer. The gmsServer just holds them. The fastgains are read from the gmsServer by the Pink script mongms.pink which displays them via a color display in the Hermes control room.

gmsClient

The directory where the official source code lies in

/hsoft/SLOW/Sources/GMS/new/

on the lxher# machines. The actual c code for gmsClient is in

/hsoft/SLOW/Sources/GMS/new/source/

and is fairly well commented.

Logfiles for the running of the program can be found,

/hsoft/SLOW/clients/gms/.

In addition to providing gmsServer with full dataflows of gains and fastgains, gmsClient also directs output to ascii files for immediate perusal by those interested:

The fastgains are written to a file called fastgains.dat in the directory (written above) where the program is written. The fastgains are written as well as the fastgains divided by the "nominal" gain of that detector.

The nominal values were chosen arbitrarily as gain values from the beginning of 1996 running.

Another ascii file is found in this directory called caloon. This is a kumac that can be used with the CAEN HV program to turn on calorimeter blocks that are found to have inordinately low gain by the GMS.

The gains (the more sophisticated calculation) are written to ascii files with name gains-?????-XXXXXXXX.dat, where ????? is the run number and XXXXXXXX is a time stamp. These files are found in yet another directory, ../cfg/, in relation to where the program is run. It is not necessary to keep them for a long time, since the gains are calculated offline (with better statistics, since the online HDC does not get all user events) along with data production. They are useful for troubleshooting in the case that something odd occurs.

Since gmsClient runs under jobctrl, it is very low maintenance. If it terminates, it is automatically restarted. When it is terminated, an email in sent to the resonsible such as:

```
Date:  Thu, 28 Nov 96 08:40:04 +0100
From:  Hermes Online <onl@dxhrb2>
To:  bains@axher1
Subject:  gmsClient terminated

Message Id :  1960
Message Type:  Online
Sender :  Oma (onl@axher4.)
Submission :  Thu Nov 28 08:40:03 1996
Valid from :  Thu Nov 28 08:39:59 1996
Valid till :  ever
Subject :  gmsClient terminated

/usf1/SLOW/r4lowlevel/bin/gmsClient
Thu Nov 28 07:20:56 MET 1996 @ axher4
--- Begin of output ----------------------------
Special ZEBRA
program gmsClient, Balijeet Singh Bains
ADAMO/TAP version 3.3 with GAF version 3.2 starting
DadID[0] (for StatusBar) = 0
DAD: reading dadinit.cnf
DAD Client Software
```

```
--- Version 1.35 (PL 24) starting up
DadID[0] (for StatusBar) = 21
DServer-dadConnect:  0 64
dadBook:  0
DaqServer-dadConnect:  0 22
dadBook:  0
gmsServer-dadConnect:  0 75
gmsfastServer-dadConnect:  0 76
DServer dadMsg:  0 68
DServer dadMsg:  0 40
Shit!  COUTAB(dataHodo) returns 167.
--- End of output ------------------------------
programm terminated Thu Nov 28 08:39:58 MET 1996
return status:  0
```

The email contains part of the logfile. Most of these terminations are as above, due to the fact that one of the servers required for running has either stopped or recently been restarted. As above, the table dataHodo in DServer has twice the number of rows as it should. So a clean exit is in order. There are however, the occasional messages of "phantom" terminations. There is no error reported, and gmsClient starts up a la jobctrl without problems. This can sometimes be accompanied by a core dump, which can possibly be explained by divide by zero errors, which can happen when there are no GMS events in a calculation period. This can be due to, for example, the filterwheel belt breaking, bad luck in the way HDC prescales user events, or the GMS timing drifting. If the crashing of gmsClient seems to coincide with the DAQ's run changes, the GMS timing is suspect. There is a bug/feature in gmsClient that it will not accept trigger 32s in coincidence with other triggers. So if the timing is drifting, and trigger 32s are in coincidence with trigger 25s, for example, then you will get no GMS events and a divide by zero will be performed. Crash. This mistiming feature occurred during the month of August and CAN happen.

gmsServer

The source code for gmsServer is found in the same place as that of gmsClient. It is well commented, like gmsClient. Also like gmsClient, it is run from its own directory, however, /hsoft/servers/gmsServer/

where you can find its jobctrl related files, such as its logfile, and its *.rz files.

It is even lower maintenance than gmsClient, since it restarts automatically upon termination. It rarely terminates, having done so only 4 times in all of 1996 running.

mongms.pink

This PinK script was kindly provided by Marc-Andre Funk, because his aesthetic programming sense was offended by the Higz window that preceded it. It is also well commented. Its source is found where the other source codes are found, and it too runs from a separate directory - /hsoft/SLOW/pinks/mongms/. Its jobctrl related files are found here. There is also in this directory a copy of the nominal.dat file found with the source codes. mongms.pink reads the fastgains from the gmsServer and divides them by their nominal values. The resulting value should be close to 1, and is depicted on a map of the detector according to a color scale. The mongms.pink display is extremely useful during datataking for detection of trips in the calorimeter and preshower.

scaler page

This program is general program in HERMES. GMS laser frequency can be checked in this program page 1.
Note : The scaler program shows GMS trigger rate, not motor frequency.

B.2 Offline Software

Offline Program “gms”

There are shell script to run the “gms”.

```
#!/bin/bash

HERMES_ROOT=/hermes/new
PEDFILE=pedestal-20020227.dat
```

```
HDC=${HERMES_ROOT}/bin/hdc
HDCPIPE=/tmp/hdc2gmsprivate

GMS=${HERMES_ROOT}/bin/gms
GMSOUT=gms2out

RUNNO=$1

rm -f $HDCPIPE
rm -f $HDCPIPE.rpid
rm -f $HDCPIPE.wpid


             ${HDC} --trigger 16 23        \
                    --read run$RUNNO       \
                    -v4                    \
                    --update off           \
                    --det HODO CALO PHMO RR HM LUMI GMS HO \
                    --write pipe $HDCPIPE  > hdc.out 2>hdc.err &

START=0
STOP=15

echo -n "Waiting for pipe to appear "
while [ $START -lt $STOP ]; do
    if [ -p $HDCPIPE ]; then
        let START=$STOP+20
        continue
    fi
    let START=$START+1
    sleep 1
    echo -n '.'
done

echo

if [ $START -le $STOP ]; then
    echo Couldn\'t find HDC pipe, so giving up.
    exit 1
fi
```

```
${GMS}  --read ${HDCPIPE}    \
        --driver WFIL        \
        --write ${GMSOUT}    \
        --odriver WFIL       \
        --gmstrig 16         \
        --pedtrig 23         \
        --pedfile ${PEDFILE} \
        --lumicode           \
        --gmsntup            \
        --ntuple gms.${RUNNO}.ntup 2>gms.err &
```

This script is just a sample. You can see help of the hdc and gms using −−help. If you use this script, you need to copy the row data file (E.P.I.O) to somewhere, for example /scratch/ etc. This can be done automatically using "linkrun" command. By this command, the row data file is copied to the /scratch/runstage/.

In addtion, if you want to see the hdc output (file), add an option "−−write file <file name>" to the hdc options. Then type "pb −fz <file name>".

Appendix C

Maintenance Procedure

The description in this section largely owes to the documentation on HERMES web[16] which was prepared by Illinois group.

Dye Change

The dye for the laser should be changed once a month. This should be done when there is NO data taking and there will not be for (to be safe) at least an hour.

First, open the laser "coffin" by removing the two wing-nuts found on its top surface. Open the box all the way. The laser will automatically shut off (to defeat the interlock, see section 2 - realignment). On top of the laser, towards its forward section, there is a removable panel. Lift this off. You will see a cuvette filled with yellow-green dye. Pull it out by its top (gently, so as not to remove the top). Hold it between thumb and forefinger so that the sides are not touched - this is important so that the sides remain as clean as possible. Take the cuvette to the second floor of the East Hall to the clean room.

In the Illinois cabinet, find a pair of gloves. Wear them to avoid dirtying the cuvette. Also there is a plastic graduated cylinder containing some dye. This is old dye. Empty the cuvette into it. There is a dark brown vial in the cabinet labelled "Coumarin 500." Also, there is handwritten on the label in black marker the word NEW. This is the dye to use. DO NOT use dye marked with any other wavelength. Use the plastic syringe in the cabinet to refill the cuvette.

NOTE: the dye is an organic dye whose effect on the human body is not completely known. It may be carcinogenic, so avoid contacting it with bare

skin.

Once the cuvette is filled, close it. If it seems dirty, use the plastic squeeze bottle of acetone and a Kimwipe to clean it. Do not use the alcohol in the hard glass bottle. That is pure alcohol needed to mix more dye.

Bring the cuvette back down to the laser. Place it back in its place. Put the removable cover back in place and close the laser "coffin." After tightening the wing-nuts, restart the laser by pushing the switch on the front of the coffin upwards.

Realignment

From time to time, you may want to realign the laser optics to get more light through to the detectors. In order to do this most efficiently, you should use a digital oscilloscope and use as its input the signal from one of the PIN photodiodes. Again, of course, only do this when data is not being taken, and to be safe, do it when there is going to be no beam for a few hours.

The signal from one of the PINs should change in magnitude in accordance with the particular filter that is in front of the laser when it fires. So you should see a rapidly changing pulse whose magnitude is $\tilde{1}00$ mV.

Now open the laser coffin. The laser is off due to the interlock mechanism. You must circumvent this. Since the laser will be on while the box is open, you must wear goggles. There are goggles in the laser box.

To circumvent the interlock, find the plug on the back of the laser which is connected to the switch on the outside of the laser coffin. Remove it. Replace it with the stand alone version found in the coffin. Now restart the laser by pushing the "enable" switch on the back of the laser upwards. You should see the signal on the oscilloscope start up again.

Now, to realign the optics, you should first try to use the fine adjustment screws found on the fiber holder. The adjustment mechanisms on the fiber holder are self-explanatory. The idea here is to adjust them such that the signal on the oscilloscope gets as large as possible. If the gross adjustments are used, you can completely ruin the alignment and you will have to "find" the beam almost entirely by trial and error. One trick is to use the main fiber. Trace it back to the main attenuator (it is orange and sits on top of the laser). Disconnect it from this attenuator and see if light is coming out ... in this way you can see if light is getting through before the PIN response is big enough to register on the scope.

Attenuation

If the laser intensity is too low (as observed by using the mymon program) and it is not yet time to change the dye, you can correct this by removing attenuation at the main attenuator.

The main attenuator lies directly on top of the laser. It is orange and can be found by tracing the main fiber (the one that directly comes from the optical mount behind the filter wheel). This main attenuator can be adjusted by means of turning the tiny screw found on its top. Clockwise attenuates the light; counterclockwise removes attenuation. Turn the screw until you reach the desired amount. You may have to close the coffin and restart the laser and run the mymon program again to see how much the laser intensity has changed. Another option is to use a digital oscilloscope, as described in the section above on realignment.

Appendix D

New Detector Installation Procedure

D.1 Online Monitoring Software Modification

For online monitoring, it is needed to add the new detector to the GMS client software (gmsClient). The "gmsClient" shoul be changed for following process ;

- Data selection :
  The detector data is selected by selecter and picked up from the DAQ data stream which are decoded by the HDC.

Another processes (e.g gain calculation process etc) are used, it is not needed to modify. The procedure which have to be modified is related to the ADAMO format data, the data is tabulated in the data stream. The data are extracted using selector. As an example for data extraction, the program pieces for H0 hodoscope are picked out as follows ;

```
#define NUMDETS 960             /* 840 + 84 + 4 + 1 + 24 + 3  + 4        */
#define NUMBINS 1               /* CALO HODO TF  NaI LUMI PIN  H0        */

.............skip...............

int idH0U , idH0L , selh0u , selh0l ;

.............skip...............
```

```
int num1,I,num2,J,num3,K,num4,L,num5,M,CaloBl,num6,N ;
int num7 ;  /* <-- Added newly for H0 */
```

In this program pices, H0 added to the GMS detectors list. Then the next pieces performs to get the ID of each H0 top (`idH0U`) and bottom (`idH0L`) from the ADAMO table.

```
idH0U = detID("H0UV");
idH0L = detID("H0LV");

.............skip...............

CRESEL(HodoId,selh0u,"H0U");
CRESEL(HodoId,selh0l,"H0L");

.............skip...............

  SELSEL(dataHodo,"dgDETS",idH0U,idH0U,selh0u,0);
  SELSEL(dataHodo,"dgDETS",idH0L,idH0L,selh0l,0);
```

In the following, H0 data are picked up from data table using selector which is declared in the above. Then the data are stored to calculate the gain.

```
num7 = COUSEL(dataHodo,selh0u);
       for (J=1;J<=num7;J++)
  {
            FETTAB(dataHodo, selh0u, J);
    K = dataHodo.iWire - 1;

    if (use_for_ped) {
hackedped[956+K] = dataHodo.iADC;
```

```
        }
               if (iTriggerMask==PEDTRIG) {     /* if ped trig            */
                   py1[956+K][pedbin]+=(double)dataHodo.iADC;
                   DetPedSum[956+K]+=(double)dataHodo.iADC;
        }
               if ((iTriggerMask==GMSTRIG)||
                   (iTriggerMask==BOTHTRIG)) {  /* if gms trig            */
                   y1x0[956+K][pedbin]+=(double)dataHodo.iADC*(1.);
                   y1x1[956+K][pedbin]+=(double)dataHodo.iADC*(double)iGmsMon;
                   y2[956+K][pedbin]+=(double)dataHodo.iADC*
                       (double)dataHodo.iADC;
                   DetGmsSum[956+K]+=(double)dataHodo.iADC;
               }
           }

    num7 = COUSEL(dataHodo,selh01);
           for (J=1;J<=num7;J++)
      {
               FETTAB(dataHodo, selh01, J);
        K = dataHodo.iWire - 1;

        if (use_for_ped) {
  hackedped[958+K] = dataHodo.iADC;
        }
               if (iTriggerMask==PEDTRIG) {     /* if ped trig            */
                   py1[958+K][pedbin]+=(double)dataHodo.iADC;
                   DetPedSum[958+K]+=(double)dataHodo.iADC;
        }
               if ((iTriggerMask==GMSTRIG)||
                   (iTriggerMask==BOTHTRIG)) {  /* if gms trig            */
                   y1x0[958+K][pedbin]+=(double)dataHodo.iADC*(1.);
                   y1x1[958+K][pedbin]+=(double)dataHodo.iADC*(double)iGmsMon;
                   y2[958+K][pedbin]+=(double)dataHodo.iADC*
                       (double)dataHodo.iADC;
                   DetGmsSum[958+K]+=(double)dataHodo.iADC;
               }
           }
```

D.2 Offline Monitoring Software Modification

The offline gain evaluation is done by GMS softwarte "newgms". Usually the newgms performs to calculate the detector gain, then outputs to a file, gains-####.dat with other hrc output files. The process of the offline program is similar to online program.

(H0 hodoscope instllation procedure, as an example)

```
#############
#           #
# gmsinit.c #
#           #
#############
```

```
  CRESEL(dataHodo,gsH0Top,"H0UV");
  CRESEL(dataHodo,gsH0Bot,"H0LV");

.........skip.........

  /* Find the top H0 detector ID */
  SELSELC(dgDETINFO,"cName","H0UV","H0UV",sDet,0);
  FETCOL(dgDETINFO,"ID",sDet,1,1,&gidH0Top);

  /* Find the bottom H0 detector ID */
  SELSELC(dgDETINFO,"cName","H0LV","H0LV",sDet,0);
  FETCOL(dgDETINFO,"ID",sDet,1,1,&gidH0Bot);
```

This program piece performs to create the selector and picked out the detector data from the table.

```
##############
#            #
# gmsevent.c #
#            #
##############
```

```
  SELSEL(dataHodo,"dgDETS",gidH0Top,gidH0Top,gsH0Top,0);
  SELSEL(dataHodo,"dgDETS",gidH0Bot,gidH0Bot,gsH0Bot,0);
```

```
.........skip.........

      /* Get the top H0 dets */
      /* Count how many there are */
      ctSelLen = COUSEL(dataHodo,gsH0Top);

      for(i=0;i<ctSelLen;i++)
        {
          /* Read in the table */
          FETTAB(dataHodo,gsH0Top,i+1);

          /* Get the index of the 'wire' for this det */
          nIndex = dataHodo.iWire;

          /* make sure the wire is within range */
          if( (nIndex < 1) || (nIndex > NUMH0S) )
            {
              /* Go to the next wire */
              continue;
            }

          /* Add on the offset, but subtract 1 for 0 based arrays */
          nIndex += OFFSETH0TOP - 1;

          /* Store the ADC for faster access */
          iADC = dataHodo.iADC;

          /* Check that the ADC is greater than 0 */
          if(iADC > 0)
            {
              /* Store the pedestal events */
              pedputvalues(iADC,nIndex);
            }

        }

      /* Get the bottom H0 dets */
      /* Count how many there are */
      ctSelLen = COUSEL(dataHodo,gsH0Bot);

      for(i=0;i<ctSelLen;i++)
        {
          /* Read in the table */
```

```
          FETTAB(dataHodo,gsH0Bot,i+1);

          /* Get the index of the 'wire' for this det */
          nIndex = dataHodo.iWire;

          /* make sure the wire is within range */
          if( (nIndex < 1) || (nIndex > NUMH0S) )
            {
              /* Go to the next wire */
              continue;
            }

          /* Add on the offset, but subtract 1 for 0 based arrays */
          nIndex += OFFSETH0BOT - 1;

          /* Store the ADC for faster access */
          iADC = dataHodo.iADC;

          /* Check that the ADC is greater than 0 */
          if(iADC > 0)
            {
              /* Store the pedestal events */
              pedputvalues(iADC,nIndex);
            }

        }

.........skip.........

      /* Get the top H0 dets */
      /* Count how many there are */
      ctSelLen = COUSEL(dataHodo,gsH0Top);

      for(i=0;i<ctSelLen;i++)
        {
          /* Read in the table */
          FETTAB(dataHodo,gsH0Top,i+1);

          /* Get the index of the 'wire' for this det */
          nIndex = dataHodo.iWire;

          /* make sure the wire is within range */
          if( (nIndex < 1) || (nIndex > NUMH0S) )
```

```
      {
        /* Go to the next wire */
        continue;
      }

    /* Add on the offset, but subtract 1 for 0 based arrays */
    nIndex += OFFSETHOTOP - 1;

    /* Store the ADC for faster access */
    iADC = dataHodo.iADC;

    /* Check that the ADC is valid */
    if(iADC>0)
      {
        /* store the GMS values */
        gmsputvalues(iADC,nIndex);
      }

  }

/* Get the bottom HO dets */
/* Count how many there are */
ctSelLen = COUSEL(dataHodo,gsHOBot);

for(i=0;i<ctSelLen;i++)
  {
    /* Read in the table */
    FETTAB(dataHodo,gsHOBot,i+1);

    /* Get the index of the 'wire' for this det */
    nIndex = dataHodo.iWire;

    /* make sure the wire is within range */
    if( (nIndex < 1) || (nIndex > NUMHOS) )
      {
        /* Go to the next wire */
        continue;
      }

    /* Add on the offset, but subtract 1 for 0 based arrays */
    nIndex += OFFSETHOBOT - 1;

    /* Store the ADC for faster access */
```

```
          iADC = dataHodo.iADC;

          /* Check that the ADC is valid */
          if(iADC>0)
            {
              /* store the GMS values */
              gmsputvalues(iADC,nIndex);
            }

        }
```

```
##############
#            #
# gmstypes.h #
#            #
##############
```

```
#define NUMHOS       2  /* Number of H0 hodoscope in one half     */

.........skip.........

#define OFFSETH0TOP      OFFSETPINS    + NUMPINS
#define OFFSETH0BOT      OFFSETH0TOP   + NUMH0S

.........skip.........

#define TOTALDETS  (OFFSETH0BOT+NUMH0S)
```

```
#############
#           #
# globals.h #
#           #
#############
```

```
int        gsH0Top;          /* H0 top selector                      */
int        gsH0Bot;          /* H0 bot selector                      */

.........skip.........
```

```
int        gidH0Top;         /* Detector ID for H0 top         */
int        gidH0Bot;         /* Detector ID for H0 bottom      */

.........skip.........

int        ganH0s[2*NUMH0S]; /* Array for filling ADC ntuple for H0  */

.........skip.........

extern int gsH0Top;          /* H0 top selector                      */
extern int gsH0Bot;          /* H0 bot selector                      */

.........skip.........

extern int ganH0s[2*NUMH0S]; /* Array for filling ADC ntuple for H0 */
```

In addition, the newgms program can aslo make a hbook file, not only gains-####.dat file. The hbook file also should be modified. The process to output the hbook file is very simple because the hbook file does not include calculated gain, the data in the file are just only raw data, GMS event data and pedestal event data.

```
#################
#               #
# gmsinitntup.c #
#               #
#################


  iptr = &ganH0s[0];
  HBNAME(2,"H0ADCs",iptr,"iH0(4)");
```

```
##################
#                #
# gmsntupevent.c #
#                #
##################


  /* Now do the HO tops */
  for(i=0;i<NUMHOS;i++)
    {
      /* Select out just the hodo wire we want */
      SELSEL(dataHodo,"dgDETS",gidHOTop,gidHOTop,gsHOTop,0);
      SELSEL(dataHodo,"iWire", i+1,      i+1,      gsHOTop,AND);

      /* Make sure we got just one wire */
      if(COUSEL(dataHodo,gsHOTop)==1)
        {
          /* Get the table entry */
          FETCOL(dataHodo,"iADC",gsHOTop,1,1,&ganHOs[i]);
        }
      else
        {
          /* this channel has problems -- set it to 0 */
          ganHOs[i]=0;
        }
    }
  /* Now do the HO bootom */
  for(i=0;i<NUMHOS;i++)
    {
      /* Select out just the hodo wire we want */
      SELSEL(dataHodo,"dgDETS",gidHOBot,gidHOBot,gsHOBot,0);
      SELSEL(dataHodo,"iWire", i+1,      i+1,      gsHOBot,AND);

      /* Make sure we got just one wire */
      if(COUSEL(dataHodo,gsHOBot)==1)
        {
          /* Get the table entry */
          FETCOL(dataHodo,"iADC",gsHOBot,1,1,&ganHOs[i+NUMHOS]);
        }
      else
        {
          /* this channel has problems -- set it to 0 */
```

```
          ganHOs[i+NUMHOS]=0;
        }
    }
```

```
#################
#               #
# gmsinitntup.c #
#               #
#################
```

```
  iptr = &ganHOs[0];
  HBNAME(2,"HOADCs",iptr,"iHO(4)");
```

Bibliography

[1] K. Ackerstaff et al., *HERMES spectrometer*, Nucl. Instrum. Meth. **A417** (1998) 230.

[2] R. Kaiser , *Particle Identification at HERMES*, HERMES internal report (1997) 97-025

[3] S. Yoneyama , *Spin Asymmetry of Kaon Productions in Polarized Deep-Inelastic Scattering on Deuterium Target By HERMES Experiment*, DESY-THESIS-2001-017 (2001)

[4] J. Ashman *et al.*, *A measurement of the spin asymmetry and determination of the structure function g_1 in deep inelastic muon-proton scattering*, Phys. Lett. **B206** (1988) 364

[5] J. Ashman *et al.*, *An investigation of the spin structure of the proton in deep inelastic scattering of polarised muons on polarised protons* , Nucl. phys. **B328** 1

[6] A. A. Sokolov and I. M. Ternov, *On Polarization and spin effects in the theory of synchrotron radiation*, Phys. Dokl. **8** (1964) 1203–1205.

[7] HERMES Collaboration, *Technical Design Report*, July 1993

[8] K. Suetsugu, *Performance of Pion Kaon and Proton Identification with Ring Imaging Čerenkov Counter of HERMES* Eprint number DESY-THESIS-2001-016

[9] HERMES Collaboration, K. Ackerstaff *et al.*, Nucl. Instrum. Methods **A417** (1998) 230. Eprint number DESY-98-057, hep-ex/9806008

[10] S. Bernreuther et al., *The HERMES back drift chambers*, Nucl. Instrum. Meth. **A416** (1998) 45–58.

[11] F. M. Menden R. Kaiser and M. C. Vetterli, *Probability Analysis of the TRD Response and the Contribution of Flus Ratios to HERMES Particle*, HERMES Internal **97-036** (1997).

[12] M. Beckmann, *et al.*, *The Longitudinal Polarimater at HERA*,Nucl. Instrum. Meth. **A** 00-046 (1998)

[13] H. Avekian *et al.*, *Performance of the Electromagnetic Calorimeter of the HERMES Experiment* (March 9,1998)

[14] M. Kobayashi *et al.*, *KEK internal report* 93-015 (1993)

[15] H. Avekian *et al.*, Nucl. Instr. and Meth. **A378** (1993)

[16] Steven Williamson (Illinois),
http://www-hermes.desy.de/groups/gmsgrp/

List of Figures

List of Tables

Acknowledgements

During my study at the Tokyo Institute of Technology and DESY, Hamburg, I was helped by a lot of people. I'd like to express my thanks to all people who supported me.

First of all, I would like to thank Prof. Toshi-Aki Shibata who gave me a chance to study the Gain Monitoring System (GMS) actually in DESY and who provided me many advices. I am indebted to Dr. Yoshiyuki Miyachi for his valuable advice and suggestions during my entire studies. I would thank Prof. Yasuhiro Sakemi for his suggestions about HERMES experiment. I wish to express my thanks to Dr. Stefan Bernreuther for reading the entire text in its original form and giving me helpful comments.

My thanks are also due to the members of HERMES collaborators with whom I worked. Many thanks to Dr. Maurice Bouwhuis who were in charge of GMS before me and gave me very kind explanation about HERMES experimental systems and details about GMS, and to Dr. Gunar Schnell who help me to build the Laser monitoring system.

I would also like to express my thank to the members of Tokyo Tech. group. Especially, Hiroshi Ohsuga, he and me had a good discussion for HERMES experiment and physics. Takuma Horaguchi, Jumpei Shirono, Hideaki Nihongi had many occasions to discuss with me about my study. It was very helpful for me.

Additionally, I thank the members of the HERMES Collaboration. Particularly, Dr. Elke-Caroline Aschenauer gave me a lot of advice and help. I received a lot of helps from the HERMES collaborators. Thanks to all of them.